ALMA MATER STUDIORUM
UNIVERSITÀ DI BOLOGNA

DOTTORATO DI RICERCA IN

SCIENZE E TECNOLOGIE AGRARIE, AMBIENTALI E ALIMENTARI

Ciclo 38

Settore Concorsuale: 07/B1 - AGRONOMIA E SISTEMI COLTURALI ERBACEI ED ORTOFLORICOLI

Settore Scientifico Disciplinare: AGR/02 - AGRONOMIA E COLTIVAZIONI ERBACEE

EFFECTS OF ROOT ARCHITECTURE OF DIFFERENT WHEAT CULTIVARS ON SOIL STRUCTURE

Presentata da: Bartolo Giuseppe Dimattia

Coordinatore Dottorato

Diana Di Gioia

Supervisore

Marco Bittelli

Co-supervisore

Silvio Salvi

Esame finale anno 2026

To my past self — who, during years of illness and rejections, never gave up on the dream of becoming a researcher. I still remember you in a hospital bed, after surgery, asking for stronger painkillers just to attend a PhD interview. Thank you for not giving up.

To the right to education,
enshrined as a pillar of equality
in the Italian Constitution.
To the beauty and dignity of a text
that reminds us that knowledge is
a common good, and that study is
not a privilege but a right.
A good that, when shared, does
not diminish but multiplies.

Acknowledgements

I would like to thank Marco Bittelli, who over these years has been not only my supervisor but also a dear friend. It is thanks to his scientific vision and determination that we implemented X-ray and Hyprop2 measurements in this project, successfully integrating them into our workflow. I am deeply grateful for the opportunity he gave me to collaborate with METER Group, which has been the most enriching experience for me both scientifically and personally. Marco's advice pushed me beyond my limits and helped me grow into an independent researcher. I am especially thankful for his insistence that I learn R and Python, and for teaching me how to write a scientific paper on my own.

I am grateful to Silvio Salvi for the trust he placed in me and for always listening with empathy and humanity. Thank you for being present whenever field trials were at risk, and for encouraging me to see things from new perspectives. I am particularly grateful for the question you once asked me: *"Why do you do research if you find it so difficult?"* — because that question sparked a constructive dialogue with myself about why I truly want to be a researcher.

My sincere thanks to Maria Hernandez Soriano for including me in the consortium, for believing in me, and for always valuing my contribution. For me, you have been not only my coordinator but also a true friend. Thank you for the laughs we shared over a beer, for introducing me to Fred, and for the many scientific discussions that have enriched me as a researcher. Although this was your first experience as coordinator of an international project, you succeeded in building a multidisciplinary consortium and in writing a proposal that was successfully funded at the international level.

Reviewer 1, your critical and rigorous comments were fundamental in improving the quality of my first article, thank you.

I would like to thank the WISH-ROOTS research consortium for always treating me with respect and valuing my contribution to the project. It has been a real pleasure to grow scientifically and personally within this network.

Thanks Roberto Tuberosa for all the conversations we had over the years and for sparking my passion for root studies. I still remember walking into your office in 2017 saying, *"I want to become an international scientist,"* and you welcomed me into your group, sending me to Belgium to carry out my thesis. Thank you also for sending me to IRSS11 in Missouri, which allowed me to meet Maria and become part of the WISH-ROOTS consortium.

My gratitude goes to George, Alina, Thomas, and Leonardo from METER Group for training me in the use of the Hyprop2, Ksat, and WP4C, and for welcoming me into your company with such

enthusiasm and trust. I am especially thankful to Wolfgang Durner for sharing with me all his knowledge on soil water retention curves (SWRCs) and on the use of the LABROS software. Seeing your passion and dedication made me realize that I could also envision a future in industry.

I would also like to thank the Department of Agricultural and Food Sciences for providing my academic training. My sincere thanks go to Elena Maria Tortorici, Sara Chetta, Eugenia Modoni and all the administrative staff for their constant support with paperwork; to Stefano, Antonio, Michael, and the technicians at the Cadriano Farm; to Angela, Orietta, and all the field workers; and to all the students who contributed to field trials and experiments. Thanks to Angela Righi for the X-ray analyses and to Giacomo Rutigliano for the aggregate analyses. I am also grateful to the genetics, crop science, and agronomy groups for the time we shared, and to Andrea Parenti for his advice and support. Special thanks go to Massimiliano Petracci, Diana Di Gioia, Giovanni Dinelli, Guido Baldoni, Lorenzo Barbanti, Enrico Noli, Marco Maccaferri, Santolo Francati, and all those who dedicated their time to help me and contribute to my training.

Thank you, Dianiele Rabboni, for helping me with the field trials. You were always there for me in the most critical moments.

My heartfelt thanks go to my dear friends and colleagues Chiara Morena and Veronica Bruno. Thank you for being there in difficult moments and for supporting me throughout this journey. I will always remember our conversations, our lunches on the lawn, and our shared frustrations about delayed orders.

I also wish to thank the Collegio Superiore, the Institute of Advanced Studies, and the International PhD College at every level. I am grateful to Beatrice Fraboni, Stefania Pellegrini, Lucia Gunella, and Michela della Vite—your humility in treating me with respect and in valuing my work has taught me much about how to be an empathetic leader. Thanks to the students of the Collegio Superiore for electing me as your representative and member of the exchange commission, and to the commission itself for always treating me as a peer. My thanks also go to the administrative staff of the Collegio Superiore for their invaluable support, and especially to Jessica for helping me with every aspect of bureaucracy.

I would like to thank Chris, Cody, Kirsten, and the entire Topp Lab at the Danforth Plant Science Center for welcoming and supporting me during my research in the United States. I will remember my time in the US as one of the best periods of my life. Thank you for making me feel valued—the culture and environment at Danforth are truly among the best I have experienced in any research center.

My thanks also go to Agnese, Roujing, Francesco, Federica, Cosmin, Ettore, Patrycja, Pietro, Andrea, and the whole I-PhD group for the scientific “aperitivi,” the stimulating discussions on a wide range of topics, and the kindness you have shown me.

I am grateful to Augusto, Laura, Marie, Margot, and Ale—it was wonderful to be part of this group. Thank you for supporting me during difficult times and for lightening my days with fun conversations and board games. With you, I truly felt at home.

Thanks to Francesco and Giusy for standing by me and making this journey lighter with your company and kindness.

A special thanks goes to Anastasia and Arina for being my “adoptive Russian moms” for three years!

I am sincerely grateful to my psychologist, who accompanied me with empathy and wisdom, making this path more sustainable both academically and personally.

I would also like to thank Leonardo, the *Radici Cosmiche* team, and the association *Casa sulle Nuvole*. Gioia, it was a pleasure to know you and to build such an ambitious project together; even though you are no longer with us, your legacy will remain in our hearts for a long time.

Last but not least, I would like to thank my family for supporting me from afar and for always sharing their pride in what I was doing. Michele and Ernesto, thank you for being worthy opponents in Pokémon and Beyblade battles. If you study hard and keep working at it, maybe one day you’ll manage to beat me (muuaahahahh).

Table of Contents

Objective

This project was conceived to explore whether—and to what extent—root morphological variability within wheat can exert a measurable influence on key soil physical properties. In particular, we aimed to determine whether genotype-dependent differences in root traits, spanning both modern wheat cultivars and traditional landraces, might modulate soil-pore morphology, hydraulic connectivity, and overall physical functionality. Establishing credible evidence for such effects would provide a conceptual basis for breeding strategies in which roots contribute actively to soil health alongside crop productivity.

To address this overarching question, the work pursued three closely interlinked objectives. First, we aimed to explore the correlations between root morphology and soil physical characteristics, addressing a knowledge gap that has so far limited investigations to comparisons between species rather than between genotypes of the same species. Second, we evaluated whether any observed genotype effects were of sufficient magnitude, to produce agronomically relevant shifts in hydraulic properties—namely, field capacity, permanent wilting point, and unsaturated conductivity—while also situating these shifts within the broader context of environmental variability. Third, by recognising the methodological challenges inherent in root phenotyping, we refined and critically compared complementary phenotyping protocols, with the aim of supplying the research community with reproducible and comparable tools for quantifying root system architecture and interpreting its impact on soil properties.

Taken together, these objectives were intended to fulfil a dual goal: (i) to lay a scientific foundation for studying the potential effect of root morphology on soil physical properties, and (ii) to establish a methodological framework capable of reliably translating basic research findings into field applications. Although the project's ambition was undeniably high—some might say optimistic—the work nonetheless produced a set of robust correlations. While not yet definitive proof of causation, these associations offer a valuable springboard for future, independent studies that can verify and extend our findings.

Introduction

1. Root System Architecture in Wheat

Wheat (*Triticum aestivum* and *Triticum durum*) is among the most important cereal crops worldwide, providing nearly 20% of human dietary calories and proteins (Ober et al. 2021). The global demand for wheat is projected to significantly increase in the coming decades, driven by population growth. Also, wheat production faces multiple challenges, including soil erosion and climate change, which intensifies the frequency and severity of extreme weather events, and a slowdown in genetic yield gains, currently plateauing around 1% annually (Hall and Richards 2013; Hickey et al. 2019).

Given these constraints, research is shifting toward improving underground traits—the roots. Root system architecture (RSA), defined as the spatial distribution and branching patterns of roots within the soil, is crucial for plant resource acquisition, particularly water and nutrients (Lynch 1995; Gregory 2006; Atkinson et al. 2019). Optimizing root traits is considered essential for a "second green revolution," emphasizing improved resource-use efficiency rather than solely increasing above ground biomass (Den Herder et al. 2010; Atkinson et al. 2019).

In the last few years, increasing attention has been paid to the preservation of ecosystem services, particularly soil health (Abbott and Manning 2015; Teague and Kreuter 2020; Lehmann et al. 2020). Consequently, root trait optimization now goes beyond resource acquisition efficiency and includes traits that enhance soil structure and function (Rojas et al. 2016; L. Wang et al. 2022; Saeed et al. 2025). These include the preservation of soil aggregates, the enhancement of microbial biodiversity, and the preservation of optimal soil hydraulic properties for plant growth (Doran et al. 1996; Arias et al. 2005; Kibblewhite, Ritz et al. 2008; Rieke et al. 2022). The development of crop varieties with root systems that not only support higher yields but also contribute to long-term soil health is now a central breeding goal (Gaiero et al. 2013; Saleem et al. 2018; Hartman and Tringe 2019). This shift underscores the dual role of root systems as agents of productivity and soil ecosystem sustainability.

In a recent article (see Chapter 2 of this thesis), we described how wheat landraces can enhance soil porosity and bioporosity, thus improving soil structure and physical health. Similarly, Chapter 3 highlights how the same wheat landrace varieties positively affect plant-available water and soil hydraulic conductivity. For the first time, we observed that different genotypes within the same species influence soil physical health differently, suggesting novel pathways for breeding programs aimed at improving resource-use efficiency.

Furthermore, wheat landraces are recognized as valuable genetic reservoirs for biodiversity and adaptive traits (Lopes et al. 2015; Adhikari et al. 2022). Our findings confirm that these varieties could effectively serve as gene donors in breeding programs aimed at developing elite cultivars with improved soil interaction traits (de Carvalho et al. 2013; Cheng et al. 2023).

Selecting wheat genotypes with more efficient RSA is now a key breeding objective, aiming to enhance yield per unit of input, improve stability under stress conditions, and provide valuable ecosystem services such as soil carbon sequestration (Lynch 2007; Kell 2011; Ober et al. 2021). Despite promising developments, root-based breeding approaches still face considerable uncertainty. Variability in environmental conditions and the complexity of root–soil interactions pose substantial challenges to achieving consistent and scalable results in diverse field conditions.

A significant obstacle is the inherent complexity of root phenotyping. Observing and accurately measuring roots is difficult because of their hidden growth within the soil (Atkinson et al. 2019). Consequently, current methodologies often yield data with limited reproducibility and comparability across experiments due to measurement errors, environmental variability, and methodological differences (Gregory et al. 2009; Li et al. 2022). To address these issues, various advanced phenotyping techniques have emerged, such as shovelomics, rhizotrons, X-ray computed tomography, and indirect root phenotyping like computational root modeling (Topp et al. 2013; Shao et al. 2021; Duncan and Topp 2022).

RSA encompasses the arrangement of seminal (embryonic) roots, nodal (crown) roots, lateral branches, and root hairs in space and time (Watt et al. 2008; Ober et al. 2021). These architectural features directly influence how plants explore soil to access resources: shallow root systems with high density facilitate phosphorus uptake (Liao et al. 2001; Zhu et al. 2005; Wang et al. 2010), while deeper roots improve access to subsoil water (Li et al. 2022; Lynch and Wojciechowski 2015) and mobile nutrients like nitrogen (Trachsel et al. 2013). Traits such as thin root diameters, greater specific root length, and increased root length density are strongly linked to enhanced performance under drought conditions (Zhu et al. 2019).

Seminal roots, originating from the embryo, are particularly important during early plant growth and can significantly affect final yield. An increased number of seminal roots typically leads to greater total root surface area, enabling more effective resource capture early in the growth cycle (Pais et al. 2022). Breeding programs have demonstrated that genotypes with more seminal roots often achieve higher yields due to improved early vigor. Conversely, fewer seminal roots may delay initial water

uptake, preserving soil moisture for critical reproductive stages under drought conditions (Xie et al. 2017; Pais et al. 2022).

The root growth angle, defined as the inclination of roots relative to vertical, is a trait with high heritability that influences overall root distribution within the soil profile (Lynch 2013; Uga et al. 2013). Narrow, steep angles direct root growth toward deeper soil layers, beneficial for accessing moisture during drought. Conversely, wide, shallow angles are advantageous in environments where nutrients are abundant in the upper soil layers or under irrigated conditions. Genetic diversity in root angles exists among wheat genotypes; traditional landraces often exhibit narrower root angles compared to modern cultivars. This genetic variation provides breeders opportunities to select for desirable root distributions using root angle or associated genetic markers (van der Bom et al. 2024; Tan et al. 2023; B. Li et al. 2022).

The "steep, cheap, and deep" root ideotype (Fig. 1), introduced by Lynch 2013, describes traits designed to optimize resource acquisition under stress conditions. It emphasizes a steep root angle to enhance deep soil exploration ("steep"), anatomical traits like root cortical aerenchyma to reduce metabolic costs ("cheap"), and overall increased rooting depth to facilitate subsoil water and nitrate uptake ("deep"). This conceptual model serves as a strategic guide for breeding wheat varieties adapted to environments characterized by drought and nitrogen limitations.

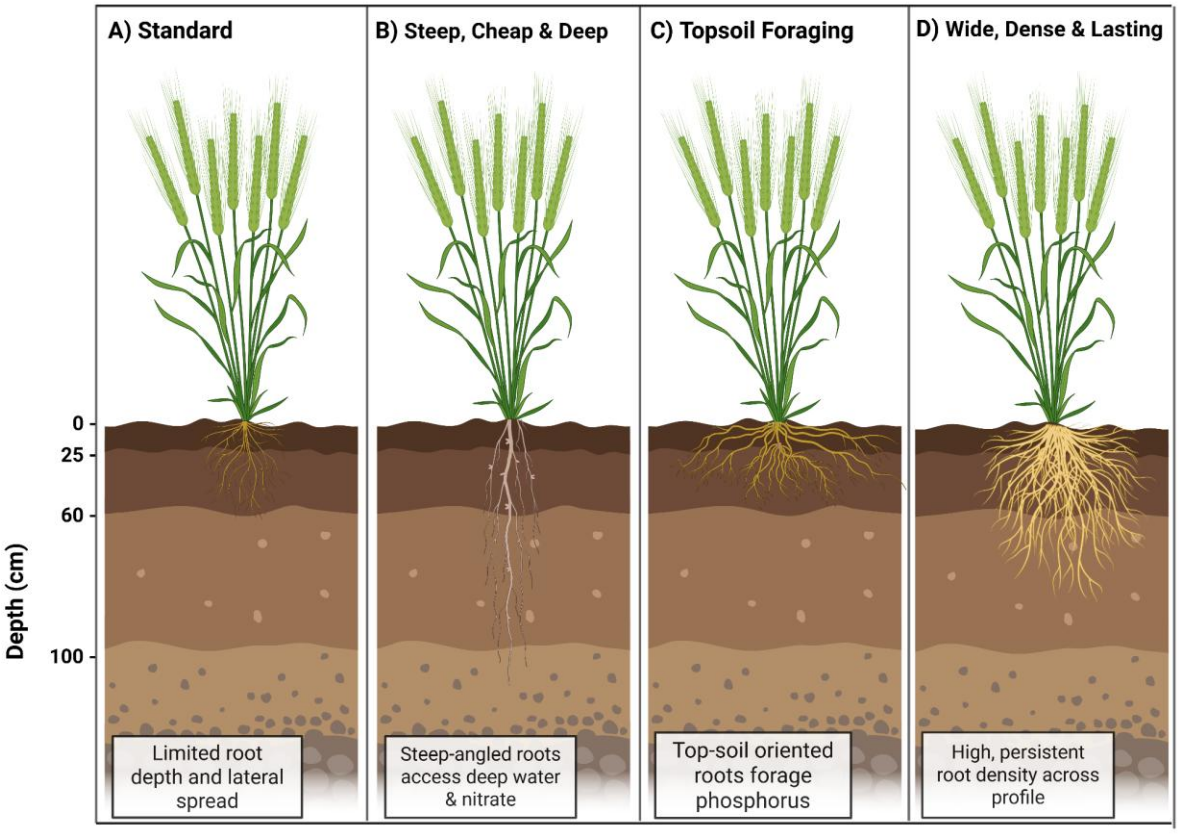

Figure 1. Root-system ideotypes in wheat across soil profile. (A) Modern cultivar with limited root depth and lateral spread (baseline). (B) Steep, Cheap & Deep ideotype: steep-angled axes explore deep water and nitrate. (C) Shallow / Top-soil foraging ideotype: surface-oriented laterals maximize phosphorus uptake. (D) Proposed Wide, Dense & Lasting ideotype: high, persistent root density throughout the profile. Soil horizons (0-25-60-100 cm) are drawn to scale. Icons generated with BioRender.com; panels B and C adapted from concepts in Lynch 2013, 2019.

In parallel with these productivity-driven strategies, growing attention is being given to root traits that contribute not only to resource capture but also to the long-term preservation of soil health. Several frameworks have been proposed to define root ideotypes that promote soil aggregation, maintain pore continuity, and support beneficial microbial habitats. Building on this perspective, during the course of this thesis, a complementary ideotype was conceived to specifically support soil physical structure—particularly aggregation stability and plant-available water.

I would like to summarize this concept in the ideotype "wide, dense, and lasting", which prioritizes a lateral root distribution ("wide") to enhance topsoil exploration and aggregate enmeshment (Erktan et al. 2016; Le Bissonnais et al. 2018), high root length density and fine root proliferation ("dense") to stabilize pore networks and promote microbial activity (Bodner et al. 2021; Jiang et al. 2023), persistent, carbon-rich root biomass ("lasting") to reinforce aggregate binding and support long-term rhizospheric carbon inputs (Hussain et al. 2021) and increases soil hydraulic properties (Dimattia et al. 2025).

My proposal does not want to replace existing models, this ideotype expands the root breeding paradigm to include traits that explicitly target the conservation of soil structure and functionality, aligning agronomic productivity with ecological resilience.

2. *Soil Health: Integrating Physical, Chemical, and Biological Dimensions for Sustainable Agro-ecosystems*

Soil health is broadly defined as the capacity of soil to function as a living system, sustaining plants, animals, and humans through its roles in food production, water regulation, nutrient cycling, and carbon storage (Doran and Zeiss 2000). Unlike fertility, which focuses primarily on nutrient availability for crops (Troeh and Thompson 2005), soil health encompasses physical, chemical, and biological dimensions (Fig. 2), each dynamically interacting with plant roots and agricultural management (Maikhuri and Rao 2012; Cardoso et al. 2013; Rattan Lal 2016). The recognition of soil as a living, functional interface rather than a passive substrate marks a paradigm shift in sustainable

agronomy, with significant implications for breeding strategies and land stewardship (Roopnarain et al. 2024).

This shift comes at a critical moment. Over the past decades, a growing body of evidence has highlighted a global decline in soil health, driven by land degradation, intensive tillage, monoculture systems, overuse of agrochemicals, and inadequate organic matter replenishment (Doran 2002; Kibblewhite et al. 2008; Montanarella et al. 2015). According to the FAO's *Status of the World's Soil Resources* report, approximately 33% of global soils are already moderately to highly degraded, with the rate of degradation exceeding the pace of regeneration in many regions. Physical degradation, including compaction and erosion, leads to reduced infiltration and water holding capacity. Chemical degradation manifests through salinization, acidification, and nutrient imbalances, while biological degradation includes a decline in microbial diversity and organic matter depletion. The loss of soil health is not only an environmental concern but it directly threatens food security, biodiversity, and climate regulation (Bagnall et al. 2021; Oliver and Gregory 2015).

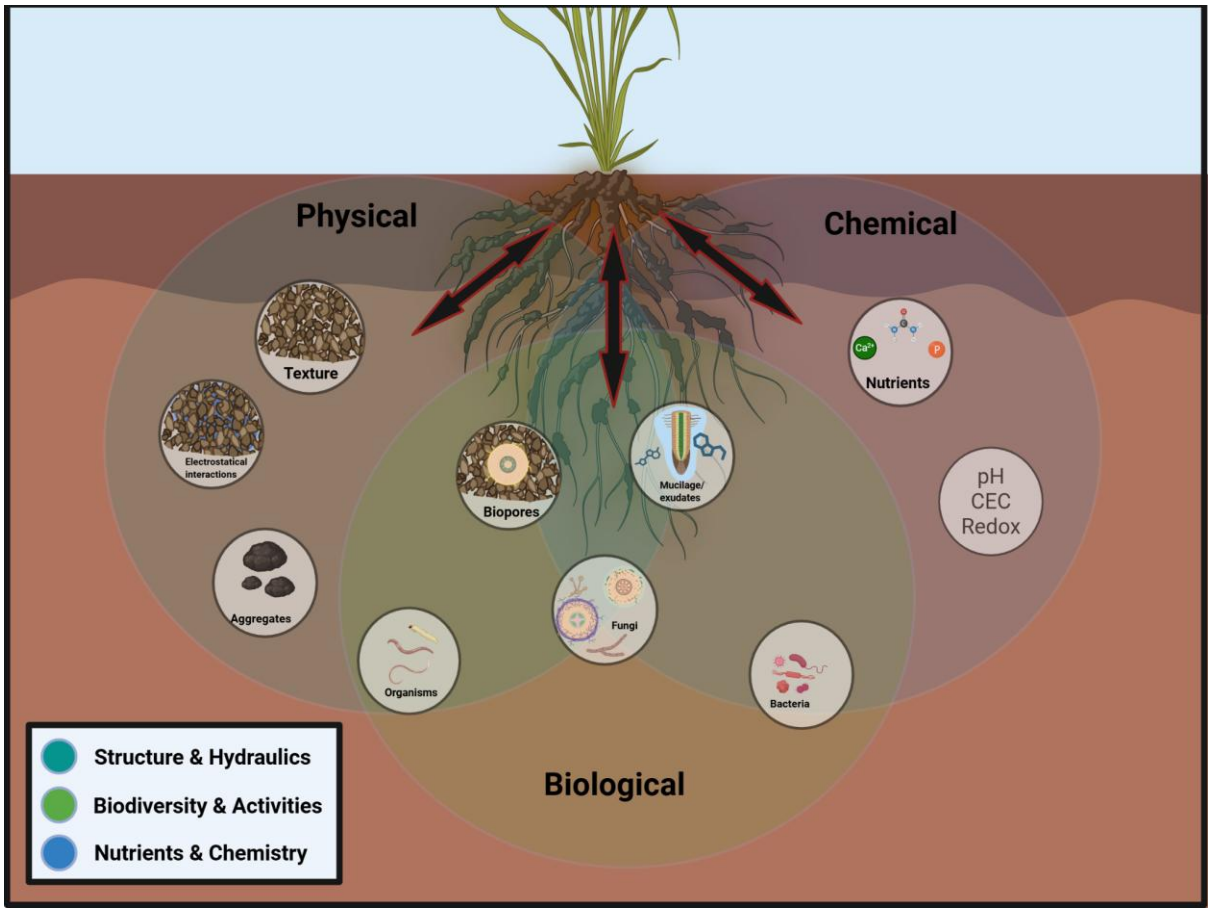

Figure 2. Conceptual framework of soil-health dimensions converging in the rhizosphere. Roots create the contact zone where physical (turquoise: structure & hydraulics), chemical (blue: nutrients & ion chemistry) and biological (green: biodiversity & activity) processes intersect. Carbon-rich

exudates (red arrows) bind particles, feed microbes and trigger ion exchange, linking the three spheres and enabling soil to function as a living, self-regulating system.

Agricultural practices play a central role in this trajectory (Tahat et al. 2020). Conventional agri-systems, characterized by deep ploughing, synthetic fertilizer dependency, and short rotations, can disrupt soil structure, accelerate carbon loss, and suppress beneficial microbial communities (Lal 2004; Kibblewhite et al. 2008). For instance, frequent tillage fragments aggregates and disrupts fungal hyphae, while bare fallows expose soil to erosion and desiccation. The repeated use of chemical herbicides and pesticides can further reduce microbial richness and lead to unintended shifts in soil food webs (Edwards and Pimentel 1989; Daisley 2022). Moreover, simplified cropping systems often fail to replenish organic carbon inputs and lead to the homogenization of root traits, reducing the functional diversity of rhizospheric interactions (Baldwin et al. 2022).

Contrariwise, a range of soil-regenerative practices has been shown to restore or enhance soil health across its three dimensions. Minimum or no-till systems help maintain aggregate stability, protect pore networks, and reduce erosion risk (Six et al. 2000b). Recent studies also highlight the potential of functional root traits as a bridge between management and soil health (de la Fuente et al. 2020; Hallett et al. 2022). Root systems that promote aggregation, maintain rhizospheric carbon flow, or support beneficial microbial consortia can amplify the positive effects of regenerative practices (Le Bissonnais et al. 2018).

Roots are, in fact, an integral component of the biological dimension of soil health, which encompasses the diversity, abundance, and activity of organisms within the soil matrix from bacteria and fungi to nematodes, earthworms, and microarthropods (Lehman et al. 2015). These organisms regulate decomposition, form symbiotic relationships with plant roots, enhance nutrient availability, and contribute to the stabilization of soil structure through physical and biochemical interactions. Within this framework, the rhizosphere—the narrow zone of intense biological activity surrounding roots—acts as a critical hotspot for nutrient cycling and microbial dynamics, and now also considered as an extended plant phenotype (de la Fuente et al. 2020). Root exudates, composed of sugars, amino acids, organic acids, and secondary metabolites, selectively shape the composition and function of rhizospheric microbiomes, in turn modulating plant access to both nutrients and water (Tarafdar 2022).

From a chemical standpoint, healthy soils maintain balanced pH levels, appropriate cation exchange capacity (CEC), and adequate reserves of macro- and micronutrients. These characteristics ensure the soil's ability to buffer external inputs, support microbial processes, and provide nutrients in plant-

available forms (Kibblewhite et al. 2008). However, nutrient availability is not static: it depends on interactions with organic matter, mineral weathering, redox dynamics, and microbial activity (Huang et al. 2005; Sanyal and Majumdar 2009; Kleber et al. 2021).

Soil physical health is the least visible yet most structurally defining component and constitutes the central focus of this thesis. It refers to the optimal state of soil structure and physical properties that underpin sustainable agricultural productivity, water management, and ecosystem functioning. It is characterized by several key indicators including soil texture, bulk density, soil porosity, aggregate stability, hydraulic conductivity, infiltration capacity, soil compaction, crust formation, and resistance to erosion (Indoria et al. 2017).

Soil texture—defined by the proportion of sand, silt, and clay—sets the physical foundation, influencing not only the water-holding capacity but also aeration and aggregation potential. However, texture alone does not determine soil functionality. Two soils of similar texture can differ widely in hydraulic behavior depending on their structural organization and biological activity (Jarvis et al. 2007). The arrangement and binding of individual sand, silt, and clay particles into aggregates is defined as soil structure (Bronick and Lal 2005; Ghezzehei 2012; Yudina and Kuzyakov 2023). Aggregates formed by organic residues, microbial by-products, root exudates, root bindings, and fungal hyphae, provide stability and resistance to external forces such as rainfall and mechanical disturbances (Six et al. 2004; Bronick and Lal 2005).

Aggregate stability, specifically, is crucial as stable aggregates maintain porosity and facilitate aeration and water infiltration (Six et al. 2004). Conversely, frequent tillage disrupts aggregate formation, reduces organic matter content, and accelerates structural degradation. Conservation agriculture (CA), integrating minimum or zero tillage, continuous residue retention, and diversified crop rotations, significantly enhances aggregate stability and soil structure over time (Six et al. 2000a). Organic residues and minimal soil disturbance under CA stimulate microbial activity and root proliferation, thereby promoting more resilient aggregate structures compared to conventional tillage (Govaerts et al. 2009).

Bulk density is another pivotal indicator, representing soil compaction levels and influencing root penetration, aeration, and water infiltration (Unger and Kaspar 1994). Excessive mechanical disturbances in conventional agriculture often lead to temporary reductions in bulk density, followed by increases due to compaction from rainfall and machinery (Osunbitan et al. 2005). Under CA, bulk density generally improves in the medium to long term due to continuous organic residue and root

activity and reduced mechanical pressure, though initially higher bulk densities can occur due to the absence of tillage-induced loosening (He et al. 2009).

Surface sealing and soil crusting significantly affect soil-water dynamics. These processes occur when raindrop impacts disperse soil particles, creating a compacted layer that reduces infiltration and aeration (Nciizah and Wakindiki 2015; Valentin and Bresson 2020). Conventional agri-systems exacerbate crust formation through repeated exposure of bare soils. By contrast, minimum tillage or non-tillage significantly reduces crusting through continuous soil cover provided by crop residues and plant root activity thereby protecting soil surfaces from raindrop impacts and enhancing infiltration and aeration (Cassel et al. 1995).

Porosity encompasses both macropores, essential for rapid water movement and aeration, and micropores, crucial for water retention (Luxmoore 1981). Root growth, activity and decay foster stable aggregates and biological activity, creating a more favorable pore network for both water infiltration and retention compared to conventional practices (Gliński and Lipiec 2018).

Soil porosity directly influences the soil hydraulic properties that are a key component of the soil health, as they regulate the storage, availability, and movement of water and nutrients within the soil (Assouline and Or 2013; Horton et al. 1994). Proper understanding and accurate estimation of these properties are fundamental for optimizing water management, improving agricultural productivity, and ensuring ecosystem sustainability. Two fundamental hydraulic properties are primarily assessed: the soil water retention curve (SWRC) and hydraulic conductivity (K) (Clapp and Hornberger 1978; Genuchten and Nielsen 1985; Bittelli et al. 2015).

The SWRC, describes the relationship between soil water content (θ) and matric potential (ψ). Matric potential indicates the energy state of water in the soil, reflecting how tightly water is retained by soil particles. Two critical points on the SWRC are the field capacity (FC) and the permanent wilting point (PWP). Field capacity represents the water content held in the soil after excess water has drained by gravity, typically corresponding to a matric potential of approximately -10 to -33 kPa. The permanent wilting point is defined as the moisture content at which plants can no longer extract sufficient water, usually corresponding to a matric potential around -1500 kPa. The water retained between these two points constitutes the plant-available water (PAW), crucial for plant growth and survival, particularly during dry periods (Bittelli et al. 2015).

Hydraulic conductivity (K), on the other hand, quantifies the soil's ability to transmit water under a hydraulic gradient, directly influencing infiltration rates, drainage, and water redistribution within the

soil profile. Saturated hydraulic conductivity (Ksat) is specifically measured under saturated conditions and is a key indicator of soil permeability and drainage capacity. Unsaturated hydraulic conductivity describes water movement when the soil is below saturation, relevant to water dynamics under typical field conditions (Mualem 2018).

Several empirical models have been developed to mathematically describe the SWRC. Among these, the most widely used is the unimodal van Genuchten equation:

$$\theta(\psi) = \theta_r + \frac{\theta_s - \theta_r}{[1 + (\alpha|\psi|)^n]^m}$$

where θs and θr represent the saturated and residual water content, respectively; α, n, and m (where m = 1 - 1/n) are shape parameters that must be fitted from experimental data. Other commonly employed models include Brooks-Corey, Campbell, and Kosugi, each suited to different soil types and research objectives (Bittelli et al. 2015).

However, soils often exhibit complex pore structures (Durner 1994) resulting from biological activity, such as root growth, microbial processes, and soil fauna movements. These biological activities create a heterogeneous distribution of pore sizes, often leading to a bimodal pore size distribution characterized by distinct macropore and micropore domains (Stolpovsky et al. 2012). Macropores, frequently created by root penetration and biological activity, allow rapid water movement and infiltration, whereas micropores retain water against gravity, supplying plants over extended periods (Colombi et al. 2017).

In Chapter 3 of this thesis, we adopted a bimodal van Genuchten model, better suited for soils influenced by root-induced structural modifications (Durner 1994). This model separately describes two distinct pore systems by employing two sets of parameters, accurately capturing the dual behavior of structured soils (see Chapter 3). The selection of this bimodal approach allows us to illustrate how root architecture influences soil porosity and consequently alters the hydraulic characteristics, providing a framework for analyzing root-soil interactions.

3. Root–Soil Interactions: From Live Architecture to Post-Senescence Legacies

Roots play a fundamental role in shaping the physical, chemical, and microbiological dimensions of soil health (Jin et al. 2017). As dynamic interfaces between plants and the soil environment, roots modulate key soil processes that determine nutrient availability, water dynamics, and microbial community structure (Hartman and Tringe 2019). Their impact is particularly relevant in the context

of sustainable agriculture, where improving soil function through root-based strategies is seen as a promising approach to enhance productivity while maintaining ecosystem resilience (Lynch et al. 2022).

From a physical standpoint, roots are major agents of soil structure formation. As they grow and penetrate the soil matrix, they exert mechanical pressure that can break compacted layers and create macropores, enhancing porosity and water infiltration (Jin et al. 2013). Root decay, in turn, leaves behind biopores that facilitate gas exchange and root proliferation for subsequent crops (Xiong et al. 2022; Wendel et al. 2022). Root exudates, including mucilage—a gel-like substance secreted by root tips—also contribute to the stabilization of soil aggregates by increasing cohesion between particles and maintaining moisture around the root zone (Carminati et al. 2010).

Aggregation is one of the most crucial physical processes influenced by roots. Stable aggregates improve water retention, reduce erosion, and create habitats for soil microorganisms (Amézketa 1999). Root hairs, root length density, and rooting depth have all been positively associated with increased aggregate stability (Graf and Frei 2013; Le Bissonnais et al. 2018; Xiao et al. 2020; Capri et al. 2023). However, not all traits have shown consistent results. For example, high root diameter has been linked in some studies to improved macroporosity, while others found no clear relationship, suggesting that the influence of certain architectural traits may depend on context-specific interactions with soil type and management (G. Bodner, Leitner, and Kaul 2014; Shi et al. 2021).

On the chemical front, roots influence nutrient dynamics both directly and indirectly. They excrete organic acids, enzymes, and chelating compounds that alter pH, mobilize nutrients, and affect mineral weathering (Dakora and Phillips 2002). By releasing labile carbon sources, roots also feed microbial populations that play critical roles in nutrient cycling, including nitrogen fixation and phosphorus solubilization. This rhizosphere priming effect creates a chemically distinct microenvironment that differs significantly from the bulk soil (Dotaniya and Meena 2015).

Microbiologically, roots act as powerful selectors and organizers of microbial communities (Philippot et al. 2013). The rhizosphere hosts a higher abundance and diversity of microorganisms compared to bulk soil, primarily driven by root exudation patterns and plant genotype (Berendsen et al. 2012; Mendes et al. 2013; Chaparro et al. 2013). Some root traits, such as a dense and finely branched architecture, increase root surface area and exudate release, fostering microbial hotspots. Others, such as the presence of aerenchyma, may influence oxygen availability and shape aerobic versus anaerobic microbial niches. Yet, despite growing interest in identifying root traits that enhance beneficial

microbial associations, results remain mixed, and trait-microbiome linkages are often context-dependent and species-specific (Freschet et al. 2021; Freschet et al. 202b).

Root physiological traits, especially exudation, strongly shapes rhizosphere hydraulics. Viscous polysaccharides (mucilage) secreted by root tips and hairs coat mineral surfaces, glue particles into micro-aggregates (Fig. 3), and line pore walls; this simultaneously enlarges water-holding capacity at low matric potentials and alters soil wettability as the profile dries (Carminati et al. 2016; Benard et al. 2019). Because the amount and chemistry of exudates vary with genotype, developmental stage, and abiotic stress, their hydraulic impact is likewise genotype- and environment-dependent.

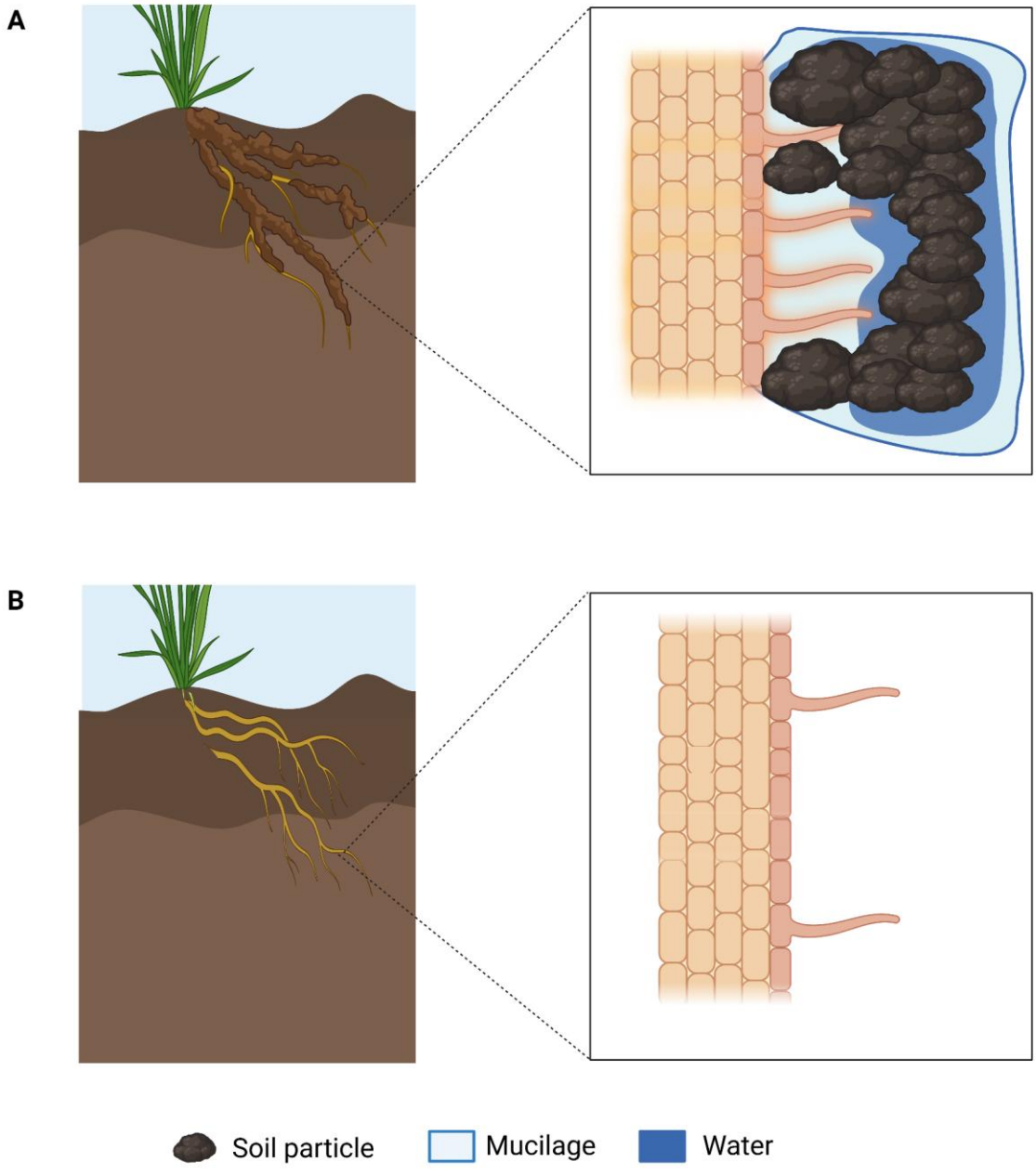

Figure 3. (A) Detail of a root with high root hair density, releasing abundant mucilage that promotes the formation of micro-aggregates around the root surface. Mucilage (light blue) coats mineral particles and pore walls, enhancing water retention (dark blue) under low matric potential and modifying soil wettability upon drying. In contrast, (B) shows roots with low hair density and minimal exudate release, resulting in limited soil aggregation and a less hydraulically functional root–soil interface. The hydraulic effects of exudation are highly dependent on genotype, developmental stage, soil and environmental conditions.

Other physiological traits act on longer timescales. Root longevity and the degree of lignification determine how long axial and lateral roots persist before decaying; their decomposition could generate transient biopores that improve vertical connectivity, while highly lignified walls delay pore collapse and prolong this conductive pathway (Zhou et al. 2020).

Despite growing recognition of mucilage as a key modulator of water retention and microbial activity, its in-situ dynamics remain difficult to quantify, limiting current models of root-soil hydraulic feedbacks (Naveed et al. 2019).

Overall, the effect of roots on soil health is a complex systems with coupled processes. For instance, roots affects soil microbes that in turn affects the chemical composition of the pore space affecting root growth and functioning. Root affects soil physical properties, for instance porosity, that in turn affects the availability of gases and water to microbes and so forth. Moreover, in the majority of cases, the phenomena are non linear, where for instance the effect of key physical parameters such soil temperature and water availability, are non-linearly related to microbial growth or chemical cycles such as the carbon or the nitrogen cycles. Dealing with such a complex, coupled and non-linear system is certainly a very challenging task.

Given this complexity and the methodological possibilities available in our laboratory, this thesis focuses specifically on RSA as a key lever for influencing soil physical properties. In fact, RSA plays a crucial role in determining how roots explore and interact with the soil environment, affecting processes such as resource acquisition and structural modification (Rogers and Benfey 2015; Koevoets et al. 2016; Lombardi et al. 2021; Maqbool et al. 2022; Zhiyong et al. 2022). While there is substantial evidence that certain RSA configurations can promote soil aggregation, enhance porosity, improve water retention, and foster microbial colonization, the specific contribution of individual root traits to these processes remains unclear. Further research is needed to disentangle the causal mechanisms and identify which traits most effectively drive improvements in soil structure and function (Bardgett et al. 2014).

In the following chapters, we investigate how genotypic variation in wheat root architecture modulates soil structure and hydraulic behavior, with a particular emphasis on the rhizosphere versus bulk soil distinction. While biochemical effects mediated by exudates and mucilage are acknowledged, the primary focus remains on the mechanical and structural effects of root growth and organization.

Beyond their role in soil aggregation and biopore formation, specific root architectural and morphological traits significantly modulate soil hydraulic properties, including water retention, saturated and unsaturated hydraulic conductivity, and pore network connectivity (Fig. 4). Root length density, diameter, branching intensity, and rooting depth are key traits determining the extent and configuration of pore networks, directly shaping water flow paths and soil porosity (Passioura 2002; Bardgett et al. 2014).

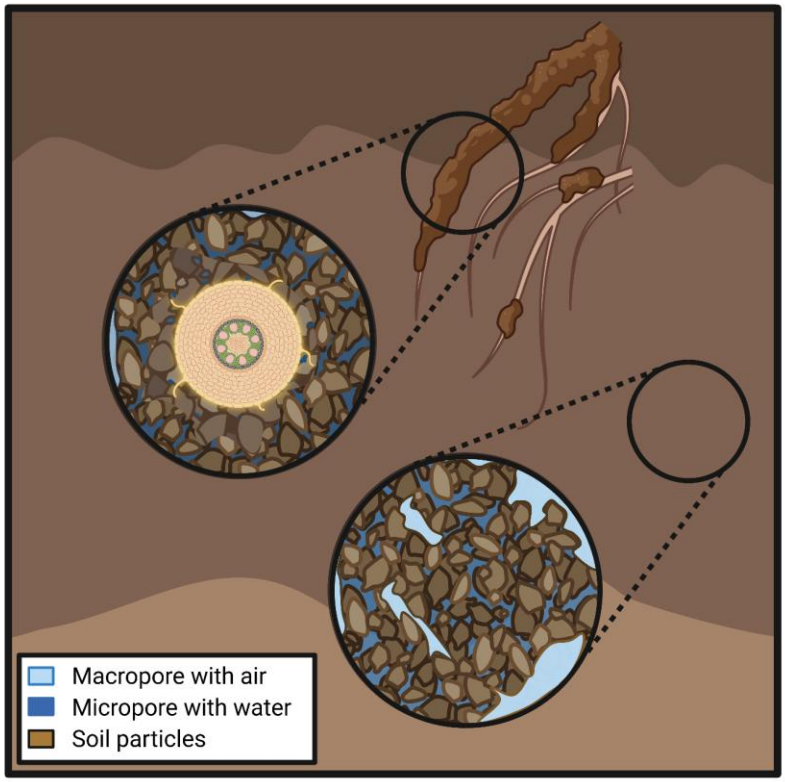

Figure 4. Roots are thicker than the surrounding soil pores and through their growth locally compact the matrix, redistributing soil particles into a denser arrangement. This mechanical pressure can promote new aggregate formation and alter the balance between macro- and micro-porosity, ultimately reshaping the soil's hydraulic and structural properties.

Long, dense and fine root systems with high number of root hairs occupy and stabilize smaller soil pores, enhancing soil water retention particularly at lower matric potentials (Zarebanadkouki et al. 2016; Lucas et al. 2019; Amtmann et al. 2022). Conversely, thicker roots, typically associated with taproot architectures or basal seminal root segments, actively promote the formation of larger macropores and soil fissures, facilitating preferential water flow and enhancing saturated hydraulic conductivity (Amtmann et al. 2022; Kohli et al. 2022). Furthermore, rooting depth and root branching significantly affect vertical and horizontal water redistribution (Fig. 5); deeply rooted plants stabilize deeper soil layers and provide access to subsoil moisture during drought, while shallow, densely branched systems enhance surface water uptake during lighter rainfall events (Uga et al. 2013; J. Lynch 2013).

On multi-season timescales the rhizosphere no longer behaves like the hydrated shell measured around living roots. As soon as drying begins, roots shrink and detach from the soil matrix, forming a micrometre-scale gap that cuts rhizosphere conductivity; re-wetting only partly reseals this gap, so the original hydraulic benefit is never fully restored (Carminati et al. 2010; Carminati and Vetterlein 2013; Ahmed et al. 2016). Meanwhile the mucilage that had increased water retention when fresh dehydrates, turns hydrophobic and slows infiltration, with the strength of this effect differing among genotypes that secrete larger or smaller amounts (Naveed et al. 2019). After complete senescence the remaining root skeleton leaves a genotype-specific pore architecture: thick, lignified axes persist as stable macropores that sustain preferential flow, whereas dense mats of fine roots decompose quickly and the small pores they create tend to collapse or become hydrophobic (Colombi et al. 2017; Lucas et al. 2019). Consequently, hydraulic measurements made around fresh, turgid roots capture only a transient state; the legacy inherited after root death can differ in both magnitude and direction, and must be considered when linking specific RSA traits to long-term soil function.

It is important to clarify that the effects of roots on soil physical properties strongly depend on soil type and climatic conditions. Thick roots may indeed compact the surrounding soil, but they might also exert enough force to break apart macroaggregates, paradoxically generating smaller pores during their growth. In contrast, fine and elongated roots can entangle and bind microaggregates into larger structures, thereby increasing soil macroporosity. From this perspective, investigating these mechanisms is crucial to determine when and where such knowledge can be applied. There is no universally superior ideotype; rather, root effects are context-dependent—emerging under specific environmental conditions and soil types—and, if deeply understood, could be harnessed to support local or regional adaptation while reducing external agricultural inputs. These processes, in my view, should be a central focus of breeding programs, especially in perennial crops and no-till systems,

where prolonged root presence and minimal soil disturbance may significantly influence long-term soil functionality.

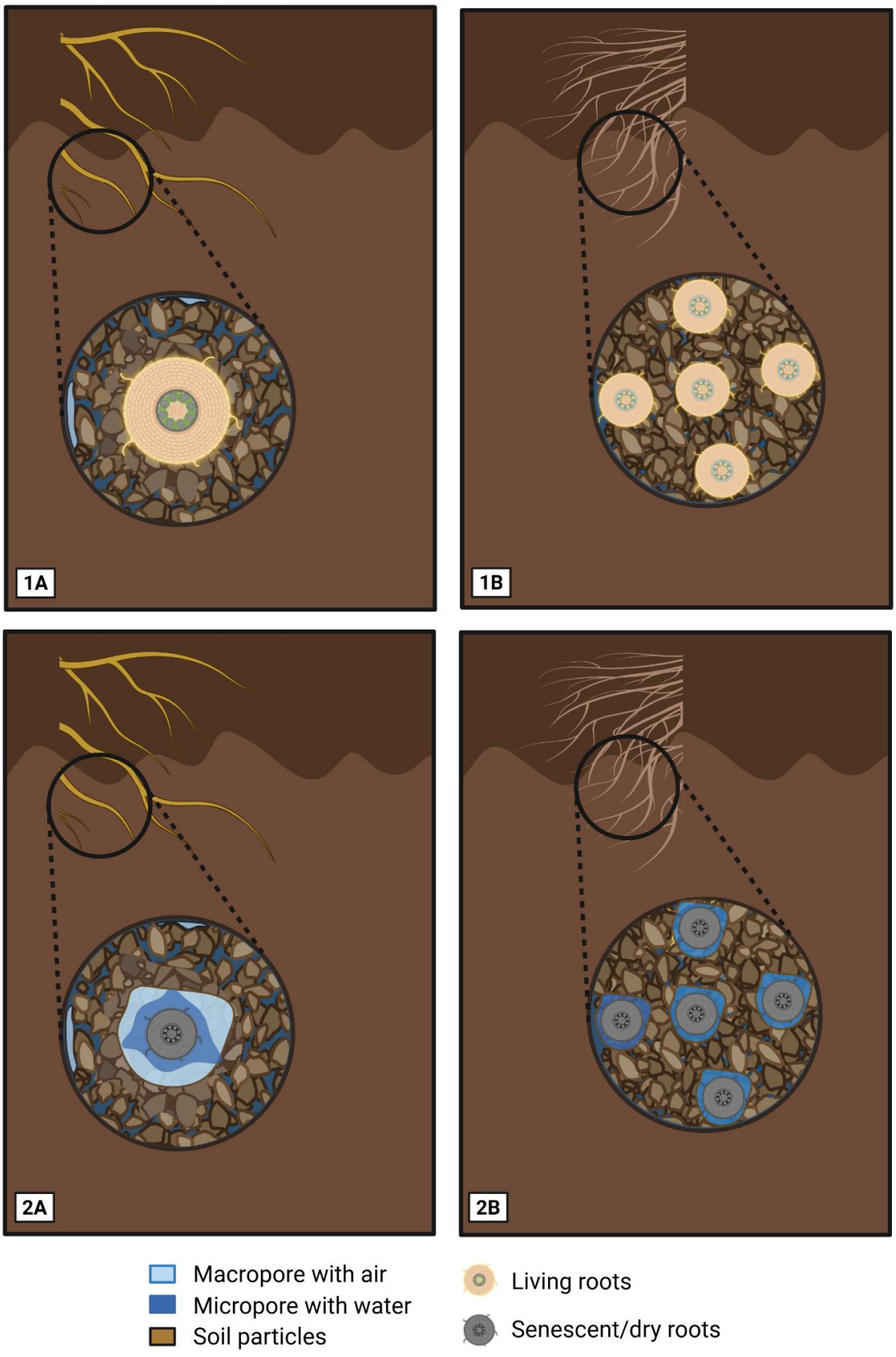

Figure 5. (1A) Living coarse roots compact the immediate rhizosheath but leave the surrounding bulk soil largely unaltered, thereby increasing adjacent microporosity. (1B) Living dense fine roots invade and occlude macropores, lowering overall macroporosity; their high root-length density raises bulk density and reduces hydraulic conductivity. (2A) Senescent coarse roots shrink, forming continuous axial channels that act as preferential flow paths: saturated hydraulic conductivity rises, water is stored at lower matric potentials (larger pores), and water held at high tensions declines. (2B) Senescent dense fine roots leave many small, disconnected biopores; conductivity remains low, but water retention at higher tensions increases. As a result, plant-available water responds in a texture- and climate-dependent manner: coarse roots tend to raise plant-available water in heavy soils under humid conditions, whereas dense fine roots tend to raise plant-available water in lighter soils and in arid environments.

References

Abbott, L. K., and D. A. C. Manning. n.d. “Soil Health and Related Ecosystem Services in Organic Agriculture.” https://ageconsearch.umn.edu/record/230386/.

Adhikari, Sneha, Jyoti Kumari, Sherry Rachel Jacob, Pramod Prasad, O. P. Gangwar, Charu Lata, Rajnikant Thakur, et al. 2022. “Landraces-Potential Treasure for Sustainable Wheat Improvement.” *Genetic Resources and Crop Evolution* 69 (2): 499–523.

Ahmed, Mutez Ali, Eva Kroener, Pascal Benard, Mohsen Zarebanadkouki, Anders Kaestner, and Andrea Carminati. 2016. “Drying of Mucilage Causes Water Repellency in the Rhizosphere of Maize: Measurements and Modelling.” *Plant and Soil* 407 (1-2): 161–71.

Amézketa, E. 1999. “Soil Aggregate Stability: A Review.” *Journal of Sustainable Agriculture* 14 (2-3): 83–151.

Amtmann, Anna, Malcolm J. Bennett, and Amelia Henry. 2022. “Root Phenotypes for the Future.” https://cgspace.cgiar.org/bitstreams/dc0d3387-101c-4bfb-8ee9-3350c7de5680/download.

Arias, M. E., J. A. González-Pérez, F. J. González-Vila, and A. S. Ball. 2005. “Soil Health: A New Challenge for Microbiologists and Chemists.” *International Microbiology* 8 (1): 13–21.

Assouline, Shmuel, and Dani Or. 2013. “Conceptual and Parametric Representation of Soil Hydraulic Properties: A Review.” *Vadose Zone Journal: VZJ* 12 (4): 1–20.

Atkinson, Jonathan A., Michael P. Pound, Malcolm J. Bennett, and Darren M. Wells. 2019. “Uncovering the Hidden Half of Plants Using New Advances in Root Phenotyping.” *Current Opinion in Biotechnology* 55 (February):1–8.

Bagnall, Dianna K., John F. Shanahan, Archie Flanders, Cristine L. S. Morgan, and C. Wayne Honeycutt. 2021. “Soil Health Considerations for Global Food Security.” *Agronomy Journal* 113 (6): 4581–89.

Baldwin-Kordick, Rebecca, Mriganka De, Miriam D. Lopez, Matt Liebman, Nick Lauter, John Marino, and Marshall D. McDaniel. 2022. “Comprehensive Impacts of Diversified Cropping on Soil Health and Sustainability.” *Agroecology and Sustainable Food Systems* 46 (3): 331–63.

Bardgett, Richard D., Liesje Mommer, and Franciska T. De Vries. 2014. “Going Underground: Root Traits as Drivers of Ecosystem Processes.” *Trends in Ecology & Evolution* 29 (12): 692–99.

Benard, Pascal, Mohsen Zarebanadkouki, and Andrea Carminati. 2019. “Physics and Hydraulics of

the Rhizosphere Network." *Journal of Plant Nutrition and Soil Science* 182 (1): 5–8.

Berendsen, Roeland L., Corné M. J. Pieterse, and Peter A. H. M. Bakker. 2012. "The Rhizosphere Microbiome and Plant Health." *Trends in Plant Science* 17 (8): 478–86.

Bittelli, M., G. S. Campbell, and F. Tomei. 2015. "Soil Physics with Python: Transport in the Soil-Plant-Atmosphere System." https://books.google.com/books?hl=it&lr=&id=kzXCCAAAQBAJ&oi=fnd&pg=PP1&dq=soil+physics+with+python&ots=iLzt0x4N-h&sig=nShe4aI7uEIAxI5D4MnsBp-DlIU.

Bodner, Gernot, Axel Mentler, and Katharina Keiblinger. 2021. "Plant Roots for Sustainable Soil Structure Management in Cropping Systems." *The Root Systems in Sustainable Agricultural Intensification*. Wiley. https://doi.org/10.1002/9781119525417.ch3.

Bodner, G., D. Leitner, and H-P Kaul. 2014. "Coarse and Fine Root Plants Affect Pore Size Distributions Differently." *Plant and Soil* 380 (1-2): 133–51.

Bom, Frederik J. T. van der, Alwyn Williams, Nelly S. Raymond, Samir Alahmad, Lee T. Hickey, Vijaya Singh, and Michael J. Bell. 2024. "Root Angle, Phosphorus, and Water: Interactions and Effects on Durum Wheat Genotype Performance in Drought-Prone Environments." *Plant and Soil* 500 (1-2): 69–89.

Bronick, C. J., and R. Lal. 2005. "Soil Structure and Management: A Review." *Geoderma* 124 (1-2): 3–22.

Capri, C., M. Gatti, A. Fiorini, Federico Ardenti, V. Tabaglio, and S. Poni. 2023. "A Comparative Study of Fifteen Cover Crop Species for Orchard Soil Management: Water Uptake, Root Density Traits and Soil Aggregate Stability." *Scientific Reports* 13 (January). https://doi.org/10.1038/s41598-023-27915-7.

Cardoso, Elke Jurandy Bran Nogueira, Rafael Leandro Figueiredo Vasconcellos, Daniel Bini, Marina Yumi Horta Miyauchi, Cristiane Alcantara dos Santos, Paulo Roger Lopes Alves, Alessandra Monteiro de Paula, André Shigueyoshi Nakatani, Jamil de Moraes Pereira, and Marco Antonio Nogueira. 2013. "Soil Health: Looking for Suitable Indicators. What Should Be Considered to Assess the Effects of Use and Management on Soil Health?" *Scientia Agricola* 70 (4): 274–89.

Carminati, Andrea, Ahmad B. Moradi, Doris Vetterlein, Peter Vontobel, Eberhard Lehmann, Ulrich Weller, Hans-Jörg Vogel, and Sascha E. Oswald. 2010. "Dynamics of Soil Water Content in the Rhizosphere." *Plant and Soil* 332 (1-2): 163–76.

Carminati, Andrea, and Doris Vetterlein. 2013. “Plasticity of Rhizosphere Hydraulic Properties as a Key for Efficient Utilization of Scarce Resources.” *Annals of Botany* 112 (2): 277–90.

Carminati, A., M. Zarebanadkouki, E. Kroener, M. A. Ahmed, and M. Holz. 2016. “Biophysical Rhizosphere Processes Affecting Root Water Uptake.” *Annals of Botany* 118 (4): 561–71.

Carvalho, Miguel A. A. Pinheiro de, Penelope J. Bebeli, Eliseu Bettencourt, Graça Costa, Sonia Dias, Teresa M. M. Dos Santos, and Jan J. Slaski. 2013. “Cereal Landraces Genetic Resources in Worldwide GeneBanks. A Review.” *Agronomy for Sustainable Development* 33 (1): 177–203.

Cassel, D. K., C. W. Raczkowski, and H. P. Denton. 1995. “Tillage Effects on Corn Production and Soil Physical Conditions.” *Soil Science Society of America Journal. Soil Science Society of America* 59 (5): 1436–43.

Chaparro, J., D. Badri, and J. Vivanco. 2013. “Rhizosphere Microbiome Assemblage Is Affected by Plant Development.” *The ISME Journal* 8 (November):790–803.

Cheng, Shifeng, Cong Feng, L. Wingen, Hong Cheng, Andrew B. Riche, Mei Jiang, M. Leverington-Waite, et al. 2023. “Harnessing Landrace Diversity Empowers Wheat Breeding.” *bioRxiv* 632 (October):823–31.

Clapp, R. B., and G. M. Hornberger. 1978. “Empirical Equations for Some Soil Hydraulic Properties.” *Water Resources Research*. https://doi.org/10.1029/WR014i004p00601.

Colombi, Tino, Serge Braun, Thomas Keller, and Achim Walter. 2017. “Artificial Macropores Attract Crop Roots and Enhance Plant Productivity on Compacted Soils.” *The Science of the Total Environment* 574 (January):1283–93.

Daisley, Brendan A. 2022. “Deteriorating Microbiomes in Agriculture-the Unintended Effects of Pesticides on Microbial Life.” *Microbiome Research Reports* 1 (1).

Dakora, Felix D., and Donald A. Phillips. 2002. “Root Exudates as Mediators of Mineral Acquisition in Low-Nutrient Environments.” In *Food Security in Nutrient-Stressed Environments: Exploiting Plants’ Genetic Capabilities*, 201–13. Dordrecht: Springer Netherlands.

Den Herder, Griet, Gert Van Isterdael, Tom Beeckman, and Ive De Smet. 2010. “The Roots of a New Green Revolution.” *Trends in Plant Science* 15 (11): 600–607.

Doran, John W. 2002. “Soil Health and Global Sustainability: Translating Science into Practice.”

Agriculture, Ecosystems & Environment 88 (2): 119–27.

Doran, John W., and Michael R. Zeiss. 2000. “Soil Health and Sustainability: Managing the Biotic Component of Soil Quality.” *Applied Soil Ecology: A Section of Agriculture, Ecosystems & Environment* 15 (1): 3–11.

Doran, J., M. Sarrantonio, and M. Liebig. 1996. “Soil Health and Sustainability.” *Advances in Agronomy* 56:1–54.

Dotaniya, M. L., and V. D. Meena. 2015. “Rhizosphere Effect on Nutrient Availability in Soil and Its Uptake by Plants: A Review.” *Proceedings of the National Academy of Sciences, India. Section B* 85 (1): 1–12.

Duncan, Keith E., and Christopher N. Topp. 2022. “Phenotyping Complex Plant Structures with a Large Format Industrial Scale High-Resolution X-Ray Tomography Instrument.” *Methods in Molecular Biology (Clifton, N.J.)* 2539:119–32.

Durner, W. 1994. “Hydraulic Conductivity Estimation for Soils with Heterogeneous Pore Structure.” *Water Resources Research*. https://doi.org/10.1029/93WR02676.

Edwards, Clive A., and David Pimentel. 1989. “Impact of Herbicides on Soil Ecosystems.” *Critical Reviews in Plant Sciences* 8 (3): 221–57.

Erktan, Amandine, Lauric Cécillon, Frank Graf, Catherine Roumet, Cédric Legout, and Freddy Rey. 2016. “Increase in Soil Aggregate Stability along a Mediterranean Successional Gradient in Severely Eroded Gully Bed Ecosystems: Combined Effects of Soil, Root Traits and Plant Community Characteristics.” *Plant and Soil* 398 (1-2): 121–37.

Freschet, Grégoire T., Loïc Pagès, Colleen M. Iversen, Louise H. Comas, Boris Rewald, Catherine Roumet, Jitka Klimešová, et al. 2021. “A Starting Guide to Root Ecology: Strengthening Ecological Concepts and Standardising Root Classification, Sampling, Processing and Trait Measurements.” *The New Phytologist* 232 (3): 973–1122.

Freschet, Grégoire T., Catherine Roumet, Louise H. Comas, Monique Weemstra, A. Glyn Bengough, Boris Rewald, Richard D. Bardgett, et al. 2021. “Root Traits as Drivers of Plant and Ecosystem Functioning: Current Understanding, Pitfalls and Future Research Needs.” *The New Phytologist* 232 (3): 1123–58.

Fuente Cantó, Carla de la, Marie Simonin, Eoghan King, Lionel Moulin, Malcolm J. Bennett, Gabriel Castrillo, and Laurent Laplaze. 2020. “An Extended Root Phenotype: The

Rhizosphere, Its Formation and Impacts on Plant Fitness." *The Plant Journal: For Cell and Molecular Biology* 103 (3): 951–64.

Gaiero, Jonathan R., Crystal A. McCall, Karen A. Thompson, Nicola J. Day, Anna S. Best, and Kari E. Dunfield. 2013. "Inside the Root Microbiome: Bacterial Root Endophytes and Plant Growth Promotion." *American Journal of Botany* 100 (9): 1738–50.

Genuchten, M., and D. R. Nielsen. 1985. "On Describing and Predicting the Hydraulic Properties of Unsaturated Soils." *Annales Geophysicae* 3:615–27.

Ghezzehei, T. A. 2012. "Soil Structure." *Handbook of Soil Science* 2:1–17.

Gliński, Jan, and Jerzy Lipiec. 2018. *Soil Physical Conditions and Plant Roots: 0*. CRC Revivals. Boca Raton, FL: CRC Press.

Govaerts∗, B., N. Verhulst∗, A. Castellanos-Navarrete, K. D. Sayre, J. Dixon, and L. Dendooven. 2009. "Conservation Agriculture and Soil Carbon Sequestration: Between Myth and Farmer Reality." *Critical Reviews in Plant Sciences* 28 (3): 97–122.

Graf, Frank, and Martin Frei. 2013. "Soil Aggregate Stability Related to Soil Density, Root Length, and Mycorrhiza Using Site-Specific Alnus Incana and Melanogaster Variegatus S.l." *Ecological Engineering* 57 (August):314–23.

Gregory, Peter J., A. Glyn Bengough, Dmitri Grinev, Sonja Schmidt, W. Bill T. B. Thomas, Tobias Wojciechowski, and Iain M. Young. 2009. "Root Phenomics of Crops: Opportunities and Challenges." *Functional Plant Biology: FPB* 36 (11): 922–29.

Gregory, P. J. 2006. "Roots, Rhizosphere and Soil: The Route to a Better Understanding of Soil Science?: Roots, Rhizosphere and Soil." *European Journal of Soil Science* 57 (1): 2–12.

Hall, Antonio J., and Richard A. Richards. 2013. "Prognosis for Genetic Improvement of Yield Potential and Water-Limited Yield of Major Grain Crops." *Field Crops Research* 143 (March):18–33.

Hallett, Paul D., Maria Marin, Gary D. Bending, Timothy S. George, Chris D. Collins, and Wilfred Otten. 2022. "Building Soil Sustainability from Root-Soil Interface Traits." *Trends in Plant Science* 27 (7): 688–98.

Hartman, Kyle, and Susannah G. Tringe. 2019. "Interactions between Plants and Soil Shaping the Root Microbiome under Abiotic Stress." *The Biochemical Journal* 476 (19): 2705–24.

He, Jin, Qingjie Wang, Hongwen Li, J. N. Tullberg, A. D. McHugh, Yuhua Bai, Xuemin Zhang, Neil McLaughlin, and Huanwen Gao. 2009. “Soil Physical Properties and Infiltration after Long-term No-tillage and Ploughing on the Chinese Loess Plateau.” *New Zealand Journal of Crop and Horticultural Science* 37 (3): 157–66.

Hickey, Lee T., Amber N Hafeez, Hannah Robinson, Scott A. Jackson, Soraya C. M. Leal-Bertioli, Mark Tester, Caixia Gao, Ian D. Godwin, Ben J. Hayes, and Brande B. H. Wulff. 2019. “Breeding Crops to Feed 10 Billion.” *Nature Biotechnology* 37 (7): 744–54.

Horton, R., M. D. Ankeny, and R. R. Allmaras. 1994. “Effects of Compaction on Soil Hydraulic Properties.” In *Developments in Agricultural Engineering*, edited by B. D. Soane and C. van Ouwerkerk, 11:141–65. Developments in Agricultural Engineering. Elsevier.

Huang, Pan-Ming, Ming-Kuang Wang, and Chih-Yu Chiu. 2005. “Soil Mineral–organic Matter–microbe Interactions: Impacts on Biogeochemical Processes and Biodiversity in Soils.” *Pedobiologia* 49 (6): 609–35.

Hussain, Sadam, Saddam Hussain, Ru Guo, Muhammad Sarwar, Xiaolong Ren, Djordje Krstic, Zubair Aslam, et al. 2021. “Carbon Sequestration to Avoid Soil Degradation: A Review on the Role of Conservation Tillage.” *Plants* 10 (10): 2001.

Indoria, A. K., K. L. Sharma, K. Sammi Reddy, and Srinivasa Rao. 2017. “Role of Soil Physical Properties in Soil Health Management and Crop Productivity in Rainfed Systems-I:Soil Physical Constraints and Scope.” *Current Science* 112 (12): 2405.

Jarvis, N., M. Larsbo, S. Roulier, A. Lindahl, and L. Persson. 2007. “The Role of Soil Properties in Regulating Non-equilibrium Macropore Flow and Solute Transport in Agricultural Topsoils.” *European Journal of Soil Science* 58 (1): 282–92.

Jiang, Xusheng, Xuemei Zhong, Guo Yu, Xuehong Zhang, and Jie Liu. 2023. “Different Effects of Taproot and Fibrous Root Crops on Pore Structure and Microbial Network in Reclaimed Soil.” *The Science of the Total Environment* 901 (165996): 165996.

Jin, Kemo, Jianbo Shen, Rhys W. Ashton, Ian C. Dodd, Martin A. J. Parry, and William R. Whalley. 2013. “How Do Roots Elongate in a Structured Soil?” *Journal of Experimental Botany* 64 (15): 4761–77.

Jin, Kemo, Philip J. White, William R. Whalley, Jianbo Shen, and Lei Shi. 2017. “Shaping an Optimal Soil by Root–soil Interaction.” *Trends in Plant Science* 22 (10): 823–29.

Kell, Douglas B. 2011. “Breeding Crop Plants with Deep Roots: Their Role in Sustainable Carbon, Nutrient and Water Sequestration.” *Annals of Botany* 108 (3): 407–18.

Kibblewhite, M. G., K. Ritz, and M. J. Swift. 2008. “Soil Health in Agricultural Systems.” *Philosophical Transactions of the Royal Society of London. Series B, Biological Sciences* 363 (1492): 685–701.

Kleber, Markus, Ian C. Bourg, Elizabeth K. Coward, Colleen M. Hansel, Satish C. B. Myneni, and Naoise Nunan. 2021. “Dynamic Interactions at the Mineral–organic Matter Interface.” *Nature Reviews. Earth & Environment* 2 (6): 402–21.

Koevoets, Iko T., Jan Henk Venema, J. Theo M. Elzenga, and Christa Testerink. 2016. “Roots Withstanding Their Environment: Exploiting Root System Architecture Responses to Abiotic Stress to Improve Crop Tolerance.” *Frontiers in Plant Science* 7 (August):1335.

Kohli, Pawandeep S., Kanika Maurya, Jitendra K. Thakur, Rahul Bhosale, and Jitender Giri. 2022. “Significance of Root Hairs in Developing Stress-Resilient Plants for Sustainable Crop Production.” *Plant, Cell & Environment* 45 (3): 677–94.

Lal, R. 2004. “Soil Carbon Sequestration Impacts on Global Climate Change and Food Security.” *Science (New York, N.Y.)* 304 (5677): 1623–27.

Lal, Rattan. 2016. “Soil Health and Carbon Management.” *Food and Energy Security* 5 (4): 212–22.

Le Bissonnais, Yves, Iván Prieto, Catherine Roumet, Jérôme Nespoulous, James Metayer, Sylvain Huon, Mario Villatoro, and Alexia Stokes. 2018. “Soil Aggregate Stability in Mediterranean and Tropical Agro-Ecosystems: Effect of Plant Roots and Soil Characteristics.” *Plant and Soil* 424 (1-2): 303–17.

Lehmann, Johannes, Deborah A. Bossio, Ingrid Kögel-Knabner, and Matthias C. Rillig. 2020. “The Concept and Future Prospects of Soil Health.” *Nature Reviews. Earth & Environment* 1 (10): 544–53.

Lehman, R., C. Cambardella, D. Stott, V. Acosta-Martínez, D. Manter, J. Buyer, J. Maul, et al. 2015. “Understanding and Enhancing Soil Biological Health: The Solution for Reversing Soil Degradation.” *Sustainability* 7 (January):988–1027.

Li, Anchang, Lingxiao Zhu, Wen-Li Xu, Liantao Liu, and Guifa Teng. 2022. “Recent Advances in Methods for in Situ Root Phenotyping.” *PeerJ* 10 (July). https://doi.org/10.7717/peerj.13638.

Liao, H., G. Rubio, X. Yan, A. Cao, K. M. Brown, and J. P. Lynch. 2001. “Effect of Phosphorus

Availability on Basal Root Shallowness in Common Bean." *Plant and Soil* 232 (1-2): 69–79.

Li, Baoru, Xiying Zhang, Shigenori Morita, Nobuhito Sekiya, Hideki Araki, Huijie Gu, Jie Han, Yang Lu, and Xiuwei Liu. 2022. "Are Crop Deep Roots Always Beneficial for Combating Drought: A Review of Root Structure and Function, Regulation and Phenotyping." *Agricultural Water Management* 271 (107781): 107781.

Lombardi, Marco, Laura De Gara, and Francesco Loreto. 2021. "Determinants of Root System Architecture for Future-Ready, Stress-Resilient Crops." *Physiologia Plantarum* 172 (4): 2090–97.

Lopes, Marta S., Ibrahim El-Basyoni, Peter S. Baenziger, Sukhwinder Singh, Conxita Royo, Kursad Ozbek, Husnu Aktas, et al. 2015. "Exploiting Genetic Diversity from Landraces in Wheat Breeding for Adaptation to Climate Change." *Journal of Experimental Botany* 66 (12): 3477–86.

Lucas, Maik, Steffen Schlüter, Hans-Jörg Vogel, and Doris Vetterlein. 2019. "Roots Compact the Surrounding Soil Depending on the Structures They Encounter." *Scientific Reports* 9 (1): 16236.

Luxmoore, R. 1981. "Micro-, Meso-, and Macroporosity of Soil." *Soil Science Society of America Journal* 45 (May):671–72.

Lynch, J. 1995. "Root Architecture and Plant Productivity." *Plant Physiology* 109 (1): 7–13.

———. 2007. "Roots of the Second Green Revolution." *Australian Journal of Botany* 55 (September):493–512.

———. 2013. "Steep, Cheap and Deep: An Ideotype to Optimize Water and N Acquisition by Maize Root Systems." *Annals of Botany* 112 (2): 347–57.

Lynch, Jonathan P., Sacha J. Mooney, Christopher F. Strock, and Hannah M. Schneider. 2022. "Future Roots for Future Soils." *Plant, Cell & Environment* 45 (3): 620–36.

Lynch, J., and T. Wojciechowski. 2015. "Opportunities and Challenges in the Subsoil: Pathways to Deeper Rooted Crops." *Journal of Experimental Botany* 66 (8): 2199–2210.

Maikhuri, R. K., and K. S. Rao. 2012. "Soil Quality and Soil Health: A Review." *Int. J. Ecol. Environ. Sci*. https://www.researchgate.net/profile/Arvind-Singh-21/post/soil_quality_data/attachment/5a966c6d4cde266d588e2942/AS%3A598930626715648%401519807597077/download/1491561070soil+important+articles.pdf.

Maqbool, Saman, Muhammad Adeel Hassan, Xianchun Xia, Larry M. York, Awais Rasheed, and Zhonghu He. 2022. “Root System Architecture in Cereals: Progress, Challenges and Perspective.” *The Plant Journal: For Cell and Molecular Biology* 110 (1): 23–42.

Mendes, Rodrigo, Paolina Garbeva, and Jos M. Raaijmakers. 2013. “The Rhizosphere Microbiome: Significance of Plant Beneficial, Plant Pathogenic, and Human Pathogenic Microorganisms.” *FEMS Microbiology Reviews* 37 (5): 634–63.

Montanarella, L., Daniel Jon Pennock, N. Mckenzie, M. Badraoui, V. Chude, I. Baptista, T. Mamo, et al. 2015. “World’s Soils Are under Threat.” *Soil* 2 (December):79–82.

Mualem, Yechezkel. 2018. “Hydraulic Conductivity of Unsaturated Soils: Prediction and Formulas.” In *SSSA Book Series*, 799–823. Madison, WI, USA: Soil Science Society of America, American Society of Agronomy.

Naveed, M., M. A. Ahmed, P. Benard, L. K. Brown, T. S. George, A. G. Bengough, T. Roose, N. Koebernick, and P. D. Hallett. 2019. “Surface Tension, Rheology and Hydrophobicity of Rhizodeposits and Seed Mucilage Influence Soil Water Retention and Hysteresis.” *Plant and Soil* 437 (1): 65–81.

Nciizah, Adornis D., and Isaiah I. C. Wakindiki. 2015. “Soil Sealing and Crusting Effects on Infiltration Rate: A Critical Review of Shortfalls in Prediction Models and Solutions.” *Archiv Fur Acker- Und Pflanzenbau Und Bodenkunde* 61 (9): 1211–30.

Ober, Eric S., Samir Alahmad, James Cockram, Cristian Forestan, Lee T. Hickey, Josefine Kant, Marco Maccaferri, et al. 2021. “Wheat Root Systems as a Breeding Target for Climate Resilience.” *Theoretical and Applied Genetics* 134 (6): 1645–62.

Oliver, M. A., and P. J. Gregory. 2015. “Soil, Food Security and Human Health: A Review: Soil, Food Security and Human Health.” *European Journal of Soil Science* 66 (2): 257–76.

Osunbitan, J. A., D. J. Oyedele, and K. O. Adekalu. 2005. “Tillage Effects on Bulk Density, Hydraulic Conductivity and Strength of a Loamy Sand Soil in Southwestern Nigeria.” *Soil & Tillage Research* 82 (1): 57–64.

Passioura, J. B. 2002. “‘Soil Conditions and Plant Growth.’” *Plant, Cell & Environment* 25 (2): 311–18.

Philippot, Laurent, Jos M. Raaijmakers, Philippe Lemanceau, and Wim H. van der Putten. 2013. “Going back to the Roots: The Microbial Ecology of the Rhizosphere.” *Nature Reviews.*

Microbiology 11 (11): 789–99.

P Pais, Isabel, Rita Moreira, José N. Semedo, Fernando H. Reboredo, Fernando C. Lidon, José Coutinho, Benvindo Maçãs, and Paula Scotti-Campos. 2022. “Phenotypic Diversity of Seminal Root Traits in Bread Wheat Germplasm from Different Origins.” *Plants* 11 (21): 2842.

Rieke, Elizabeth L., Dianna K. Bagnall, Cristine L. S. Morgan, Kade D. Flynn, Julie A. Howe, Kelsey L. H. Greub, G. Mac Bean, et al. 2022. “Evaluation of Aggregate Stability Methods for Soil Health.” *Geoderma* 428 (116156): 116156.

Rogers, Eric D., and Philip N. Benfey. 2015. “Regulation of Plant Root System Architecture: Implications for Crop Advancement.” *Current Opinion in Biotechnology* 32 (April):93–98.

Rojas, Ronald Vargas, Moujahed Achouri, Jerry Maroulis, and Lucrezia Caon. 2016. “Healthy Soils: A Prerequisite for Sustainable Food Security.” *Environmental Earth Sciences* 75 (3). https://doi.org/10.1007/s12665-015-5099-7.

Roopnarain, A., M. V. Kidson, B. Mndzebele, M. C. Hernandez-Soriano, and B. Ndaba. 2024. “Role of Targeted Breeding to Improve Wheat Production on the Marginal Lands of Africa.” In *The Marginal Soils of Africa*, 229–52. Cham: Springer Nature Switzerland.

Saeed, Qudsia, Adnan Mustafa, Shahzaib Ali, Lasisi Hammed Tobiloba, Ansa Rebi, Sadia Babar Baloch, Muhammad Zahid Mumtaz, Muhammad Naveed, Muhammad Farooq, and Xiankai Lu. 2025. “Advancing Crop Resilience through Nucleic Acid Innovations: Rhizosphere Engineering for Food Security and Climate Adaptation.” *International Journal of Biological Macromolecules* 310 (Pt 2): 143194.

Saleem, Muhammad, Audrey D. Law, Mohammad Radhi Sahib, Zahida H. Pervaiz, and Qingming Zhang. 2018. “Impact of Root System Architecture on Rhizosphere and Root Microbiome.” *Rhizosphere* 6 (June):47–51.

Sanyal, S. K., and K. Majumdar. 2009. “Nutrient Dynamics in Soil.” *Journal of the Indian Society of Soil Science* 57 (4): 477–93.

Shao, M. R., N. Jiang, M. Li, A. Howard, K. Lehner, J. L. Mullen, S. L. Gunn, J. K. McKay, and C. N. Topp. 2021. “Complementary Phenotyping of Maize Root System Architecture by Root Pulling Force and X-Ray Imaging.” *Plant Phenomics (Washington, D.C.)* 2021 (November):9859254.

Shi, Xiaoqing, Tianling Qin, Denghua Yan, Fuqiang Tian, and Hao Wang. 2021. “A Meta-Analysis

on Effects of Root Development on Soil Hydraulic Properties." *Geoderma* 403 (115363): 115363.

Six, J., H. Bossuyt, S. Degryze, and K. Denef. 2004. "A History of Research on the Link between (micro)aggregates, Soil Biota, and Soil Organic Matter Dynamics." *Soil & Tillage Research* 79 (1): 7–31.

Six, J., E. T. Elliott, and K. Paustian. 2000a. "Soil Macroaggregate Turnover and Microaggregate Formation: A Mechanism for C Sequestration under No-Tillage Agriculture." *Soil Biology & Biochemistry* 32 (14): 2099–2103.

———. 2000b. "Soil Structure and Soil Organic Matter II. A Normalized Stability Index and the Effect of Mineralogy." *Soil Science Society of America Journal. Soil Science Society of America* 64 (3): 1042–49.

Stolpovsky, K., M. Gharasoo, and M. Thullner. 2012. "The Impact of Pore-Size Heterogeneities on the Spatiotemporal Variation of Microbial Metabolic Activity in Porous Media." *Soil Science* 177 (February):98–110.

Tahat, Monther M., Kholoud M. Alananbeh, Yahia A. Othman, and Daniel I. Leskovar. 2020. "Soil Health and Sustainable Agriculture." *Sustainability*, June. https://doi.org/10.3390/su12124859.

Tan, Jianbiao, Weichen Yu, Yang Liu, Youzheng Guo, Nan Liu, Haiman Fu, Nan Di, J. Duan, Ximeng Li, and Benye Xi. 2023. "Response of Fine-Root Traits of Populus Tomentosa to Drought in Shallow and Deep Soil." *Forests*, May. https://doi.org/10.3390/f14050951.

Tarafdar, J. C. 2022. "Role of Soil Biology on Soil Health for Sustainable Agricultural Production." In *Structure and Functions of Pedosphere*, 67–81. Singapore: Springer Nature Singapore.

Teague, Richard, and Urs Kreuter. 2020. "Managing Grazing to Restore Soil Health, Ecosystem Function, and Ecosystem Services." *Frontiers in Sustainable Food Systems* 4 (September). https://doi.org/10.3389/fsufs.2020.534187.

Topp, Christopher N., Anjali S. Iyer-Pascuzzi, Jill T. Anderson, Cheng-Ruei Lee, Paul R. Zurek, Olga Symonova, Ying Zheng, et al. 2013. "3D Phenotyping and Quantitative Trait Locus Mapping Identify Core Regions of the Rice Genome Controlling Root Architecture." *Proceedings of the National Academy of Sciences of the United States of America* 110 (18): E1695–1704.

Trachsel, S., S. M. Kaeppler, K. M. Brown, and J. P. Lynch. 2013. "Maize Root Growth Angles

Become Steeper under Low N Conditions." *Field Crops Research* 140 (January):18–31.

Troeh, F. R., and L. M. Thompson. 2005. "Soils and Soil Fertility" 489. https://library.wur.nl/WebQuery/titel/1762424.

Uga, Yusaku, Kazuhiko Sugimoto, Satoshi Ogawa, Jagadish Rane, Manabu Ishitani, Naho Hara, Yuka Kitomi, et al. 2013. "Control of Root System Architecture by DEEPER ROOTING 1 Increases Rice Yield under Drought Conditions." *Nature Genetics* 45 (9): 1097–1102.

Unger, Paul W., and Thomas C. Kaspar. 1994. "Soil Compaction and Root Growth: A Review." *Agronomy Journal* 86 (5): 759–66.

Valentin, C., and L. M. Bresson. 2020. "Soil Crusting." In *Methods for Assessment of Soil Degradation*, 89–107. Boca Raton: CRC Press.

Wang, Liyang, Zed Rengel, Kai Zhang, Kemo Jin, Yang Lyu, Lin Zhang, Lingyun Cheng, Fusuo Zhang, and Jianbo Shen. 2022. "Ensuring Future Food Security and Resource Sustainability: Insights into the Rhizosphere." *iScience* 25 (4): 104168.

Wang, Xiurong, Jianbo Shen, and Hong Liao. 2010. "Acquisition or Utilization, Which Is More Critical for Enhancing Phosphorus Efficiency in Modern Crops?" *Plant Science: An International Journal of Experimental Plant Biology* 179 (4): 302–6.

Watt, Michelle, Linda J. Magee, and Margaret E. McCully. 2008. "Types, Structure and Potential for Axial Water Flow in the Deepest Roots of Field-Grown Cereals." *The New Phytologist* 178 (1): 135–46.

Wendel, Anna S., Sara L. Bauke, Wulf Amelung, and Claudia Knief. 2022. "Root-Rhizosphere-Soil Interactions in Biopores." *Plant and Soil* 475 (1-2): 253–77.

Xiao, Lie, Kehan Yao, Peng Li, Ying Liu, Enhao Chang, Yi Zhang, and Tiantian Zhu. 2020. "Increased Soil Aggregate Stability Is Strongly Correlated with Root and Soil Properties along a Gradient of Secondary Succession on the Loess Plateau." *Ecological Engineering* 143 (105671): 105671.

Xie, Q., K. Fernando, S. Mayes, and D. Sparkes. 2017. "Identifying Seedling Root Architectural Traits Associated with Yield and Yield Components in Wheat." *Annals of Botany* 119 (May):1115–29.

Xiong, Peng, Zhongbin Zhang, and Xinhua Peng. 2022. "Root and Root-derived Biopore Interactions in Soils: A Review." *Journal of Plant Nutrition and Soil Science* 185 (5): 643–55.

Yudina, Anna, and Yakov Kuzyakov. 2023. “Dual Nature of Soil Structure: The Unity of Aggregates and Pores.” *Geoderma* 434 (116478): 116478.

Zarebanadkouki, Mohsen, Félicien Meunier, Valentin Couvreur, Jimenez Cesar, Mathieu Javaux, and Andrea Carminati. 2016. “Estimation of the Hydraulic Conductivities of Lupine Roots by Inverse Modelling of High-Resolution Measurements of Root Water Uptake.” *Annals of Botany* 118 (4): 853–64.

Zhiyong, Zhang, Fan Baomin, Song Chao, Zhang Xiaoxian, Zhao Qingwen, and Ye Bing. 2022. “Advances in Root System Architecture: Functionality, Plasticity, and Research Methods.” *Journal of Resources and Ecology* 14 (1). https://doi.org/10.5814/j.issn.1674-764x.2023.01.002.

Zhou, Yangyan, Yue Zhang, Xuewen Wang, Xiao Han, Yi An, Shiwei Lin, Chao Shen, et al. 2020. “Root-Specific NF-Y Family Transcription Factor, PdNF-YB21, Positively Regulates Root Growth and Drought Resistance by Abscisic Acid-Mediated Indoylacetic Acid Transport in Populus.” *The New Phytologist* 227 (2): 407–26.

Zhu, Jinming, S. Kaeppler, and J. Lynch. 2005. “Topsoil Foraging and Phosphorus Acquisition Efficiency in Maize (Zea Mays).” *Functional Plant Biology: FPB* 32 (8): 749–62.

Zhu, Yong-He, Jacob Weiner, Ming-Xi Yu, and Feng-Min Li. 2019. “Evolutionary Agroecology: Trends in Root Architecture during Wheat Breeding.” *Evolutionary Applications* 12 (4): 733–43.

Chapter 1

Experimental Site and Baseline Characterisation

Field trials were established at the Cadriano experimental station, Bologna, Italy (44.5491 °N, 11.4130 °E). The site experiences a sub-humid temperate climate, with a long-term mean annual temperature of 12.8 °C and a mean annual precipitation of 924 mm. In autumn 2022, the field was staked out with centimetre-precision global positioning system (GPS) receivers. The resulting xyz coordinates were imported into AutoCAD (Ridder 2014) to create a two-dimensional geospatial map and to fix each plot at the exact same position for the duration of the multi-year study (Fig. 1).

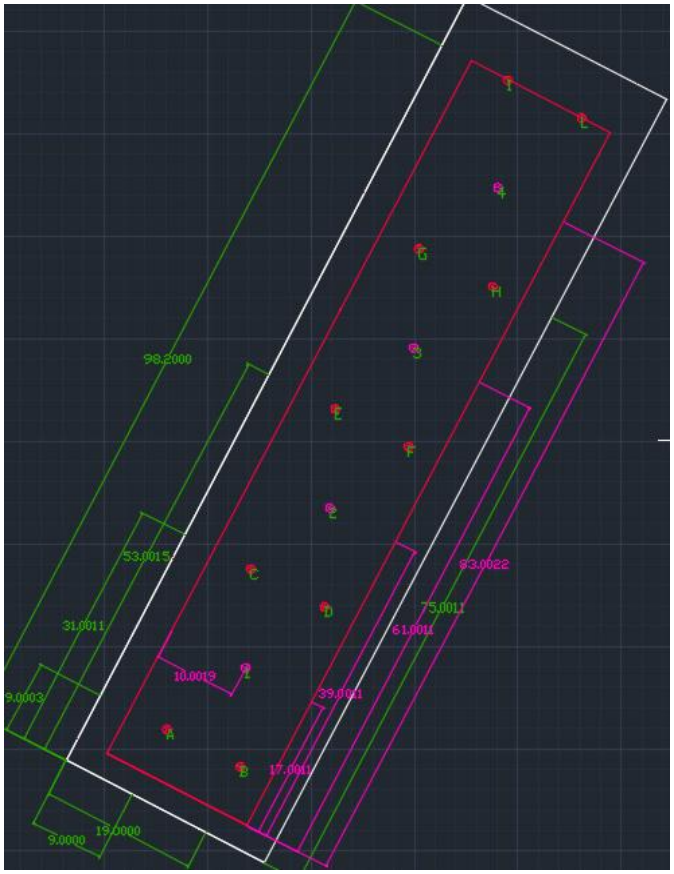

Figure 1. The red rectangle bounds the sown area. Green polylines form the geo-referenced grid. Red circles locate the primary baseline sites (triplicate cores at 0–30, 30–60 and 60–90 cm for texture, aggregates, chemistry and microbiome). Fuchsia polylines mark the secondary grid for soil-physics work, and the corresponding fuchsia circles show where undisturbed cylinders were taken for hydraulic tests and X-ray CT.

Baseline sampling points were geo-referenced on the CAD map. At each node, triplicate soil cores were collected at 0–30, 30–60, and 60–90 cm to profile chemical, physical, and microbiological gradients. Subsamples were split and processed as follows (Fig. 2):

- Chemical assays. Air-dried, < 2 mm fractions were analysed for total carbon, total nitrogen, ammonium-N, nitrate-N, and N15, together with routine macro- and micronutrient determinations (Jackson et al. 1997; Norman and Bremner 1965; Yeomans and Bremner 1991).
- Physical assays. Additional aliquots were subjected to laser diffraction for particle-size distribution, wet-sieving for macro-aggregate stability, and X-ray computed-tomography–based measurements of pore architecture; intact cores were also used for hydraulic conductivity and water-retention curves (Singh and Verdi 2024; Six et al. 2000; Black and Whittig 1965).
- Microbiological assays. Field-moist material was stored at −20 °C for potential nitrification rates and microbiome analysis (Fierer 2017).

This integrated protocol provides a comprehensive baseline against which treatment-induced changes can be quantified throughout the experiment.

Figure 2. Composite cores from each sampling node were air-dried, sieved to < 2 mm, and partitioned into separate aliquots for chemical, physical, and microbiological assays, establishing the reference dataset for subsequent field-scale evaluations.

To balance our ambition for broad genetic coverage with the practical limits of labour and funding, we drew on two complementary wheat collections whose contrasting functional traits were likely to modulate soil properties. From the Watkins panel (Wingen et al. 2014) of bread wheat (*Triticum aestivum*), we chose seven genetically distinct landraces and added the elite cultivar ‘Paragon’ to serve as a modern reference. From Durum Panel 1 we selected eight durum landraces, a single emmer

wheat (*T. dicoccum*) accession and, as an elite check, the widely grown cultivar Bologna (Mazzucotelli et al. 2020). Each entry received an internal alphanumeric code (Table 1) to streamline data handling.

Table 1. Genotypes included in the field experiment and their assigned numeric codes.

Genotype	Number
RUSSELLO_SG7	1
KYPEROUNDA_L28	2
TETRA-IPK251	3
SENATORE_CAPPELLI	4
HAURANI	5
MENCEKI_L36	6
DICOCCUM_MOLISE_COLLI	7
SVEVO	8
ALTAR_C84	9
MONASTIR	10
Wat 238	11
Wat 496	12
Wat 579	13
Wat 580	14
Wat 784	15
Wat 387	16
Wat 560	17
Paragon	18
Bologna	19
Wat 746	20

Using the statistical software R (Knezevic, Streibig, and Ritz 2007), we then generated a completely randomised block layout that would give robust replication without exceeding the capacity of our field team. Six blocks were established (A; B; C; D; E; F), and within every 6 m² plot the genotypes were allocated entirely at random (Fig. 3). This design maintains sufficient statistical power to detect genotype effects while remaining feasible within the available human and financial resources.

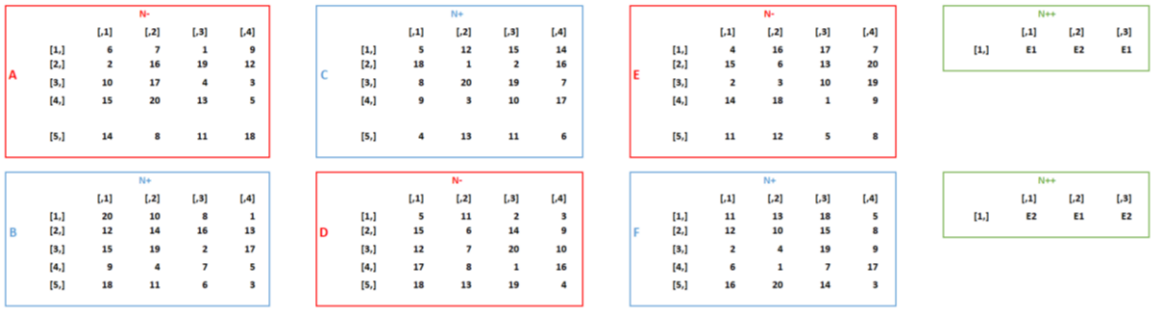

Figure 3. Each square represents a block with twenty polts; numbers correspond to the genotype codes in Table 1. Block colours denote nitrogen rate: red = N^- (48 kg N ha^{-1}), blue = N^+ (80 kg N ha^{-1}), and green = N^{++} (160 kg N ha^{-1}). The two green blocks are planted only with the regional check cultivars Bologna and Monastir, providing an agronomic benchmark.

Blocks B, C and F were assigned the low-nitrogen treatment (48 kg N ha^{-1}, N^-), whereas blocks A, D and E received the moderate rate (80 kg N ha^{-1}, N^+). Two supplementary micro-blocks were established outside the main RCBD and sown exclusively with the widely grown cultivars Bologna and Monastir; these controls were fertilised at the regional standard of 160 kg N ha^{-1} (N^{++}). The final seeding map was drafted in AutoCAD and geo-referenced in QGIS (Fig. 4), a workflow that not only guaranteed centimetre-level sowing accuracy but also enables future production of spatially explicit soil-property maps.

Figure 4. Final representation of the imported CAD layer into QGIS ensures centimetre-accurate sowing and provides a spatial framework for integrating future drone imagery and soil-property maps.

Sowing was carried out on **26 November 2022** with a precision plot drill. Immediately afterwards, the entire trial area was covered with a translucent polyethylene film and enclosed by a bird-proof net to promote uniform emergence and minimise vertebrate damage (Fig. 5).

Figure 5. (A) Precision plot drill used for sowing on 26 November 2022. (B) Experimental blocks after sowing, covered with a protective plastic film and surrounded by perimeter netting.

Once the plastic cover had been removed on 19 December 2022, the trial was inspected every week. Ground checks were complemented by unmanned-aerial-vehicle (UAV) flights that produced high-resolution orthophotos of the entire site. The imagery proved invaluable for pinpointing plots with poor emergence; these localised gaps were hand-reseeded within a fortnight to restore stand uniformity (Fig. 6).

Figure 6. Variations in canopy density are clearly visible; the pale, bare-soil patches were subsequently hand-reseeded to ensure a uniform plant stand across all plots.

Liquid ammonium sulphate enriched with N15 was applied by hand with a backpack sprayer at two key growth stages—tillering (13 February 2023) and stem elongation (17 April 2023) (Fig. 7). The low-, moderate- and high-nitrogen treatments received 24, 40 and 80 kg N ha^{-1} per application, giving seasonal totals of 48, 80 and 160 kg N ha^{-1}, respectively.

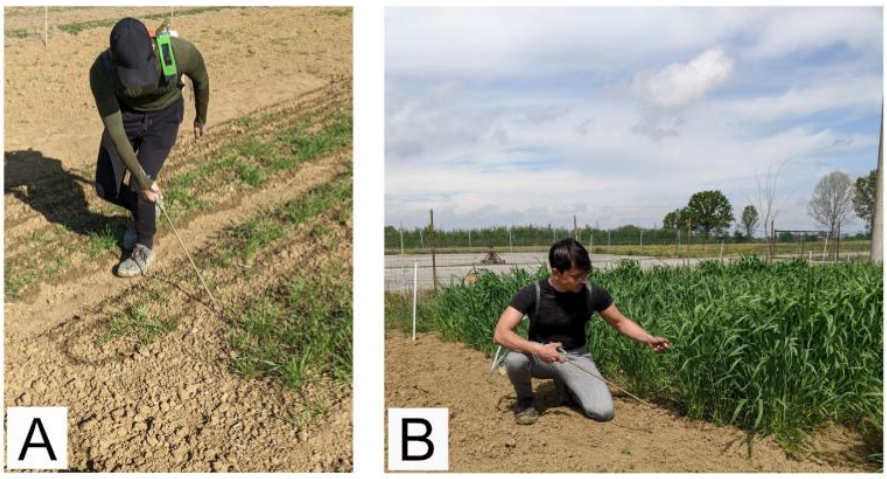

Figure 7. Liquid ammonium sulphate enriched with N15 application at tillering (A) and stem elongation (B).

Between three and five days after each fertiliser application, rhizosphere soil was sampled from every plot (Fig. 8). Three sub-samples per plot were taken and combined in a composed sample.

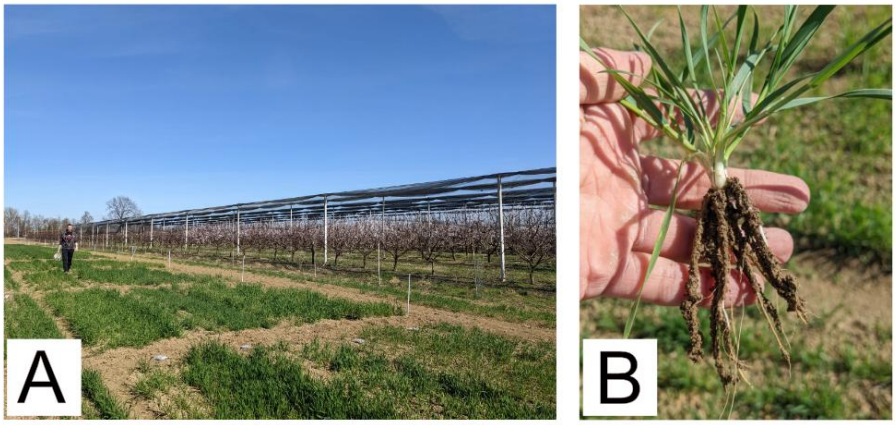

Figure 8. (A) Field technician collecting rhizosphere soil samples. (B) Roots with an adhering rhizosheet of soil. Rhizosphere samples were flash-frozen at −20 °C for subsequent laboratory determination of potential nitrification rates, whereas the soil adhering to the rhizosheath was shipped on dry ice to BiomeMaker (Madrid, Spain) for high-throughput profiling of the resident microbiome.

The soil retrieved from each plot was subsequently partitioned for three key indicators of soil function:

1. Potential nitrification rate, determined by incubating field-moist subsamples under aerobic conditions with ammonium amendment and measuring the accumulation of nitrate over 24 h.
2. Rhizosphere microbiome diversity, assessed by 16S rRNA/ITS amplicon sequencing from the rhizosheath fraction.
3. Aggregate stability, quantified by wet-sieving to obtain the mean weight diameter (MWD) of water-stable aggregates.

The field trial was inspected weekly to ensure agronomic integrity (Fig. 10) and to record key phenological variables—plant density (m^2), canopy height, and growth stage. These time-series measurements guided the scheduling of the final destructive operations: shovelomics at full anthesis and grain harvest at physiological maturity.

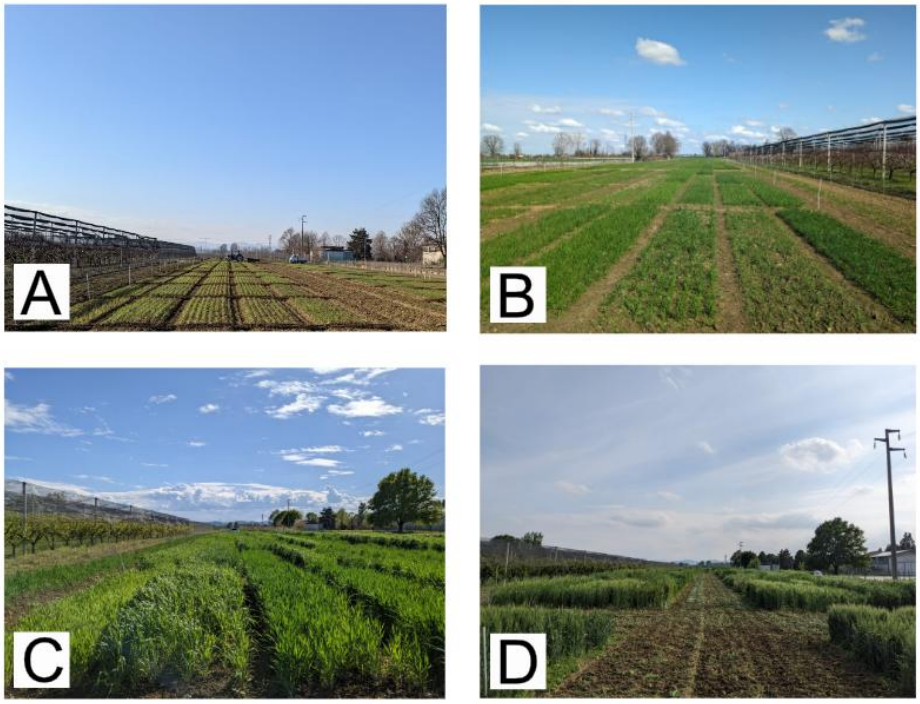

Figure 10. Different growth stages of wheat in the same area of the experimental field: emergence (A), tillering (B), stem elongation (C), and flowering (D).

Root phenotyping through shovelomics was carried out at anthesis, between May 15th and May 25th, 2023, depending on the phenological timing of each wheat genotype. From each plot, rhizospheric soil monoliths containing between six and ten plants were excavated. Among these, three representative plants per plot were selected for root phenotyping, following the methodology described in Chapter 4 of this thesis.

Grain harvest was performed manually using a sickle on July 15th, 2023. The entire experimental field was harvested within approximately seven days. From each plot, 5 grams of grains were finely ground and stored for subsequent analysis of N15 content in the caryopsis.

For the collection of samples destined for X-ray computed tomography and for the analysis of soil hydraulic properties—corresponding to the studies presented in Chapters 2 and 3, respectively—custom aluminum sampling rings had to be designed. To this end, a CAD model of standardized aluminum cylinders (Fig. 11) was created and provided to a local manufacturer, who fabricated the rings according to specifications.

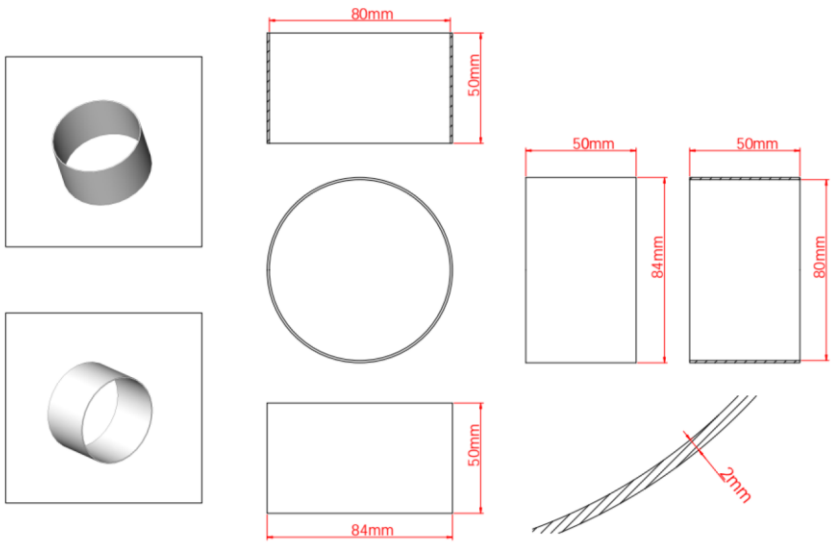

Figure 11. Design of the aluminium sampling ring used for undisturbed samples of rhizosphere soil.

To select the genotypes to be analyzed via X-ray tomography and hydraulic property measurements—given the higher cost and technical complexity of these methods—I used root architectural traits as a proxy for potential soil-structuring effects. Specifically, root images obtained from the shovelomics campaign were analyzed using RhizoVision Explorer (Seethepalli et al. 2021), and a principal component analysis (PCA) was performed to identify the main axes of variation (Fig. 12).

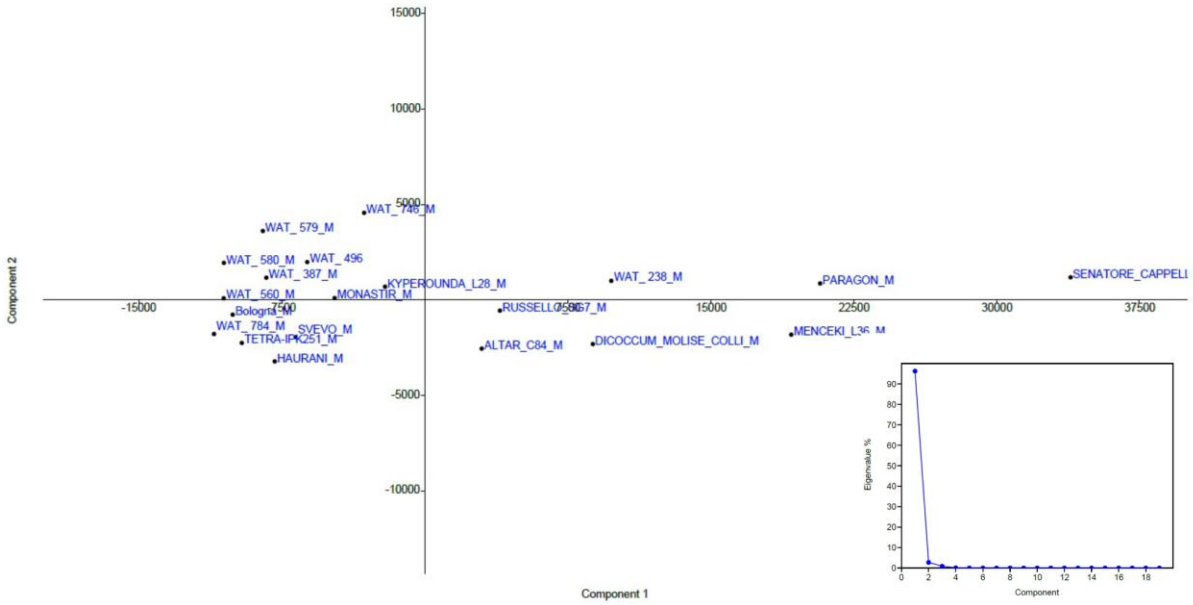

Figure 12. Principal component analysis (PCA) of root traits obtained from shovelomics for 20 wheat

genotypes. The inset in the bottom right corner shows the proportion of variance explained by each principal component.

The first principal component (PC1) accounted for approximately 92% of the total variance and was strongly associated with root length and diameter traits. Genotypic effects explained the vast majority of the phenotypic variation, suggesting strong genetic control over root architectural diversity. Based on this analysis, we selected genotypes that maximized the diversity in root traits, while also considering phylogenetic distance and agronomic relevance. For the X-ray tomography study, we selected Watkins (a *T. aestivum* landrace), Paragon (a modern elite *T. aestivum* cultivar), and Senatore Cappelli (a *T. durum* landrace). For the hydraulic properties study, the Bologna variety was additionally included, as it exhibited a markedly reduced root system compared to the others, making it an interesting contrasting genotype.

On November 7th, 2023, the field was prepared through minimum tillage (not exceeding 15 cm depth), and the second sowing was carried out on November 27th, 2023. The trial was repeated in a mirrored layout relative to the first year and concluded with the second harvest on July 7th, 2024.

References

Black, C. A., and L. D. Whittig. 1965. “X-Ray Diffraction Techniques for Mineral Identification and Mineralogical Composition.” In *Methods of Soil Analysis. Part 1. Physical and Mineralogical Properties, Including Statistics of Measurement and Sampling*. American Society of Agronomy, Soil Science Society of America.

Fierer, Noah. 2017. “Embracing the Unknown: Disentangling the Complexities of the Soil Microbiome.” *Nature Reviews. Microbiology* 15 (10): 579–90.

Jackson, G. D., G. D. Kushnak, G. R. Carlson, and D. M. Wichman. 1997. “Correlation of the Olsen Phosphorus Soil Test: Spring Wheat Response.” *Communications in Soil Science and Plant Analysis* 28 (9-10): 813–22.

Knezevic, Stevan Z., Jens C. Streibig, and Christian Ritz. 2007. “Utilizing R Software Package for Dose-Response Studies: The Concept and Data Analysis.” *Weed Technology: A Journal of the Weed Science Society of America* 21 (3): 840–48.

Mazzucotelli, Elisabetta, Giuseppe Sciara, Anna M. Mastrangelo, Francesca Desiderio, Steven S. Xu, Justin Faris, Matthew J. Hayden, et al. 2020. “The Global Durum Wheat Panel (GDP): An International Platform to Identify and Exchange Beneficial Alleles.” *Frontiers in Plant Science* 11 (December):569905.

Norman, A. G., and J. M. Bremner. 1965. “Isotope-Ratio Analysis of Nitrogen in Nitrogen-15 Tracer Investigations.” In *Methods of Soil Analysis. Part 2. Chemical and Microbiological Properties*. American Society of Agronomy, Soil Science Society of America.

Ridder, Detlef. 2014. *AutoCAD 2015*. PDF. 2014th ed. bhv Einsteigerseminar. Frechen, Germany: MITP.

Seethepalli, Anand, Kundan Dhakal, Marcus Griffiths, Haichao Guo, Gregoire T. Freschet, and Larry M. York. 2021. “RhizoVision Explorer: Open-Source Software for Root Image Analysis and Measurement Standardization.” *bioRxiv*. bioRxiv. https://doi.org/10.1101/2021.04.11.439359.

Singh, Amninder, and Amir Verdi. 2024. “Estimating the Soil Water Retention Curve by the HYPROP-WP4C System, HYPROP-Based PCNN-PTF and Inverse Modeling Using HYDRUS-1D.” *Journal of Hydrology* 639 (131657): 131657.

Six, J., K. Paustian, E. T. Elliott, and C. Combrink. 2000. “Soil Structure and Organic Matter I.

Distribution of Aggregate-size Classes and Aggregate-associated Carbon." *Soil Science Society of America Journal. Soil Science Society of America* 64 (2): 681–89.

Wingen, Luzie U., Simon Orford, Richard Goram, Michelle Leverington-Waite, Lorelei Bilham, Theofania S. Patsiou, Mike Ambrose, Jo Dicks, and Simon Griffiths. 2014. "Establishing the A. E. Watkins Landrace Cultivar Collection as a Resource for Systematic Gene Discovery in Bread Wheat." *Theoretical and Applied Genetics* 127 (8): 1831–42.

Yeomans, J. C., and J. M. Bremner. 1991. "Carbon and Nitrogen Analysis of Soils by Automated Combustion Techniques." *Communications in Soil Science and Plant Analysis* 22 (9-10): 843–50.

Chapter 2

Root traits of different wheat cultivars influence soil structure: an X-ray computed tomography and root morphology study

Bartolo Giuseppe Dimattia[1], Angela Righi[1,2], Matteo Bettuzzi[3], John Koestel[4], Maria Pia Morigi[3], Rosa Brancaccio[3,6], Silvio Salvi[1], Maria C. Hernandez-Soriano[5], and Marco Bittelli[1]*

[1]Department of Agricultural and Food Sciences, University of Bologna, Viale Fanin, 44, 40125, Bologna, Italy

[2]Department of Agronomy, Food, Natural resources, Animals and Environment – DAFNAE, University of Padova, Viale Dell'Università 16, 35020 Legnaro (PD), Italy3Department of Physics and Astronomy, "Augusto Righi", University of Bologna, Viale Berti Pichat 6/2, 40127, Bologna, Italy

[4]Soil Quality and Soil Use, Agroscope, Reckenholzstrasse 191, Zürich, CH-8046, Switzerland

[5]John Innes Centre, Norwich Research Park, Norwich, NR4 7UH, United Kingdom

[6] Department of Physics and Earth Science, University of Ferrara, via Saragat 1, 44121 Ferrara

*Corresponding author: marco.bittelli@unibo.it

Published in Geoderma. DOI: https://doi.org/10.1016/j.geoderma.2025.117349

Abstract

Plant roots play a fundamental role in maintaining soil health. Although a broad range of root traits have been reported, few studies have attempted to link root morphology with soil structure. Here, we used shovelomics to characterize the root morphology of a wheat cultivar (Paragon), and two landraces (Senatore-Cappelli, and Watkins238), and advanced soil pore and root network X-ray computed tomography to assess their impact on soil morphology at cylinder and aggregate scales. Bare soil was analyzed as a control. Minkowski functionals and percolation theory parameters were computed to characterize soil pore network morphology. Bioporosity at the cylinder scale was significantly different for all cultivars compared to the bare soil. Bare soil presented the largest structural pore volume and the smallest biopore volume, this suggesting rapid degradation of biopores. At the cylinder scale, biopore characteristics were significantly different between Senatore-Cappelli and Watkins238, with Senatore-Cappelli exhibiting more pores with diameters >1 mm. The parameters from percolation theory revealed notable differences between the rhizospheric and bare soil samples. We found significant differences between genotypes, finding statistically significant correlations among root morphology parameters and pore network geometry.

Total imaged porosity and total root volume were limited descriptors of the effect of roots on soil structure, which is better quantified by pore network connectivity measurements. Our findings confirm previous studies on the relationship between root traits and soil properties and highlight the potential of our experimental approach to explore how different genotypes may influence soil morphology, paving the way for future applications in plant phenotyping.

1. Introduction

Soil structure, defined as the spatial arrangement of soil particles and pores, is a fundamental parameter for soil quality (Dexter, 1988, Young, 2001). Soil pores provide a habitat for microorganisms and play a major role in infiltration, root growth and carbon turnover (Kravchenko et al., 2017). Soil structure is also directly linked to soil hydraulic properties (e.g. water retention and hydraulic conductivity) that determine the availability of water for plants and soil microbial communities and key processes such as gas exchange, thermal properties, soil organic matter transformations, nutrient dynamics and root penetration (Horn et al., 1994, Bittelli et al., 2015).

A vast number of soil processes depend indeed on its complex structure, but its characterization and quantification remain challenging due to: (a) the various hierarchies of scales ranging from very small pores, to aggregates and large cavities and (b) the multitude of complex shapes and geometries that are difficult to interpret (Yudina and Kuzyakov, 2023).The interactions between plants roots and soil add additional levels of complexity. Plant roots can significantly affect soil physical structure through the formation and activity of biopores, modification of the density and distribution of soil pores, and by affecting the soil's capacity to retain water and air. Previous research has indicated that different root phenotypes can significantly impact soil structure by forming pore spaces, influencing water infiltration, and facilitating aggregate formation (De La Fuente Cantò at al., 2020). Considering that crop production claims nearly one third of the world land (Ritchie et Roser, 2019), it is crucial to introduce root traits in crop systems that can improve soil structure parameters such as porosity and aggregation (Lal, 2015). Reducing the detrimental impact of crop production on agricultural land remains a key goal of policies such as the European Green Deal (Montanarella and Panagos, 2021). Therefore, immediate measures to reverse current trends in soil degradation and restore and support soil productivity require strategies that preserve soil structure (Lal, 2009). Wheat landraces are a valuable source of genetic diversity (Cheng et al., 2024) for the introduction of root traits in modern cultivars that can be beneficial for soil structure (Marone et al., 2021). Accordingly, crops that improve soil physical properties have become a major breeding target (Lynch, 2022). Particularly, identifying root traits in wheat cultivars that can enhance soil productivity and breeding them into commercial elite cultivars is a key goal for improving crop yields (Ober et al., 2021). Wheat is a target crop since it plays a key role in global food security due to its nutritional and economic value (Shiferaw et al., 2013). Therefore, identifying root traits in wheat that enhance soil structure can advance our capability to support sustainable and profitable wheat production. Current collections of wheat cultivars such as the A.E. Watkins238 landrace collection (Wingen et al., 2014, Cheng et al., 2024) and the Global Durum Wheat Panel (Mazzucotelli et al., 2020) are untapped sources of diversity to identify root traits that have been lost through breeding and modern agricultural practices

and breed them into modern cultivars. Root traits such as root depth, root length, xylem diameter and root hairs can improve water use efficiency by enhancing soil structure (Wasson et al., 2012). Root traits associated to the relationship between soil structure and soil biota play a key role in reshaping and modifying plant performance and crucial soil biological processes such as nutrient cycling (Brussaard, 2012; Rabot et al., 2018). Importantly, it is well established that root systems, particularly fine roots, induce specific structural changes by increasing pore space heterogenization and promoting aggregate coalescence (Carminati et al., 2010, Mooney et al., 2012, Bodner et al., 2014) Overall, the root morphology and processes associated with the rhizosphere significantly contribute to structural dynamics and function through bioturbation (Meysman et al., 2006; Lucas et al., 2019a).

According to Pagliai and Vignozzi (2002), the most relevant approach to assessing soil structural properties is the characterization of the pore system. For this reason, and for the ability to measure further and more detailed morphological properties, X-ray computed tomography (CT) is now increasingly used to assess soil and root structure (Bardgett et al., 2014 Young et al., 2022). In recent years, several studies have explored the impact of roots on morphological assessment of soil structure, primarily focusing on comparing how different ecosystems and cultivation methods shape soil pore structure (Kuka et al., 2013; Burr-Hersey et al., 2020; Kan et al., 2023).

While extensive research has explored the reciprocal relationship between soil structure and root growth (Tracy et al., 2012; Dal Ferro et al., 2014; Mawodza et al., 2020; Giuliani et al., 2024), investigations into the effects of root growth on soil structure have primarily relied on soil water retention curves (Angers and Caron, 1998; Logsdon, 2013; Bodner et al., 2014; Scholl et al., 2014). However, methods that are based on the capillary bundle model (Childs and Collis-George, 1948) often lack the ability to provide a comprehensive morphological characterization of the pore space due to oversimplification of the soil geometry (Hunt et al., 2013). This critique becomes even more pertinent when considering biopores, which possess distinct geometries and topologies (Leue et al., 2019).

Helliwell et al. (2019) investigated the impact of different plant species and their interaction with different soil types while Phalempin et al. (2021) assessed bulk density in the rhizosphere for different soil conditions. Here, for the first time we examined the impact of the genetic diversity of three wheat cultivars with different root morphological features on soil structure. The cultivars were selected from a preliminary screening of root morphology on a set of 20 wheat cultivars. We quantified the impact of the contrasting root morphology of an elite cultivar (Paragon) and two landraces (Watkins238 and Senatore-Cappelli, hereafter referred to as Senatore) grown in a field trial on key soil morphological and topological properties, both in soil cores and soil aggregates. Root crown morphology was determined using shovelomics and broken roots (Trachsel et al., 2011).

The results presented in this paper advance our understanding of the relevance of root traits to support soil structure.

2. Materials and methods

2.1 Field Trial

The field trial was conducted at the experimental farm of the University of Bologna in Cadriano (44°3255 N, 11°2452 E, 26 m a.s.l.), located in the Pianura Padana valley, in northern Italy. The area is characterized by a subhumid climate with a mean annual temperature of 12.8°C and an average annual precipitation of 924 mm. The soil is classified as loam, consisting of 11.6% clay, 52.8% silt, and 35.6% sand, with a bulk density between 1.1 and 1.3 g/cm^3.

Following a preliminary screening of the root morphology of 20 wheat cultivars and varieties, the following were selected based on contrasting root morphology: a bread wheat landrace (Watkins238), the bread cultivar Paragon, and the durum wheat landrace Senatore-Cappelli. The selection aimed at maximizing diversity in root architecture while also considering species differences and their breeding history of each genetic diversity. We intentionally selected: (i) an elite bread wheat variety with a robust root system, (ii) a durum wheat landrace characterized by a highly branched root system, (iii) a bread wheat landrace with fewer but slightly thicker roots. This selection ensures a broad spectrum of root system variability. Additionally, by incorporating both elite and landrace varieties from different species, we aim to capture variability not only in root traits but also in their evolutionary and breeding trajectories. For further clarity, we have included a PCA plot (available in the supplementary material) that visually represents the divergence among these genotypes.

The three selected cultivars are phylogenetically distinct and sourced from two collections of tetraploids (Maccaferri et al., 2016, Mazzucotelli et al., 2020) and hexaploidy wheat (Wingen et al., 2014). These cultivars were sown in 6 x 1-meter (6 m^2) plots for the first time on November 26, 2022, on soil that had not undergone any tillage in the previous two years. Each cultivar was grown in three different plots according to a randomized experimental design. The field was not cultivated and not tilled for two years to reduce the potential effect of other crops or tillage on soil structure. The plants were subjected to two rounds of nitrogen fertilization at a rate of 24 kg/ha: the first on February 13, 2023, during the tillering stage, and the second on April 17, 2023, during the stem elongation stage. Wheat was harvested on June 10th, 2023.

2.2 Sample collection

Undisturbed soil cores were collected in October 2023 using an Eijkelkamp soil sampler. The samples were collected between rows and at the center of each plot between residual wheat plants. After harvesting the wheat in June 2023, no other crop was cultivated, and no tillage was performed.

Additionally, samples of bare soil were collected outside the plots of the rhizosphere as a control. The bare soil had been grown by weeds prior to October 2022 but been bare after that date. Sampling was conducted at a soil depth of 10 cm (corresponding to the bottom of the sampler), using an aluminum cylinder, which was selected due to its suitability for X-ray analysis (Koestel et al., 2018). The cylinder used had an internal diameter of 8 cm, a height of 5 cm and had a wall thickness of 2 mm. Three undisturbed bare soil samples were collected as controls (bare soil) and three for each cultivar.

The samples were preserved at a constant temperature of 18°C and covered with aluminum foil to prevent soil shrinkage. Any excess soil protruding from the aluminum cylinder was removed. Following the X-ray scanning of the undisturbed soil cylinder, sub-samples of soil aggregates were collected and used for scanning at a higher resolution for the aggregate soil structure analysis. X-ray analysis was therefore performed on the whole soil cylinder and on aggregates, as detailed below.

2.3.1 Root phenotyping

Root phenotyping of the selected cultivars was conducted on May 27, 2023, during the flowering stage, to ensure complete root development using shovelomics (Trachsel et al., 2011). A 40 cm long and 30 cm deep soil block was excavated with a shovel. The analysis was performed for three plants for each plot (cultivars), for a total of eighteen plants per cultivar. After washing the roots of the excavated plants, three plants were selected for phenotyping as representative of the plants collected per plot regarding average number of tillers, plant height and root system size. Plants with visible malformations, signs of disease, or damaged root systems were excluded. Shovelomics was performed using two methods: whole root (crown) and broken root image analysis (Trachsel et al., 2011).

Whole roots were photographed with a black matte background (Fig.1). The plants were positioned 80 cm above the ground, with the camera placed 80 cm away from the black matte background and 80 cm above the ground surface. To provide a comprehensive view of the root system morphology in three dimensions, each plant was photographed first from a frontal view, then rotated 90 degrees, and photographed again. The values of the root traits were therefore an average of both two-dimensional (2-D) images (Liu et al., 2021).

Broken roots were also imaged following the whole root analysis. The seminal and nodal roots were separated from the main culm and arranged in a plexiglass tank placed over an Epson Expression 12000XL Pro scanner, filled with 1.5 L of water to prevent overlapping. The main culm of the plant was identified based on its greater height than the other tillering culms. A reference marker was included, and the tank was covered with a matte black lid to reduce reflections and interference. Images were captured at a minimum resolution of 600 DPI (Fig. 2). To maintain image quality, the

water was replaced every 10 samples.

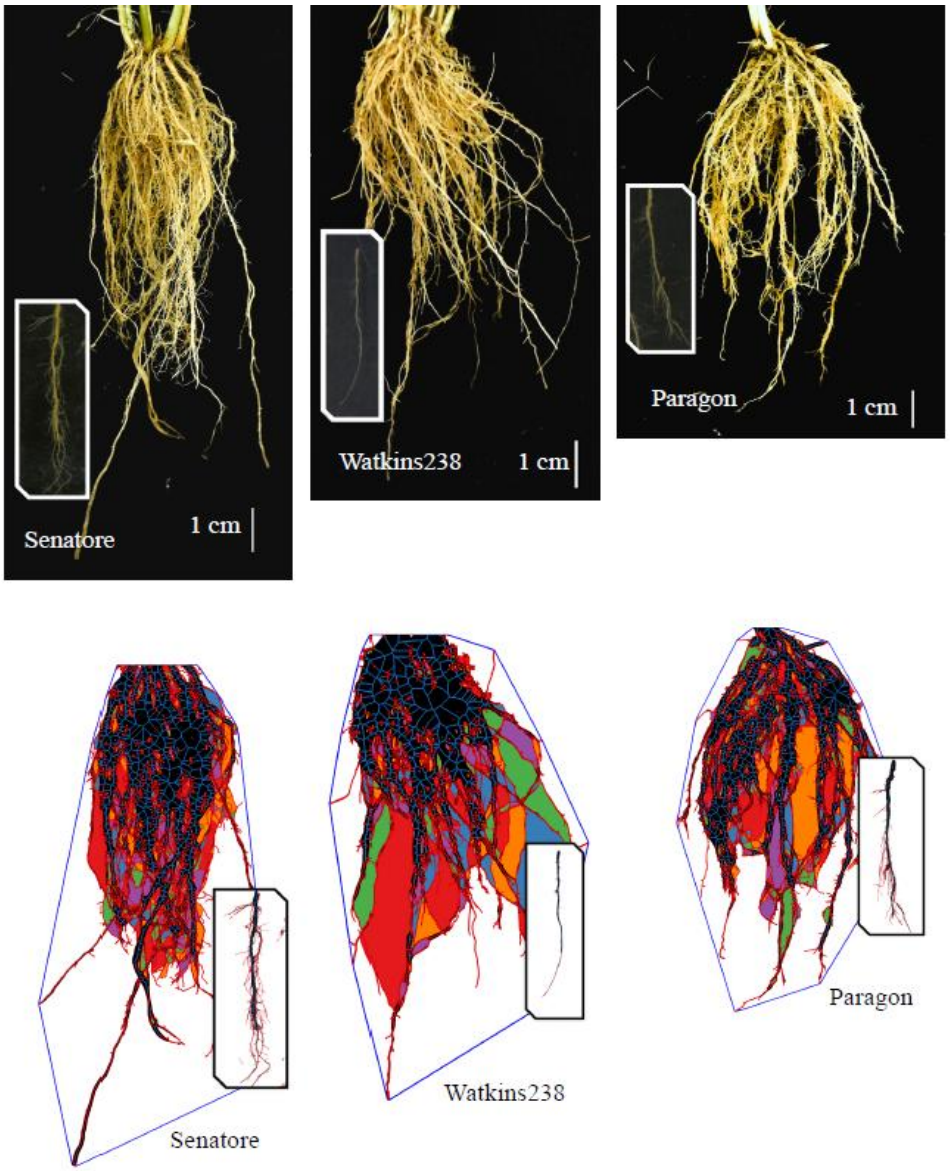

Figure 1. Photos of the root crowns of the three wheat cultivars (top) and the corresponding image analysis output from RhizoVision Explorer (bottom). In the RhizoVision Explorer output, root segments are color-coded based on their diameter: red lines represent Range 1 roots (0–1.6 mm), while blue lines represent Range 2 roots (>1.6 mm). The colored regions within the roots indicate fragmented root morphological patterns, highlighting structural variations. The outer blue contour delineates the convex hull area, which represents the minimum convex boundary enclosing the root system.

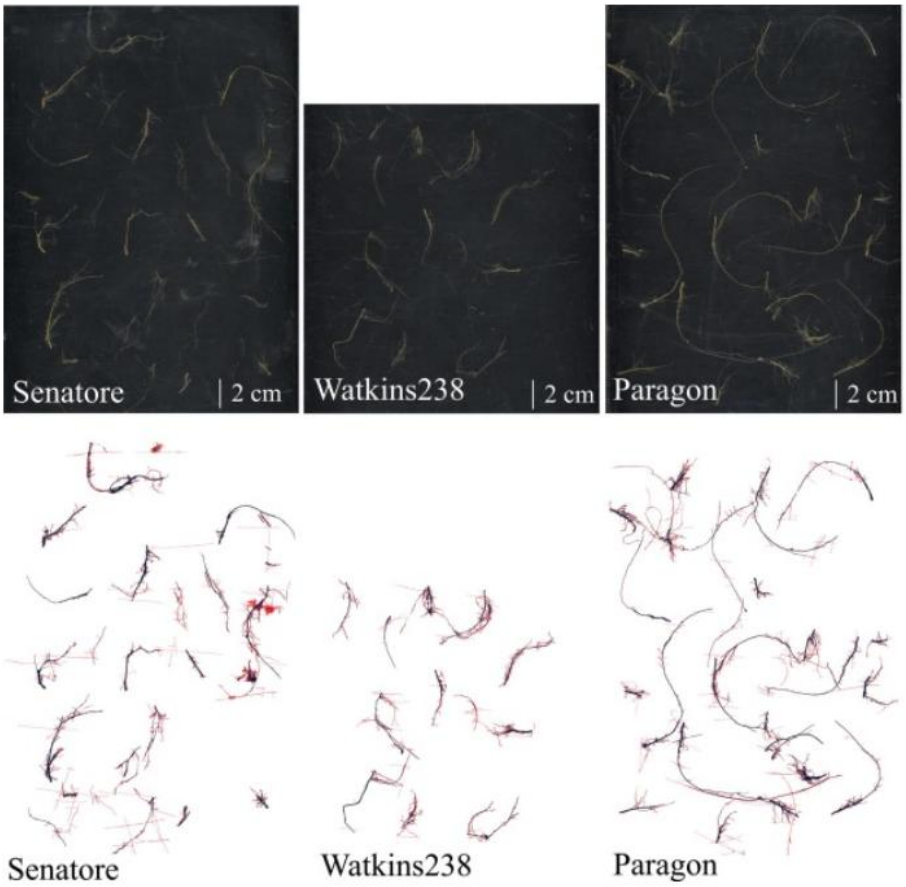

Figure 2. Photos of the dissected main culm of the three wheat cultivars (top) and the corresponding image analysis output from RhizoVision Explorer (bottom). In the RhizoVision Explorer output, root segments are color-coded based on their diameter: red lines represent Range 1 roots (0–0.5 mm), while blue lines represent Range 2 roots (>0.5 mm).

2.3.2 Root image analysis

Root image analysis was performed using RhizoVision Explorer software for both the whole-root and broken-root methods (Seethepalli et al., 2021). This software has been extensively validated and utilized in previous research within the shovelomics framework (Bucksch et al., 2014; Le Marié et al., 2019; Seethepalli et al., 2021; Xu et al., 2022; Prince et al., 2022; Weihs et al., 2024). RhizoVision Explorer provides two distinct analytical modalities: "whole-root analysis," used to evaluate entire root system images, and "broken-root analysis," which examines root fragments obtained after sectioning.

For whole-root analysis, focusing specifically on crown images, an image threshold value of 170 was employed to achieve precise segmentation of the root structures. Pixel-to-millimeter conversion was accomplished using a known-length reference scale and the Fiji software (Schindelin et al., 2012), with a resulting pixel-to-mm ratio of 8.6 pixels/mm, equivalent to an approximate resolution of 116 µm per pixel. Thirty-two root traits were derived from whole-root images, among which six key traits were selected due to their relevance to the study objectives and support in the literature: network area, convex hull area, root holes, shallow angle frequency, and steep angle frequency (Trachsel et al., 2011; Maccaferri et al., 2016; Ober et al., 2021). The parameter initially named "root holes," indicative of disconnected root segments, was renamed for clarity as "fragmented root morphological pattern". This trait, determined by analyzing the inverted segmented images (Seethepalli et al., 2021), quantifies the branching degree and structural complexity of the root system. Higher values for this trait denote greater complexity and branching, potentially reflecting enhanced soil exploration capability, nutrient and water uptake efficiency, and improved soil aggregation capacity (Balashov and Bazzoffi, 2003).

For the broken-root image analysis, thresholding levels were set differently to enhance segmentation accuracy: 200 for fine roots and 170 for axial roots. Root diameters were categorized into two narrower classes: root diameter range 1 (0–0.5 mm) and root diameter range 2 (>0.5 mm), enabling a more precise assessment of detailed root topology. Pixel-to-millimeter conversion followed the identical approach as described for whole-root analysis, ensuring consistency between methods. Further details regarding RhizoVision parameterization and image analysis are provided in the Materials and Methods section.

A total of twenty-two root traits were extracted from broken-root images. To facilitate direct comparison with the whole-root analysis, five critical traits were prioritized: number of root tips, root length in diameter range 1 (0–0.5 mm), root length in diameter range 2 (>0.5 mm), branching points, branching frequency, as well as average and maximum root diameter. The total root length was computed by summing the root length of diameter range 1 and diameter range 2 classes.

The two analytical methods employed are complementary: whole-root analysis provides comprehensive information regarding overall root system architecture, whereas broken-root analysis offers detailed insights into finer structural and topological root characteristics. However, traits such as root tips, branching frequency, and branching points should be interpreted with caution, as they may be slightly overestimated due to background noise or limitations in feature detection inherent to the analysis software (RhizoVision Explorer).

2.4 X-ray scanning

X-ray images were taken with two different cone-beam X-ray CT systems at the Department of Physics and Astronomy at the University of Bologna. The X-ray scanning processes were controlled remotely by means of in-house proprietary software developed for research purposes (Zagaglia, 2012). Images of the undisturbed cylinders were collected using a PXS10-65 W MicroFocus X-ray tube (Thermo Kevex X-ray LLC) with a tungsten anode, a Varian PaxScan 2520D flat-panel detector and a Physik Instrumente M-038 PD1 precision rotary stage. The operating voltage was set to 130 kV, and the beam current was set to 240 µA. An optical lead filter of 0.3 mm was used to reduce beam-hardening effects. A total of 900 projections were acquired over a rotation of 360 degrees, and ideally, the number of projections should be the same as the number of horizontal pixels, which is 1500 in the detector. However, since the object did not occupy the entire field of view, 900 projections resulted in an optimal approximation. The exposure time per radiograph was adjusted to 250 ms, and the projection was averaged from 8 consecutive radiographs to reduce image noise. The voxel size was approximately 63 µm. We estimated the X-ray image resolution to be three times greater than this value, i.e., approximately 190 µm.

For the soil aggregates, a PXS10-65 W MicroFocus X-ray source was used in combination with a Photonic Science VHR 1:1 X ray camera and a Physik Instrumente M-037 precision rotary stage. Since the object size and the distance between the tube and the detector were significantly smaller than those of the ring sample, it was possible to work with a lower voltage, which we set to 110 kV and an electron current of 70 µA. We added an iron filter of 0.1 mm thickness. The exposure time per radiograph was set to 2 s. Again, we collected 900 projections over a rotation of 360 degrees, and each projection was averaged again from 8 consecutive radiographs. The voxel size was approximately 9 µm, resulting in an estimated image resolution of 27 µm. Fig. 3 illustrates the X-ray imaging systems for the cylinder and the aggregates collected from each measured cylinder.

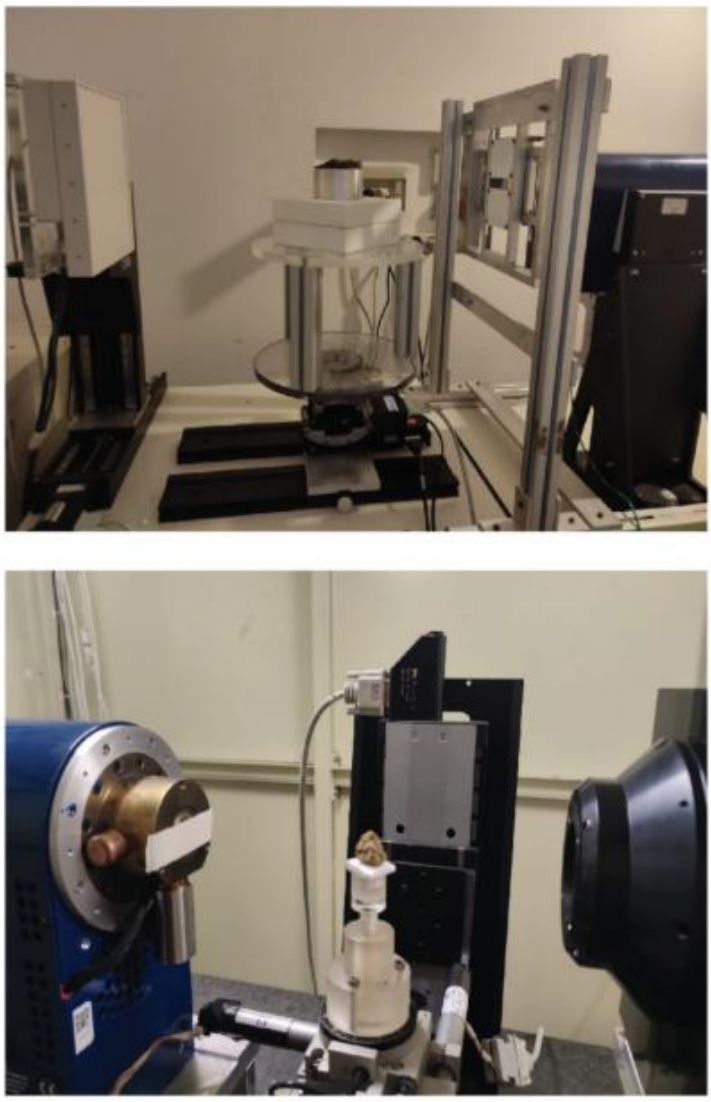

Figure 3. Setup system with a soil sample on the rotating axis. In the upper picture the measurement of the cylinder sample and the in the lower picture one of the collected aggregates from each sample.

The tomographic reconstruction software PARREC (Brancaccio et al., 2011) was used to filter the projections to remove imaging artifacts. This was performed in two steps. The first step was the application of a local threshold filter, using the local standard deviation for thresholding. Secondly, the projections were converted to sinograms and ring artifacts caused by malfunctioning detector pixels were corrected. Then the sinograms were re-converted to projections and a back-projection Feldkamp algorithm was used to reconstruct the sequence of frontal slices of each sample. Finally, 3D images were obtained by means of rendering software VGStudio Max 2.0 by Volume Graphics.

2.5 Image processing

2.5.1 Denoising

Digital images consistently contain noise to some extent, this being defined as casual brightness variation, i.e., that is not present in the original object. This can be due to measuring instruments, data transmission or quantization. Schlüter et al. (2014) reviewed the best denoising methods for micro tomography images and indicated that a nonlocal means filter is especially suitable for soil-like materials. This filter is based on the replacement of the gray level of a given pixel with an average of the gray levels of similar pixels, which allows overcoming the issues associated with the classical principle of denoising based on neighborhood values. As a 3-D implementation of a non-local means filter is not available as a Fiji plugin, we applied a 2-D non-local means filter (Buades et al., 2011) in all three different dimensions as described in Nitzbon et al. (2022). The smoothing factor was set to 1, and the noise standard deviation sigma was set to be auto estimated.

2.5.2 Calibration and segmentation

To segment the images from each sample series, i.e., the cylinder and aggregate samples, with the same value, a calibration was performed beforehand. The following steps were carried out using the SoilJ plugin (Koestel, 2018). First, the 3-D cylinder outlines were delineated. Then, the gray values were rescaled to the 0.1-percentile of each cross-sectional histogram and the gray value of the aluminum wall. The rationale behind this approach is that the 0.1-percentile corresponds to air-filled pores (see Koestel et al., 2020). For the aggregates, calibration was performed by using values of the 10 and 60-percentiles since there was no aluminum wall to use as an upper reference. The 0.6 was found to correspond to the matrix gray value. After the gray-value calibration, joint histograms, i.e., a single representation of gray-values intensity distributions from all slices of all the scanned samples, were compiled from the cylinder and aggregate scale images, respectively. and used to compute threshold values with different methods: Otsu, Minimumn, Isodata, Renyi Entropy, Maximum Entropy, Huang, Li and Yen (Prewitt and Mendelsohn, 1966; Ridler and Clavard, 1978; Otsu, 1979; Kapur et al., 1985; Huang and Wang, 1995; Yen et al., 1995). The gray value used as a threshold for segmentation was the average of all the global method thresholds listed before. Once the images were binarized into imaged pores, a morphological opening (erosion followed by dilation) of a cubic structural element of 2 voxels was performed. This approach allows for overcoming the fact that objects smaller than 3 voxels are likely to be noise.

2.5.3 Biopore extraction

Pores of different sizes and shapes belong to two main categories: abiotic pores and biopores. Among the abiotic pores are textural pores which originate from the arrangement of primary particles (sand, silt, and clay), and affect soil structure at the macroscale, such as the typical formation of cracks in silty soil. Biopores are the result of biological activity; in particular, in the rhizosphere, they are the result of root exploration, which pushes mineral particles and organic substances aside (Lucas et al., 2019a). Once the root decomposes, the biopore persists as a tubular structure in soil. We used the workflow described by Lucas et al. (2019b) implemented in SoilJ to extract the biopores from the binarized images.

2.6 X-ray CT image Analysis

To characterize the soil structure, four Minkowski functionals and three percolation theory parameters were computed from the binarized images for the total imaged porosity and the bioporosity, and at both cylinder and aggregate scale. The Minkowski functionals, or the quermass integral, are described as the "intrinsic volume" of an object and are valuable tools for describing soil structural properties since they are scale invariant (Vogel et al., 2010) and express information on the topology of the porous material through the Euler number (Renard and Allard, 2013; Armstrong et al., 2018). Negative values of the Euler number denote a higher number of redundant paths within pore-clusters than the number of isolated pore-clusters. Pore morphology and connectivity are also defined through the parameters obtained from percolation theory (Liu and Regenauer-Lieb, 2011; Koestel et al., 2020). The three parameters that best describe the connectivity of a system are the connection probability (Γ), which measures the likelihood of two random pore voxels being connected, and thus belong to the same cluster; the percolation threshold (PT), indicating the minimum porosity needed for a continuous pore network; and the critical diameter, representing the largest pore size that allows fluid flow through the soil. Thus, these parameters were computed to investigate soil morphology.

The first Minkowski functional, the phase volume fraction (M0), represents the most basic characteristic of porosity, i.e., its total volume. The second indicator, the surface area (M1), represents the area of the total imaged porosity, which is a relevant indicator of water adsorption and chemical exchanges between the solid and fluid phases. The third functional, the mean curvature (M2), is affected by the pore shape and is a relevant indicator of soil mechanical properties (Vogel et al., 2010). Finally, the fourth functional measures the total curvature. If it is divided by 4π, the Euler characteristic (M3) is obtained. The Euler characteristics is a topological property that carries information on the local connectivity of a porous medium (Renard and Allard, 2013). Negative values of the Euler number denote a higher number of redundant paths within pore-clusters than the number

of isolated pore-clusters.

In the natural sciences, connectivity is also defined through the parameters obtained via the percolation theory paradigm (Liu and Regenauer-Lieb, 2011; Renard and Allard, 2013). Originally, percolation theory investigated at which porosity two opposite sides of an infinite domain become connected. Applied to soil science, it has been used to evaluate if an imaged soil pore-network contains a connected pore-cluster that spans from top to bottom surface of a soil sample (Jarvis et al., 2017). We used three parameters from percolation theory to quantify the pore network connectivity: the connection probability (Γ), the (apparent) percolation threshold (PT), and the critical pore diameter (CPD).

The connection probability is defined as the probability that two randomly chosen pore voxels in the region of interest (ROI) are connected (i.e., they belong to the same pore cluster). Its upper bound is 1 and it may asymptotically approximate 0. Larger values indicate better interconnected pore systems. However, since the beneficial effect on total pore connectivity of a root system is given by an enhanced connectivity of the whole system itself, only the connectivity and Euler number of the whole pore system was discussed and not of the biopore system.

The apparent percolation threshold was determined using the method proposed in Liu and Regenauer-Lieb. (2011). It refers to the minimum porosity required for a continuous network of pores to form. Note that the apparent percolation threshold strongly depends on the image resolution, since it only expresses percolation properties for pores with diameters larger than the image resolution. Pores with smaller diameter may well percolate at lower porosities but are not resolved by the image data. A higher percolation threshold indicates that the gap needed to bridge for obtaining a pore connection from top to bottom of the ROI is larger. The critical pore diameter is only defined if at least one percolating pore cluster exists. Then it corresponds to the bottleneck in the pore connection from top to bottom, i.e., it is equivalent to the diameter of the largest sphere that could be moved from top to bottom through the pore system. In undisturbed soils, the square of the critical pore diameter is correlated with the saturated hydraulic conductivity (Koestel et al., 2018b, Schlüter et al., 2020).

The labels for the morphological parameters for the cylinder and aggregate were chosen as follow: M0, M1, M2, M3, Γ and PT for the cylinder analysis and μM0, μM1, μM2, μM3, μΓ and μPT for the aggregate sub samples.

The pore size distribution (PoSD) was also extracted from both rhizospheric samples with a thickness analysis of the pore space using the maximum inscribed sphere method using the software SoilJ (Koestel, 2018), to obtain a PoSD by attributing each pore voxel to its class diameter. Nonlinear regression models were used to quantify different continuous probability distributions. The best fit was obtained for an inverse Gamma distribution (Kahle and Stamey, 2017):

$$f(x;\alpha,\beta) = \frac{\beta^{\alpha}}{\Gamma(\alpha)}(1/x)^{\alpha+1}e^{-\beta/x}$$

where α is the shape factor, which is defined as $\alpha = 2 + \mu^2/\sigma^2$ and β is the scale factor, $\beta = \mu(\alpha - 1)$. Four parameters can be extracted from each inverse Gamma distribution: shape, scale, mean and variance (α, β, μ and σ^2). Two PoSD (Pore Size Distribution) curves were obtained for the different cultivars: one derived from the aggregate samples and the other from the ring samples. The first curve represents a pore diameter range from 0.03 to 0.7 mm, while the second curve covers the range from 0.19 mm to 2 mm. The two curves overlap at approximately 0.2 mm.

2.7 Statistical analysis

Firstly, we tested whether the parameters for normal distribution by using the Shapiro-Wilk test. For those parameters that didn't adjust to normal distribution, a nonparametric Kruskal-Wallis test was used to assess differences among the cultivars and between the cultivars and the control for parameters that were normally distributed, Tukey's post-hoc analysis was performed to identify which cultivars primarily contributed to the significant differences. For non-normally distributed parameters, the Conover post-hoc test was used instead (Dinno et al., 2024). In the case of bioporosity the analysis was performed only on geometrical properties, i.e., the first three MF. Connectivity parameters were excluded because biopores can be linked by structural pores without a tubular shape, which the plugin cannot detect, and this would have led to misleading results.

The PoSD curves, modeled as inverse Gamma functions, were compared using the Kolmogorov–Smirnov (KS) test.

The impact of the root traits of the cultivar and varieties on soil morphology was determined using an ANOVA and a Tukey post hoc analysis. To investigate the relationships between soil pore-network properties and root traits, linear regression models were used to evaluate all the interactions of the soil and root variables. The statistical analyses were performed using R software (RStudio, 2020). To analyze the effect of each root trait on the soil morphological parameters, data from the cultivars was combined. Since we wanted to explore the effects of root morphological traits on soil structure this analysis was conducted with the bioporosity parameters only. The analysis was conducted by using a mixed linear model (LMM) providing 96 combinations, where each root trait was analyzed in terms of its effect on the morphological parameters of the bioporosity alone.

3. Results and discussion

3.1 Root traits

The genotype Senatore-Cappelli exhibited a statistically significant bigger convex hull and network area compared to Paragon and Watkins238 ($p < 0.05$). There were no significant differences in the frequency of root angles among the cultivars ($p > 0.05$). The genotype Paragon exhibited significantly higher values of root tips, branching points, and total root length compared to Senatore Cappelli ($p < 0.05$). Watkins238 showed significantly lower values for root tips, branching points, and total root length compared to both Paragon and Senatore Cappelli (all $p < 0.001$). Senatore Cappelli and Watkins238 presented significantly smaller average and maximum root diameter compared to Paragon ($p < 0.001$ and $p < 0.01$, respectively). Branching frequency was significantly lower in both Senatore Cappelli and Watkins238 compared to Paragon (both $p < 0.001$). Finally, the root length within diameter ranges 1 and 2 was significantly lower in Senatore Cappelli and Watkins238 compared to Paragon ($p < 0.01$ and $p < 0.001$, respectively).

Table 1. Mean values of root traits for the three wheat cultivars. Mean values associated with different letters indicate statistically significant differences ($p < 0.05$, Tukey's test).

Root trait	p_value[1]	Paragon	Senatore Cappelli	Watkins 238
		Whole root analysis		
Network area (mm^2)	**	4435 ± 361^{a}	5667 ± 391^{b}	4145 ± 454^{a}
Convex area (mm^2)	**	15002 ± 1460^{a}	16291 ± 2206^{b}	14714 ± 1659^{a}
Shallow angle frequency	ns	0.22 ± 0.02^{a}	0.24 ± 0.01^{a}	0.23 ± 0.01^{a}
Steep angle frequency	ns	0.51 ± 0.02^{a}	0.46 ± 0.01^{a}	0.48 ± 0.02^{a}
Fragmenter root morphological pattern	*	451 ± 27^{a}	637 ± 86^{b}	636 ± 75^{a}
		Broken root analysis		
Root tips	***	894 ± 127^{b}	506 ± 60^{b}	237 ± 45^{a}
Total root length (mm)	***	6086 ± 828^{ab}	3200 ± 416^{b}	1353 ± 322^{a}
Root length diameter range 2 (mm)	***	1157 ± 100^{b}	546 ± 175^{a}	283 ± 42^{a}
Root length diameter range 1 (mm)	***	4928 ± 734^{b}	2654 ± 743^{a}	1170 ± 249^{a}
Branching points	***	3479 ± 612^{ab}	1447 ± 189^{b}	635 ± 165^{a}
Branching frequency (mm^{-1})	***	0.69 ± 0.08^{b}	0.35 ± 0.01^{a}	0.29 ± 0.03^{a}
Max root diameter (mm)	**	1.93 ± 0.50^{b}	1.17 ± 0.13^{a}	1.19 ± 0.56^{a}
Root diameter (mm)	***	0.93 ± 0.09^{b}	0.56 ± 0.01^{a}	0.60 ± 0.02^{a}

[1]) p values of ANOVA genotypic effect, with *, ** or *** representing $p < 0.1$, <0.05 or <0.01, respectively.

3.2Minkowski Functionals and Percolation Properties

3.2.1.1 Cylinder scale, total imaged porosity.

No statistically significant differences were observed among the cultivars or between the bare and rhizospheric soil for the geometric and topological characteristics of the Minkowski functionals (Fig. 4). The analysis of the critical diameter at the cylinder scale did not reveal any significant differences between the samples, with a mean value of 0.06 mm.

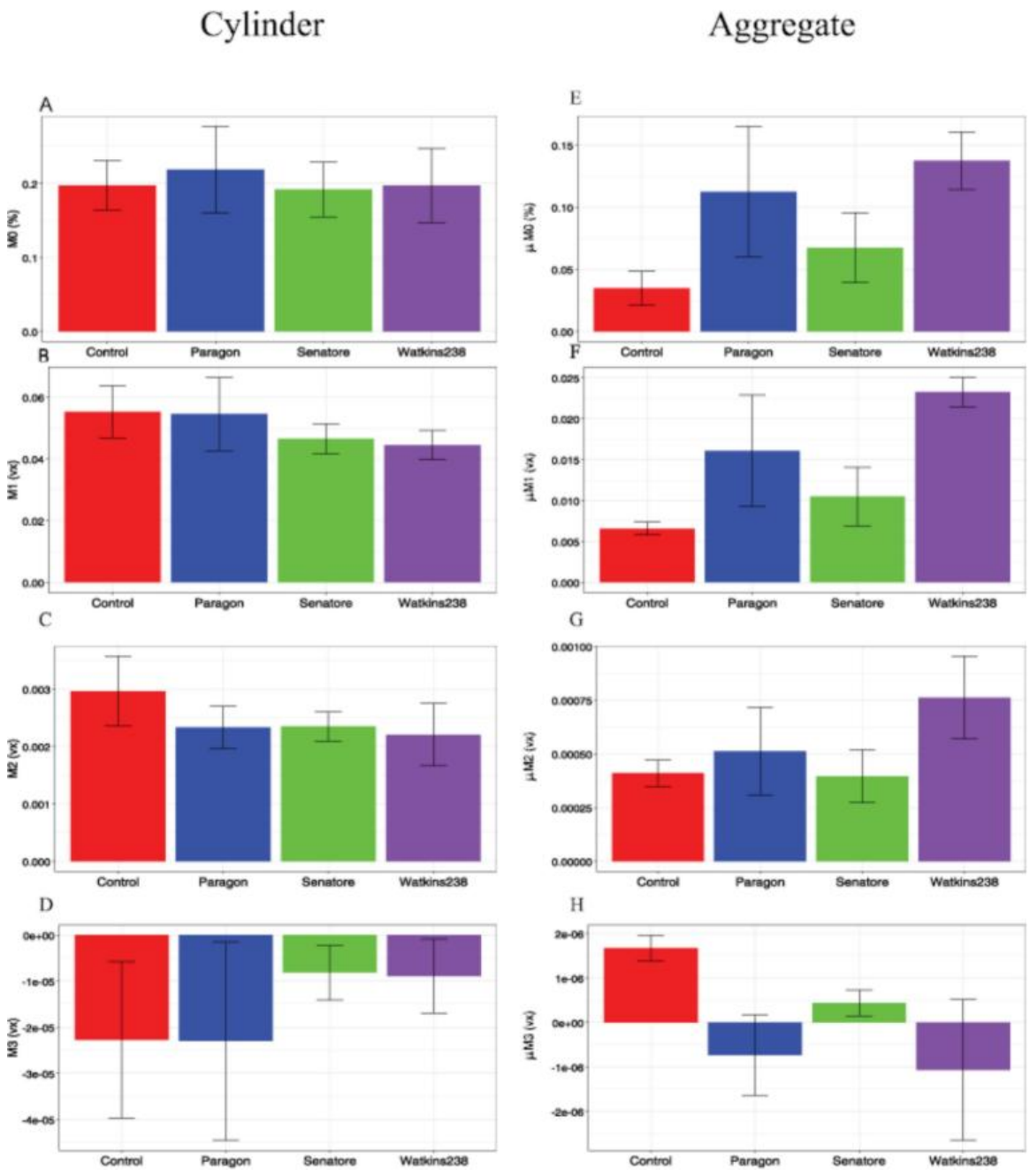

Figure 4. Values of M0 (pore volume), M1 (surface area), M2 (mean curvature) and M3 (Euler number) for the bare (red bar) and rhizospheric soil from the three wheat cultivars (blue, green and purple bars) from the cylinder and the aggregate setups. The values are computed for the total imaged porosity.

From the analysis of total imaged porosity, the only parameter non-normally distributed was the connection probability and the values, for both rhizosphere and bare soil samples were comparable and showed no significant differences. The percolation threshold is the minimum porosity required

within the analyzed volume to form at least one "percolating" cluster, i.e., a cluster that spans from one end to the other of a 3D image in a finite system, such as our tomography-scanned volume. This parameter does not depend solely on the amount of porosity but also on morphological properties of the pore network, such as anisotropy (Jarvis et al., 2017) and pore size distribution (Huang, 2021). Consequently, higher connectivity is often associated with a lower percolation threshold. The percolation threshold revealed notable differences between rhizospheric and bare soil samples (Fig. 5), being significantly higher in bare soil ($p < 0.01$) than in rhizospheric soil. The observation of similar total connection probabilities between rhizospheric and control soils, along with significantly higher percolation threshold values for bare soil, suggests that bare soil contains clusters large enough to support connectivity comparable to that of root-explored soils. However, these clusters are less uniformly distributed within the volume, resulting in lower levels of percolation compared to rhizospheric soil.

This highlights the importance of using a broad set of parameters to describe the morphology of the pore phase from multiple perspectives. Since a high percolation threshold indicates highly disconnected porosity or non-conducting regions (Daigle et al., 2019; Soto-Gómez et al., 2020), this finding evidences the beneficial effect of wheat roots on soil structure. Root activity promotes a more connected pore network, reducing the percolation threshold and enhancing total connectivity. Our results are consistent with Lucas et al. (2019a), who emphasized the critical role of connected pores formation in plant growth that facilitates access to deeper soil layers and mitigates the impact of soil compaction.

Figure 5. Values of the connection probability and the percolation threshold for the cylinder and the aggregate, for the control (red bar) and three cultivars (blue, green and purple bars). The values are computed for the total imaged porosity.

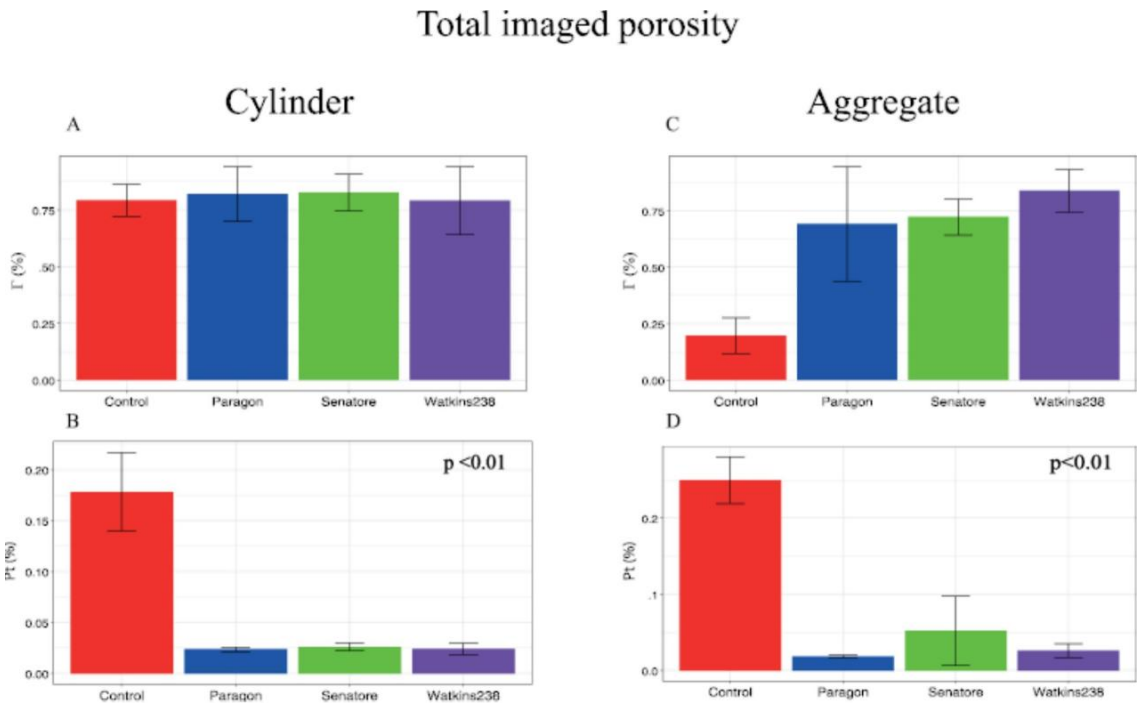

Figure 5. Values of the connection probability and the percolation threshold for the cylinder and the aggregate, for the control (red bar) and three cultivars (blue, green and purple bars). The values are computed for the total imaged porosity.

3.2.1.2. Cylinder *scale, bioporosity.*

Xiong et al., 2022, stated the importance of biopores smaller than 2 mm, which is the case of the ones observed at both scales in this study, since they consistently promote plant growth by enhancing root-soil interactions, nutrient uptake, and water absorption. The bioporosity network is presented in Fig. 6, while Fig. 7 illustrates the morphological functions (MFs) for the biopore networks at both the cylinder and aggregate scales. No significant differences were observed between rhizospheric and bare soils in terms of total biopore volume fraction, mean curvature, or surface area.

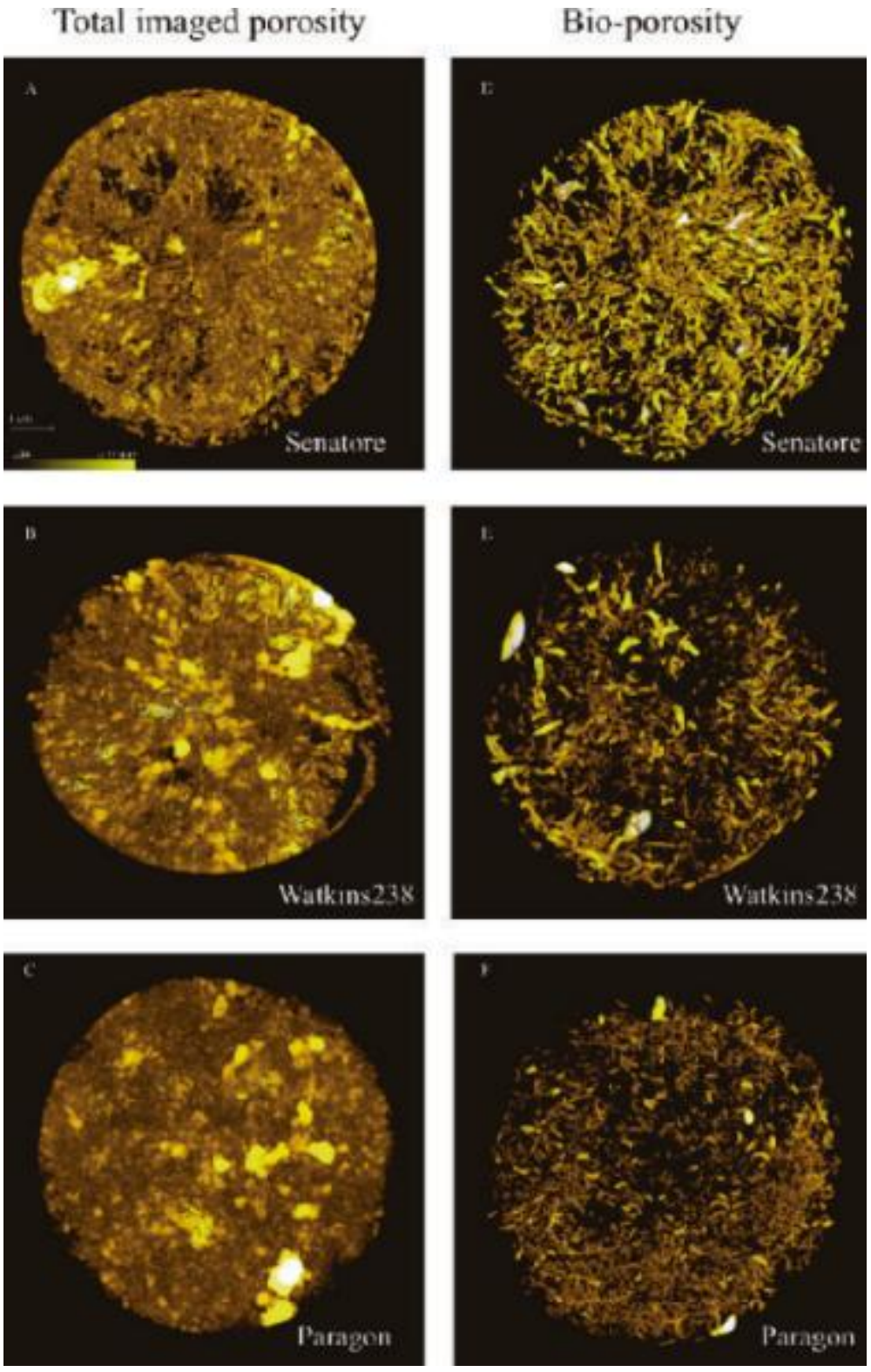
Total imaged porosity
Bio-porosity
A
Senatore
E
Senatore
B
Watkins238
F
Watkins238
C
Paragon
F
Paragon

Figure 6. Tomographic images of total imaged porosity and bioporosity for the three cultivars for the one representative cylinder sample. The color gradient is a representation of the pore diameter.

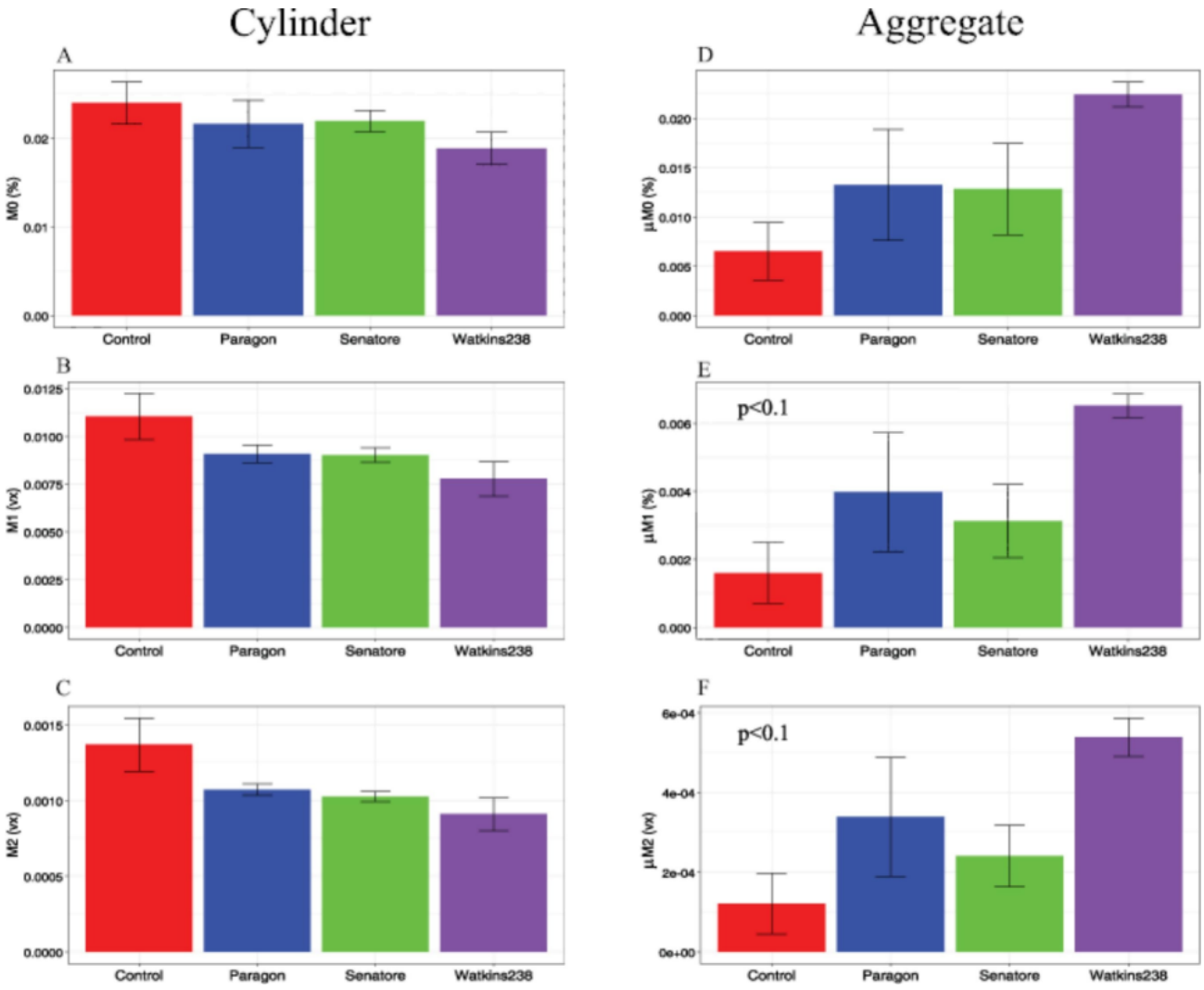

Figure 7. Values of M0 (biopore volume), M1 (surface area), M2 (mean curvature) for the cylinder and the aggregate, for the control and three cultivars. The values are computed for the imaged bioporosity.

3.2.1.3 Cylinder scale, pore size distributions

The computed frequency distribution of the pore diameters (Fig. 8) extracted from cylinder samples span a pore diameter range from 0.15 to 3 mm and it was fitted with an Inverse Gamma distribution. Each distribution was compared among the samples using the Kolmogorov-Smirnov test and the results revealed significant differences for the following pairs: Senatore-Cappelli and Paragon ($p < 0.01$), Senatore-Cappelli and Watkins238 ($p < 0.01$), Watkins238 and bare soil ($p < 0.01$), and Senatore-Cappelli and bare soil ($p < 0.1$).

To better visualize these differences, all soils were characterized by total imaged biopore diameters below 3 mm (Fig. 9) in a cumulative curve, with the most abundant diameters ranging between 0.45 and 0.8 mm.

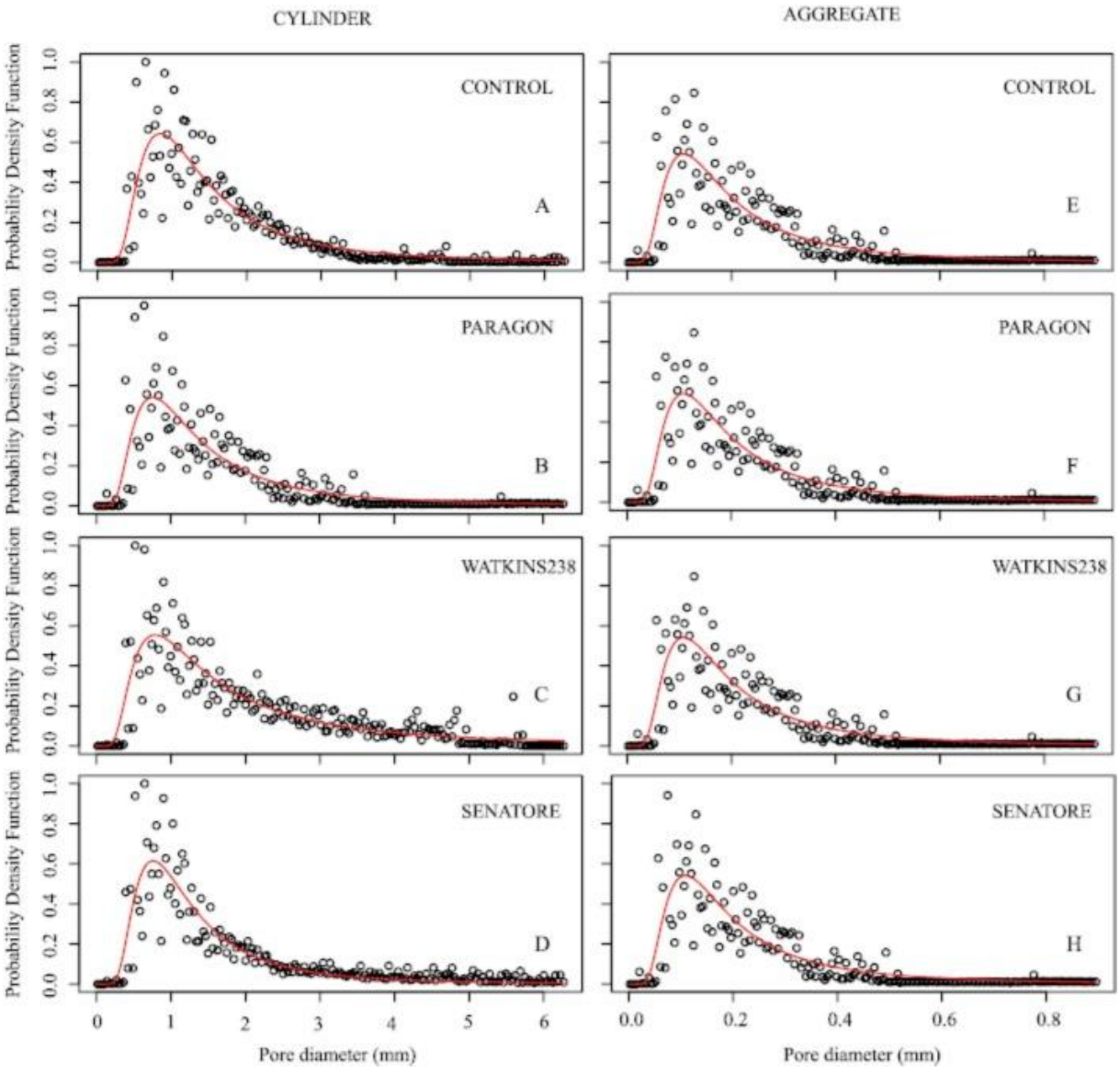

Figure 8. Probability density function (PDF) for the cylinder and aggregate samples, for the control and three cultivar samples. The red line was obtained by fitting the inverse gamma function to the experimental data (dots).

We found a significant difference in biopore size distributions between Senatore-Cappelli and Watkins238 ($p < 0.05$), with the latter one having smaller diameters. Bioporosity volumes between control and rizospheric soil within this diameter range are comparable (fig.7) indicating that the biopores produced by spontaneous vegetation from the previous year were still persistent, and the

diameters in the bare soil samples were smaller compared to the rhizospheric soil ($p < 0.01$ both for Senatore-Cappelli and Paragon respect control) (Fig. 9), which confirms the findings of Whalley et al., (2005). This is likely due to the creation of larger pores by wheat root growth.

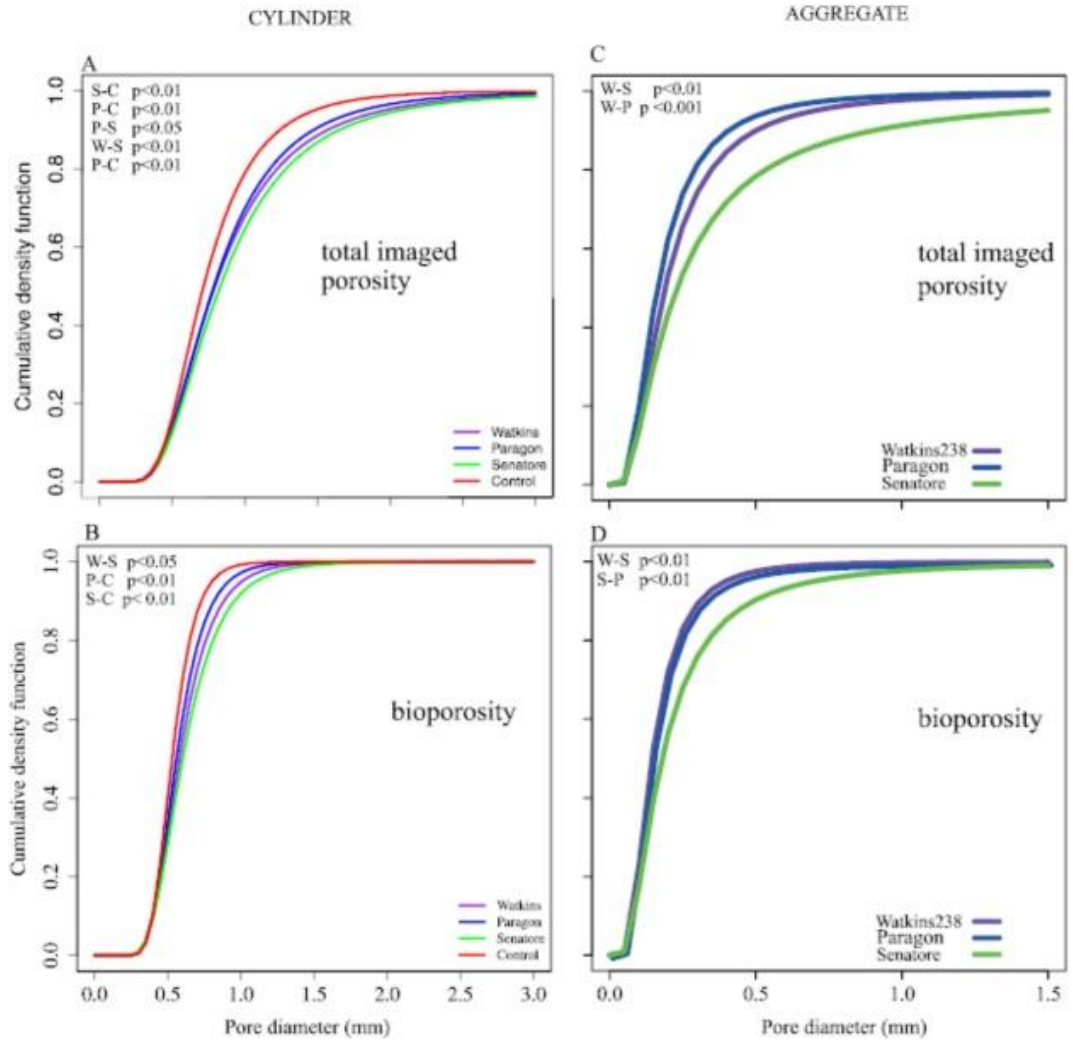

Figure 9. Modeled cumulative distribution functions for total imaged and bio-porosity for the cylinder and aggregate samples. Both curves are represented on a scale that allows visualization of their growth up to approximately 95%, for a better comparison of their differences.

3.2.2.1 Aggregate scale, total imaged porosity.

For the total imaged porosity at the aggregate scale, no statistically significant differences were observed among the rhizospheric and the bare soil, although the porosity values within the aggregate suggested that the presence of roots might result in a larger pore volume fraction ($p = 0.11$) and greater imaged pore connectivity, as indicated by lower Euler numbers (Fig. 4) Similarly to what we observed for the cylinder samples, the non-normally distributed percolation theory parameter (Fig. 5) showed significant differences between rhizospheric samples and bare soil, the percolation threshold

was higher in the control samples than in the rhizospheric values ($p < 0.01$). These results indicate that, although rhizospheric soil is known to be more compacted than bulk soil (Dexter, 1988, Whalley et al., 2005; Daly et al., 2015; Lucas et al., 2019a) it also exhibits a more connected structure (Helliwell et al., 2019), with roots promoting enhanced structural connectivity across the two scales assessed.

3.2.2.2 Aggregate scale, bioporosity

Bioporosity inside the aggregate is likely determined by the growth of fine roots (Hendriks et al., 2022) (Fig. 10).

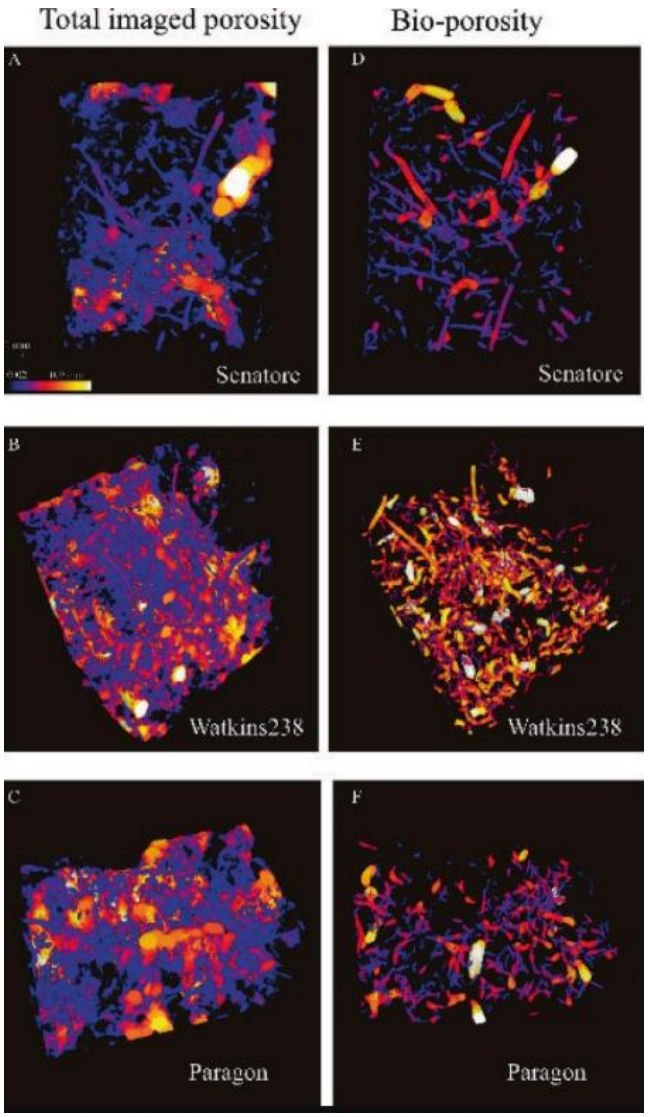

Figure 10. Tomographic images of total imaged porosity and bioporosity of the three cultivars for the one representative aggregate sample. The color shades represent the pore diameter.

In the aggregate samples, no significant differences were found for the total bioporosity fraction parameter. However, the results suggest a lower bioporosity fraction in the bare soil samples. Since this pattern was not observed at the cylinder scale, we speculate that bioporosity associated with fine root growth may be less persistent than that associated with larger roots. Interestingly, the cultivar Watkins238 showed higher values for surface area ($p < 0.1$) and mean curvature ($p < 0.1$) of the aggregates compared to bare soil samples. These two functionals likely enhance the development of the microbiome and increase the surface area available that roots encounter for exchanges of nutrients, gases and water fluxes (San Josè Martinez et al., 2015).

3.2.2.3 Aggregate scale, pore size distribution

For pore diameters ranging between 0.03 mm and 1.5 mm, the Inverse Gamma model fitting was not performed on the control samples (Fig. 9), since as indicated in Fig. 4 and 7 there was an order-of-magnitude difference in porosity between the bare and the rhizospheric soil. Consequently, illustrating a distribution function across such different volumes would not provide a representative comparison. The pairwise comparisons among the rhizospheric samples showed significant differences for Watkins238 vs. Senatore-Cappelli ($p < 0.01$) and Watkins238 vs. Paragon ($p < 0.01$). Analysis of the biopores at this resolution resulted in significant differences for Senatore-Cappelli vs. Watkins238 ($p < 0.01$) and Senatore-Cappelli vs. Paragon ($p < 0.01$). Similarly, to the bioporosity investigated in the larger diameter range, Senatore-Cappelli consistently exhibited slower increase in the curves, with 90% of bioporosity below 1 mm compared to 97% for both Watkins238 and Paragon. The Paragon and Watkins238 cultivars, which have thicker roots, may cause greater compaction of the rhizospheric soil during exploration in this size range, which may ultimately lead to enhanced soil microporosity as root decay. During the decomposition process, the substantial loss of water from roots and root hairs causes a reduction in their diameter, creating voids previously occupied by the root structures, which are subsequently filled with air (Lucas, 2022). These voids, or biopores, improve soil structure by enhancing aeration, water infiltration, and retention. Furthermore, the decomposition of roots enriches the biopore walls with nutrients and promotes microbial activity, creating hotspots for nutrient cycling and contributing to soil health and fertility (Wendel et al.,

2022), and potentially enhancing water retention and structural stability at this scale. This behavior, and our results indicating that soil underwent compaction for pores in the range between 0.1 and 0.5 mm, are consistent with previous research reporting that roots decrease porosity in rhizosphere plots, especially for macropores (> 0.25 mm) (Lucas et al., 2019a). The authors indicated that these effects depend on the initial bulk density, but that bulk density alone is not sufficient to explain this complex behavior. This was also discussed by Dexter, 2004, who reported that compaction around roots also depends on other soil physical properties such as the organic matter content and water retention capacity. The authors maintained that the ability of the roots to grow into an already connected soil affects the eventual impact on the pore size distribution. Therefore, the connectivity parameters measured in the overall imaged pore system are not only influenced by plant roots but also shape their growth, creating a dynamic relationship of mutual influence. These results may explain the scale dependent effect on the imaged pore size distribution of the three wheat cultivars that was found between the pore size ranges of 0.05 to 0.5 mm (aggregate) and 0.5 to 2 mm (cylinder), and demonstrates that the influence of the root morphology on the physical properties of a particular soil varies depending on the pore size range analyzed.

3.2 Root traits impact on total imaged porosity

The ANOVA results show that the root traits of the cultivars mainly affect the percolation threshold for both cylinder and aggregate scale, with bare soil displaying significantly higher values than Paragon, Senatore Cappelli, and Watkins238 ($p < 0.01$). These results suggest that the cultivars Paragon, Senatore Cappelli, and Watkins238 might modify specific soil characteristics. Tukey's post hoc tests confirmed these differences, suggesting a negative effect of bare soil on soil permeability. These findings are relevant to advancing our capability to introduce root traits with potential to influence the soil structure. Particular root traits showed specific correlation on soil properties (Fig. 11), showing how specific root trait could be correlated with specific soil physical property. Crown network area was positively associated with M0 ($p < 0.05$), M1 ($p = 0.05$), GAMMA ($p < 0.05$), and μPT ($p < 0.001$), while negatively affecting M2 ($p < 0.05$). Those correlations suggest decreased bulk density in the rhizospheric zone, this being consistent with previous research (Aravena et al., 2011;

Lucas et al., 2019a; Helliwell et al. 2019, Phalempin et al., 2021) that reported compaction around the growing roots.

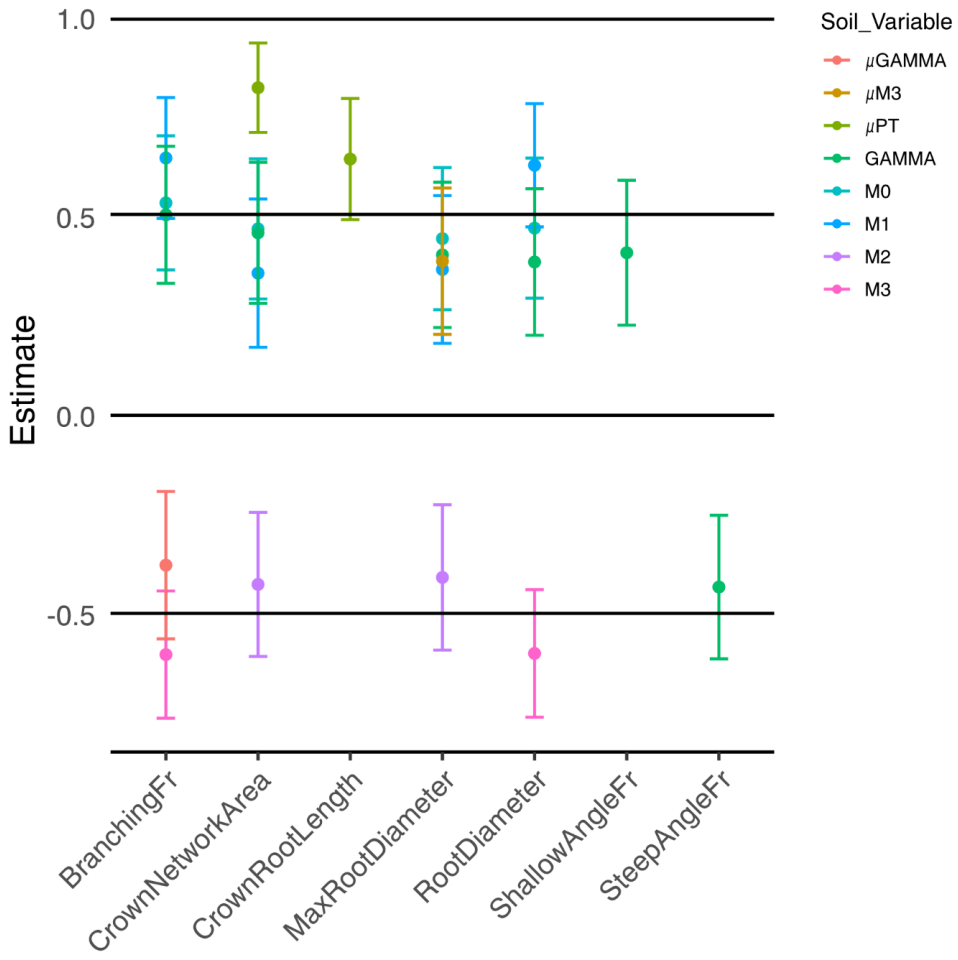

Figure 11. Effect of each root trait on the statistically significant soil morphological parameters obtained by using a mixed linear model, on total imaged porosity. When a parameter does not show it means it was not statistically significant. Symbols for the root are Avg = Average Root Diameter, Frmp = Fragmented Root Morphological Pattern, NuRT = Number of Root Tips, Per = Perimeter, ShaF/SteepF = Shallow and Steep Angle Frequency, TotaL = Total Root Length, Vol = Root Volume.

Shallow angle frequency was positively associated with GAMMA ($p < 0.05$), whereas steep angle frequency was negatively correlated with the same parameter ($p < 0.05$).

Branching frequency showed contrasting effects depending on the soil variable. It was positively associated with M0 ($p < 0.01$), M1 ($p < 0.001$), and GAMMA ($p < 0.01$), while showing a significant negative correlation with M3 ($p < 0.01$). A weaker negative association was also found with

μGAMMA (p = 0.05).

Root diameter presented a positive relationship with M0 ($p < 0.05$), M1 ($p < 0.001$), and GAMMA ($p = 0.05$), while being negatively correlated with M3 ($p < 0.01$). Maximum root diameter had a positive effect on M0 ($p < 0.05$), M1 ($p = 0.05$), GAMMA ($p < 0.05$), and μM3 ($p < 0.05$), while showing a negative correlation with M2 ($p < 0.05$). Those correlations suggest that thicker roots could decrease bulk density, confirming previous studies results (Aravena et al., 2011; Lucas et al., 2019a; Helliwell et al. 2019, Phalempin et al., 2021). Our results confirmed that root diameter might affect multiple soil properties, as previously suggested by Lu et al., 2020.

3.3 Root traits impact on soil bioporosity

The effect of the different root traits on the bioporosity morphology was assessed by combining the

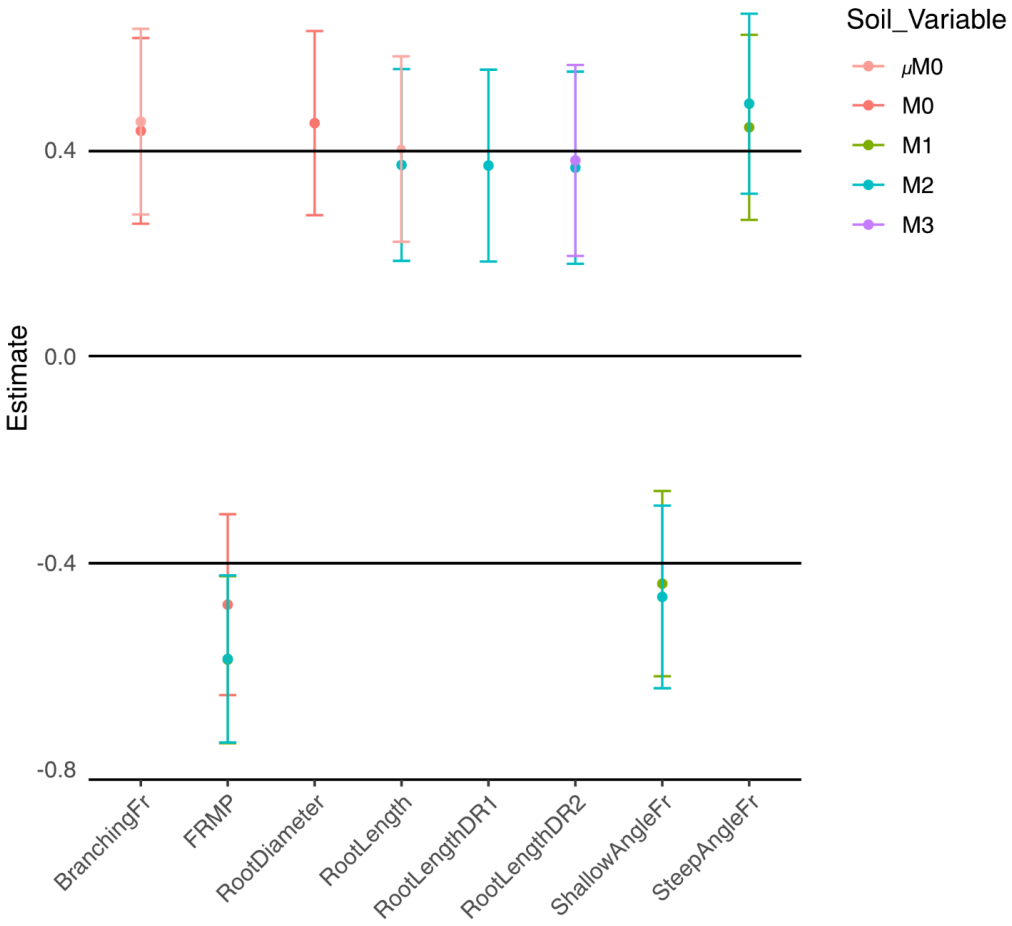

root features of the three genotypes and tested for correlation with each bioporosity parameter. Fig. 12 depicts the root traits that presented a statistically significant effect on bioporosity.

Figure 12. Effect of each root trait on the statistically significant soil morphological parameters obtained by using a mixed linear model, on bioporosity. When a parameter does not show it means it was not statistically significant. Symbols for the root are Avg = Average Root Diameter, Frmp = Fragmented Root Morphological Pattern, NuRT = Number of Root Tips, Per = Perimeter, ShaF/SteepF = Shallow and Steep Angle Frequency, TotaL = Total Root Length, Vol = Root Volume.

At the aggregate scale, branching frequency and root length were positively associated with μM0 ($p < 0.05$). At the cylinder scale, root diameter and branching frequency were positively associated with M0 ($p < 0.05$). FRMP exhibited a strong negative correlation with M0, M1, and M2 ($p < 0.01$). Interestingly, tap root length and root length showed weak positive correlations with M2 and M3 ($p = 0.05$). Shallow angle frequency was negatively associated with M1, M2. In contrast, steep angle frequency was positively correlated with M1 and M2.

*4. **Conclusion***

This study provides further insight into the potential influence of wheat root traits on soil physical properties, particularly on the pore network structure. By combining non-destructive X-ray tomography with 2D root phenotyping, we explored how different genotypes may contribute to modifying soil structure under controlled conditions. While no significant differences were detected in total porosity, our findings suggest that root development can enhance pore connectivity and reduce the percolation threshold, potentially improving water and air transport within the soil. Differences in bioporosity distribution across genotypes and scales indicate that root system morphology, including traits such as diameter, branching frequency, and root length, may play a role in shaping the rhizospheric soil. However, the observed effects appear to be scale-dependent and may vary with root persistence, compaction, and post-harvest decomposition processes. Further research is needed to validate these patterns under field conditions and assess the long-term implications of root traits on soil structure and functionality.

References

Angers, D.A., Caron, J. 1998. Plant-induced changes in soil structure: processes and feedbacks. Biogeochemistry, 42, 55–72. https://doi.org/10.1023/A:1005944025343

Aravena, J.E., Berli, M., Ghezzehei, T.A., Tyler, S.W. 2011. Effects of root-induced compaction on rhizosphere hydraulic properties—X-ray microtomography imaging and numerical simulations. Environ. Sci. Technol., 45, 425–431. https://doi.org/10.1021/es102566j

Armstrong, R.T., McClure, J.E., Robins, V., Liu, Z., Arns, C.H., Schlüter, S., Berg, S. 2018. Porous media characterization using Minkowski functionals: theories, applications and future directions. Transp. Porous Media, 123, 619–649. https://doi.org/10.1007/s11242-018-1201-4

Balashov, E., Bazzoffi, P. 2003. Aggregate water stability of sandy and clayey loam soils differently compacted with and without wheat plants. International Agrophysics, 17, 151–155.

Bardgett, R.D., Mommer, L., De Vries, F.T. 2014. Going underground: root traits as drivers of ecosystem processes. Trends in Ecology & Evolution, 29, 692–699. https://doi.org/10.1016/j.tree.2014.10.006

Bittelli, M., Campbell, G.S., Tomei, F. 2015. Soil Physics with Python: Transport in the Soil-Plant-Atmosphere Continuum. Oxford University Press, Oxford, UK. ISBN: 9780199683093.

Bodner, G., Leitner, D., Kaul, H.P. 2014. Coarse and fine root plants affect pore size distributions differently. Plant Soil, 380, 133–151. https://doi.org/10.1007/s11104-014-2079-8

Brancaccio, R., Bettuzzi, M., Casali, F., Morigi, M.P., Levi, G., Gallo, A., Marchetti, G., Schneberk, D. 2011. Real-time reconstruction for 3D CT applied to large objects of cultural heritage. IEEE Trans. Nucl. Sci., 58, 1864–1871. https://doi.org/10.1109/TNS.2011.2158850

Brussaard, L. 2012. Ecosystem services provided by the soil biota. In: Wall, D.H. (Ed.), Soil Ecology and Ecosystem Services. Oxford University Press, Oxford, UK, 45–58. https://doi.org/10.1093/acprof:oso/9780199575923.003.0005

Buades, A., Coll, B., Morel, J.M. 2011. Non-local means denoising. Image Process. Online, 1, 208–212. https://doi.org/10.5201/ipol.2011.bcm_nlm

Bucksch, A., Burridge, J., York, L.M., Das, A., Nord, E.A., Weitz, J.S., Lynch, J.P. 2014. Image-based high-throughput field phenotyping of crop roots. Plant Physiology, 166, 470–486. https://doi.org/10.1104/pp.114.243519

Burr-Hersey, J.E., Ritz, K., Bengough, G.A., Mooney, S.J. 2020. Reorganisation of rhizosphere soil pore structure by wild plant species in compacted soils. J. Exp. Bot., 71, 6107–6115. https://doi.org/10.1093/jxb/eraa323

Campiglia, E., Mancinelli, R., Radicetti, E., Marinari, S. 2011. Legume cover crops and mulches: effects on nitrate leaching and nitrogen input in a pepper crop (Capsicum annuum L.). Nutr. Cycl. Agroecosyst., 89, 399–412. https://doi.org/10.1007/s10705-010-9404-2

Carminati, A., Moradi, A., Vetterlein, D. 2010. Dynamics of soil water content in the rhizosphere. Plant Soil, 332, 163–176. https://doi.org/10.1007/s11104-010-0283-8

Cheng, S., Feng, C., Wingen, L.U., et al. 2024. Harnessing landrace diversity empowers wheat breeding. Nature, 632, 823–831. https://doi.org/10.1038/s41586-024-07682-9

Childs, E.C., Collis-George, N. 1948. Soil geometry and soil-water equilibria. Discuss. Faraday Soc., 3, 78–85. https://doi.org/10.1039/DF9480300078

Colombi, T., Walter, A. 2017. Genetic diversity under soil compaction in wheat: root number as a promising trait for early plant vigor. Frontiers in Plant Science, 8, 420. https://doi.org/10.3389/fpls.2017.00420

Daigle, H., Reece, J.S., Flemings, P.B. 2019. Evolution of the percolation threshold in muds and mudrocks during burial. Geophys. Res. Lett., 46, 5966–5973. https://doi.org/10.1029/2019GL083723

Dal Ferro, N., Sartori, L., Simonetti, G., Berti, A., Morari, F. 2014. Soil macro- and microstructure

as affected by different tillage systems and their effects on maize root growth. Soil Tillage Res., 140, 55–65. https://doi.org/10.1016/j.still.2014.02.003

Daly, K.R., Mooney, S.J., Bennett, M., Crout, N.M.J., Roose, T., Tracy, S.R. 2015. Assessing the influence of the rhizosphere on soil hydraulic properties using X-ray computed tomography and numerical modelling. J. Exp. Bot., 66, 2305–2314. https://doi.org/10.1093/jxb/eru509

De La Fuente Cantó, C., Simonin, M., King, E., Moulin, L., Bennett, M.J., Castrillo, G., Laplaze, L. 2020. An extended root phenotype: the rhizosphere, its formation and impacts on plant fitness. Plant J., 103, 951–964. https://doi.org/10.1111/tpj.14781

Dexter, A.R. 1988. Advances in characterization of soil structure. Soil Tillage Res., 11, 199–238. https://doi.org/10.1016/0167-1987(88)90002-5

Dinno, A. 2024. Conover.test: Conover-Iman Test of Multiple Comparisons Using Rank Sums. R package version 1.1.6.

Giuliani, L.M., Hallett, P.D., Loades, K.W. 2024. Effects of soil structure complexity to root growth of plants with contrasting root architecture. Soil Tillage Res., 238, 106023. https://doi.org/10.1016/j.still.2024.106023

Helliwell, J.R., Sturrock, C.J., Miller, A.J., Whalley, W.R., Mooney, S.J. 2019. The role of plant species and soil condition in the structural development of the rhizosphere. Plant Cell Environ., 42, 1974–1986. https://doi.org/10.1111/pce.13529

Hendriks, P.M., Ryan, P., Hands, P., Rolland, V., Gurusinghe, S., Weston, L., Rebetzke, G., Delhaize, E. 2022. Selection for early shoot vigour in wheat increases root hair length but reduces epidermal cell size of roots and leaves. J. Exp. Bot., 73, 1672–1684. https://doi.org/10.1093/jxb/erac048

Horn, R., Taubner, H., Wuttke, M., Baumgartl, T. 1994. Soil physical properties related to soil structure. Soil Tillage Res., 30, 187–216. https://doi.org/10.1016/0167-1987(94)90005-1

Huang, L.K., Wang, M.J.J. 1995. Image thresholding by minimizing the measures of fuzziness.

Pattern Recognit., 28, 41–51. https://doi.org/10.1016/0031-3203(94)E0043-K

Huang, X., Yang, D., Kang, Z. 2021. Impact of pore distribution characteristics on percolation threshold based on site percolation theory. Physica A: Statistical Mechanics and its Applications, 570, 125800. https://doi.org/10.1016/j.physa.2021.125800

Hunt, A.G., Ewing, R.P., Horton, R. 2013. What's wrong with soil physics? Soil Sci. Soc. Am. J., 77, 1877–1887. https://doi.org/10.2136/sssaj2013.01.0020

Jarvis, N., Larsbo, M., Koestel, J. 2017. Connectivity and percolation of structural pore networks in a cultivated silt loam soil quantified by X-ray tomography. Geoderma, 287, 71–79. https://doi.org/10.1016/j.geoderma.2016.06.026

Kahle, D., Stamey, J. 2017. invgamma: The Inverse Gamma Distribution. R package version 1.1.

Kan, X., Zheng, W., Cheng, J., Zhang, L., Li, J., Liu, B., Zhang, X. 2023. Investigating soil pore network connectivity in varied vegetation types using X-ray tomography. Water, 15, 3823. https://doi.org/10.3390/w15213823

Kapur, J.N., Sahoo, P.K., Wong, A.K.C. 1985. A new method for gray-level picture thresholding using the entropy of the histogram. Comput. Vision Graph. Image Process., 29, 273–285. https://doi.org/10.1016/0734-189X(85)90125-2

Koestel, J. 2018. SoilJ: An ImageJ plugin for the semiautomatic processing of three-dimensional X-ray images of soils. Vadose Zone J., 17, 1–7. https://doi.org/10.2136/vzj2017.03.0062

Koestel, J., Dathe, A., Skaggs, T.H., Klakegg, O., Ahmad, M.A., Babko, M., Giménez, D., Farkas, C., Nemes, A., Jarvis, N. 2018b. Estimating the permeability of naturally structured soil from percolation theory and pore space characteristics imaged by X-ray computed tomography. Water Resour. Res., 54, 2344–2360. https://doi.org/10.1029/2018WR023609

Koestel, J., Larsbo, M., Jarvis, N. 2020. Scale and REV analyses for porosity and pore connectivity measures in undisturbed soil. Geoderma, 366, 114206.

https://doi.org/10.1016/j.geoderma.2020.114206

Koestel, J., Schlüter, S. 2019. Quantification of the structure evolution in a garden soil over the course of two years. Geoderma, 338, 597–609. https://doi.org/10.1016/j.geoderma.2018.12.030

Kravchenko, A.N., Guber, A.K. 2017. Soil pores and their contributions to soil carbon processes. Geoderma, 287, 31–39. https://doi.org/10.1016/j.geoderma.2016.06.027

Kuka, K., Illerhaus, B., Fox, C.A., Joschko, M. 2013. X-ray computed microtomography for the study of the soil–root relationship in grassland soils. Vadose Zone J., 12, 1–10. https://doi.org/10.2136/vzj2013.01.0014

Lal, R. 2009. Soil and world food security. Soil Tillage Res., 102, 1–4. https://doi.org/10.1016/j.still.2008.08.001

Lal, R. 2015. Restoring soil quality to mitigate soil degradation. Sustainability, 7, 5875–5895. https://doi.org/10.3390/su7055875

Le Marié, C.A., York, L.M., Strigens, A., Malosetti, M., Camp, K.H., Giuliani, S., Lynch, J.P., Hund, A. 2019. Shovelomics root traits assessed on the EURoot maize panel are highly heritable across environments but show low genotype-by-nitrogen interaction. Euphytica, 215, 173. https://doi.org/10.1007/s10681-019-2472-8

Leue, M., Uteau-Puschmann, D., Peth, S., Nellesen, J., Kodešová, R., Gerke, H.H. 2019. Separation of soil macropore types in three-dimensional X-ray computed tomography images based on pore geometry characteristics. Vadose Zone J., 18, 180170. https://doi.org/10.2136/vzj2018.09.0170

Liu, J., Regenauer-Lieb, K. 2011. Application of percolation theory to microtomography of structured media: percolation threshold, critical exponents, and upscaling. Phys. Rev. E, 83, 016106. https://doi.org/10.1103/PhysRevE.83.016106

Liu, S., Barrow, C. S., Hanlon, M., Lynch, J. P., Bucksch, A. 2021. DIRT/3D: 3D root phenotyping

for field-grown maize (Zea mays). Plant Physiology, 187(2), 739–757. https://doi.org/10.1093/plphys/kiab311

Logsdon, S.D. 2013. Root effects on soil properties and processes: synthesis and future research needs. Adv. Agric. Syst. Model., 4, 173–196. https://doi.org/10.2134/advagricsystmodel4.c8

Lu, J., Zhang, Q., Werner, A.D., Li, Y., Jiang, S., Tan, Z. 2020. Root-induced changes of soil hydraulic properties–A review. J. Hydrol., 589, 125203. https://doi.org/10.1016/j.jhydrol.2020.125203

Lucas, M., Schlüter, S., Vogel, H.J., Vetterlein, D. 2019a. Roots compact the surrounding soil depending on the structures they encounter. Sci. Rep., 9, 16236. https://doi.org/10.1038/s41598-019-52665-w

Lucas, M., Schlüter, S., Vogel, H.J., Vetterlein, D. 2019b. Soil structure formation along an agricultural chronosequence. Geoderma, 350, 87–97. https://doi.org/10.1016/j.geoderma.2019.04.041

Lucas, M. 2022. Perspectives from the Fritz-Scheffer Awardee 2020—The mutual interactions between roots and soil structure and how these affect rhizosphere processes. J. Plant Nutr. Soil Sci., 185, 8-18.

Lynch, J.P. 2022. Harnessing root architecture to address global challenges. Plant J., 109, 415–431. https://doi.org/10.1111/tpj.15560

Maccaferri, M., El-Feki, W., Nazemi, G., Salvi, S., Canè, M.A., Colalongo, M.C., Stefanelli, S., Tuberosa, R. 2016. Prioritizing quantitative trait loci for root system architecture in tetraploid wheat. J. Exp. Bot., 67, 1161–1178. https://doi.org/10.1093/jxb/erw039

Marone, D., Russo, M.A., Mores, A., Ficco, D.B., Laidò, G., Mastrangelo, A.M., Borrelli, G.M. 2021. Importance of landraces in cereal breeding for stress tolerance. Plants, 10, 1267. https://doi.org/10.3390/plants10071267

Mawodza, T., Burca, G., Casson, S., Menon, M. 2020. Wheat root system architecture and soil

moisture distribution in an aggregated soil using neutron computed tomography. Geoderma, 359, 113988. https://doi.org/10.1016/j.geoderma.2019.113988

Mazzucotelli, E., et al. 2020. The global durum wheat panel (GDP): an international platform to identify and exchange beneficial alleles. Front. Plant Sci., 11, 569905. https://doi.org/10.3389/fpls.2020.569905

Meysman, F.J.R., Middelburg, J.J., Heip, C.H.R. 2006. Bioturbation: a fresh look at Darwin's last idea. Trends Ecol. Evol., 21, 688–695. https://doi.org/10.1016/j.tree.2006.08.002

Montanarella, L., Panagos, P. 2021. The relevance of sustainable soil management within the European Green Deal. Land Use Policy, 100, 104950. https://doi.org/10.1016/j.landusepol.2020.104950

Mooney, S.J., Pridmore, T.P., Helliwell, J., Bennett, M.J. 2012. Developing X-ray computed tomography to non-invasively image 3-D root systems architecture in soil. Plant Soil, 352, 1–22. https://doi.org/10.1007/s11104-011-1039-9

Nitzbon, J., Gadylyaev, D., Schlüter, S., Köhne, J.M., Grosse, G., Boike, J. 2022. Brief communication: Unravelling the composition and microstructure of a permafrost core using X-ray computed tomography. Cryosphere, 16, 3507–3517. https://doi.org/10.5194/tc-16-3507-2022

Ober, E.S., et al. 2021. Wheat root systems as a breeding target for climate resilience. Theor. Appl. Genet., 134, 1645–1662. https://doi.org/10.1007/s00122-021-03819-w

Otsu, N. 1979. A threshold selection method from gray-level histograms. IEEE Trans. Syst. Man Cybern., 9, 62–66. https://doi.org/10.1109/TSMC.1979.4310076

Pagliai, M., Vignozzi, N. 2002. The soil pore system as an indicator of soil quality. Adv. GeoEcol., 35, 69–80.

Phalempin, M., Lippold, E., Vetterlein, D., Schlüter, S. 2021. Soil texture and structure heterogeneity predominantly governs bulk density gradients around roots. Vadose Zone J.,

20, 5. https://doi.org/10.1002/vzj2.20147

Prewitt, J.M.S., Mendelsohn, M.L. 1966. The analysis of cell images. Ann. N.Y. Acad. Sci., 128, pp.1035–1053. https://doi.org/10.1111/j.1749-6632.1965.tb11715.x

Prince S, Anower MR, Motes CM, Hernandez TD, Liao F, Putman L, Mattson R, Seethepalli A, Shah K, Komp M, Mehta P, York LM, Young C and Monteros MJ. 2022 Intraspecific variation for leaf physiological and root morphological adaptation to drought stress in Alfalfa (Medicago sativa L.). Front. Plant Sci., 13, 795011. https://doi.org/10.3389/fpls.2022.795011

Rabot, E., Wiesmeier, M., Schlüter, S., Vogel, H.J. 2018. Soil structure as an indicator of soil functions: A review. Geoderma, 314, 122–137. https://doi.org/10.1016/j.geoderma.2017.11.009

Renard, P., Allard, D. 2013. Connectivity metrics for subsurface flow and transport. Adv. Water Resour., 51, 168–196. https://doi.org/10.1016/j.advwatres.2011.12.001

Ridler, T.W., Calvard, S. Picture thresholding using an iterative selection method. IEEE Trans. Syst. Man Cybern., 8 (1978), pp. 630–632. https://doi.org/10.1109/TSMC.1978.4310039https://doi.org/10.1109/TSMC.1978.4310039

Ritchie H. and Roser M. (2019) - “Land Use” Published online at OurWorldinData.org. Retrieved from: 'https://ourworldindata.org/land-use' [Online Resource]

RStudio Team. 2020. RStudio: Integrated Development Environment for R. RStudio, PBC., Boston, MA.

San Josè Martinez, F., Munoz Ortega, F.J., Caniego Monreal, F.J., Kravchenko, A.N., Wang, W. 2015. Soil aggregate geometry: Measurements and morphology. Geoderma, 237, 36–48. https://doi.org/10.1016/j.geoderma.2014.08.003

Schindelin, J., Arganda-Carreras, I., Frise, E., et al. 2012. Fiji: an open-source platform for biological-image analysis. Nat. Methods, 9, 676–682. https://doi.org/10.1038/nmeth.2019

Schlüter, S., Albrecht, L., Schwärzel, K., Kreiselmeier, J. 2020. Long-term effects of conventional tillage and no-tillage on saturated and near-saturated hydraulic conductivity – can their prediction be improved by pore metrics obtained with X-ray CT? Geoderma, 361, 114082. https://doi.org/10.1016/j.geoderma.2019.114082

Schlüter, S., Sheppard, A., Brown, K., Wildenschild, D. 2014. Image processing of multiphase images obtained via X-ray microtomography: a review. Water Resour. Res., 50, 3615–3639. https://doi.org/10.1002/2014WR015256

Scholl, P., Leitner, D., Kammerer, G., Loiskandl, W., Kaul, H.P., Bodner, G. 2014. Root-induced changes of effective 1D hydraulic properties in a soil column. Plant Soil, 381, 193–213. https://doi.org/10.1007/s11104-014-2119-4

Seethepalli, A., Dhakal, K., Griffiths, M., Guo, H., Freschet, G.T., York, L.M. 2021. RhizoVision Explorer: Open-source software for root image analysis and measurement standardization. AoB Plants, 13, Article plab056. https://doi.org/10.1093/aobpla/plab056

Shiferaw, B., Smale, M., Braun, H.J., Duveiller, E., Reynolds, M., Muricho, G. 2013. Crops that feed the world 10. Past successes and future challenges to the role played by wheat in global food security. Food Sec., 5, 291–317. https://doi.org/10.1007/s12571-013-0263-y

Soto-Gómez, D., Juíz, L.V., Pérez-Rodríguez, P., López-Periago, J.E., Paradelo, M., Koestel, J. 2020. Percolation theory applied to soil tomography. Geoderma, 357, 113959.https://doi.org/10.1016/j.geoderma.2019.113959

Trachsel, S., Kaeppler, S.M., Brown, K.M., Lynch, J.P. 2011. Shovelomics: high throughput phenotyping of maize (Zea mays L.) root architecture in the field. Plant Soil, 341, 75–87. https://doi.org/10.1007/s11104-010-0623-8

Tracy, S.R., Black, C.R., Roberts, J.A. 2012. Quantifying the effect of soil compaction on three varieties of wheat (Triticum aestivum L.) using X-ray micro computed tomography (CT). Plant Soil, 353, 195–208. https://doi.org/10.1007/s11104-011-1022-5

Vogel, H.J., Weller, U., Schlüter, S. 2010. Quantification of soil structure based on Minkowski functions. Comput. Geosci., 36, 1236–1245. https://doi.org/10.1016/j.cageo.2010.03.007

Wasson, A.P., Richards, R.A., Chatrath, R., Misra, S.C., Prasad, S.S., Rebetzke, G.J., ... Watt, M. 2012. Traits and selection strategies to improve root systems and water uptake in water-limited wheat crops. J. Exp. Bot., 63(9), 3485–3498. https://doi.org/10.1093/jxb/ers111

Wei, X., Guo, S., Ma, B., Palta, J.A., Ma, Y., Li, P. 2024. Wheat yield improvement is associated with altered root systems during cultivar replacement. Eur. J. Agron., 154, 127101. https://doi.org/10.1016/j.eja.2024.127101

Weihs, B.J., Tang, Z., Tian, Z., Heuschele, D.J., Siddique, A., Terrill, T.H., Zhang, Z., York, L.M., Samac, D., Zhang, Z., Xu, Z. 2024. Phenotyping alfalfa (Medicago sativa L.) root structure architecture via integrating confident machine learning with ResNet-18. Plant Phenomics. https://doi.org/10.34133/plantphenomics.0251

Wendel, A.S., Bauke, S.L., Amelung, W., Knief, C. 2022. Root-rhizosphere-soil interactions in biopores. Plant Soil, 475, 253–277. https://doi.org/10.1007/s11104-022-05406-4

Whalley, W.R., Riseley, B., Leeds-Harrison, P.B., Bird, N.R.A., Leech, P.K., Adderley, W.P. 2005. Structural differences between bulk and rhizosphere soil. Eur. J. Soil Sci., 56, 353–360. https://doi.org/10.1111/j.1365-2389.2004.00670.x

Wingen, L.U., Orford, S., Goram, R., Leverington-Waite, M., Bilham, L., Patsiou, T.S., Ambrose, M., Dicks, J., Griffiths, S. 2014. Establishing the AE Watkins landrace cultivar collection as a resource for systematic gene discovery in bread wheat. Theor. Appl. Genet., 127, 1831–1842. https://doi.org/10.1007/s00122-014-2344-5

Xiong, P., Zhang, Z., Peng, X. 2022. Root and root-derived biopore interactions in soils: A review. J. Plant Nutr. Soil Sci., 185(5), 643–655. https://doi.org/10.1002/jpln.202200003

Xu, Z., York, L. M., Seethepalli, A., Bucciarelli, B., Cheng, H., Samac, D. A. 2022. Objective phenotyping of root system architecture using image augmentation and machine learning in alfalfa (Medicago sativa L.). Plant Phenomics, 9879610.

https://doi.org/10.34133/2022/9879610

Yen, J.C., Chang, F.J., Chang, S. 1995. A new criterion for automatic multilevel thresholding. IEEE Trans. Image Process., 4, 370–378. https://doi.org/10.1109/83.366472

Young, I.M., Crawford, J.W., Rappoldt, C. 2001. New methods and models for characterising structural heterogeneity of soil. Soil Tillage Res., 61, 33–45. https://doi.org/10.1016/S0167-1987(01)00188-X

Young, I.M., Mooney, S.J., Heck, R.J., Peth, S. 2022. 40 years of X-ray CT in soil: Historical context. X-ray imaging of the soil porous architecture. Springer International Publishing. https://doi.org/10.1007/978-3-031-12176-0

Zagaglia, G. 2012. Sviluppo di un sistema tomografico trasportabile per analisi in situ di reperti paleoantropologici. Tesi di laurea magistrale, Università di Bologna, Bologna, Italia.

Acknowledgements

The research was partially funded by the project WISH-ROOTS- "Tuning the wheat root microbiome to improve soil health and optimize rhizosphere nitrogen cycling and availability" is supported by the European Join Programme Soil ERA- NET (HORIZON 2020) research and innovation programme. MCHS gratefully acknowledges funding support from the Biotechnology and Biological Sciences Research Council (BBSRC), project BB/X003000/1. Funding was also provided by the Department of Agricultural and Food Sciences, University of Bologna, through its Ph.D programme. We thank Roberto Tuberosa for useful discussion and for participation in the development and implementation of the funded project. We are also grateful to Marco Maccaferri for providing the seeds of the cultivar Senatore-Cappelli and for useful discussions, to the John Innes Centre Germplasm Resources Unit for providing the seeds of the Paragon and Watkins238 cultivars, and to Simon Griffiths and Luzie Wingen for advice on the relevance of these cultivars.

Additional support to Bartolo Giuseppe Dimattia was provided by the Collegio Superiore and the Institute of Advanced Studies of the University of Bologna, whose contribution is gratefully acknowledged.

Author contributions statement

B.G.D. contributed to the writing of the funded project, conceived the experiment, followed all the agronomic practices and management practices, collected samples and data, analyzed the data and contributed to the writing of the paper, A.R. collected the samples, performed X-ray measurements, image and statistical analysis and contributed to the writing of the paper , M.B, M.P.M. and R.B are responsible for the X-ray center and performed the X-ray imaging, J.K. is the developer of the SoilJ plugin used for image analysis, contributed to image analysis and manuscript review and writing, S.S. is the responsible for the Bologna group of the project and contributed to the field experiment, M.C.H.S is the coordinator of the project and contributed to manuscript review, and M.B contributed to data analysis and writing of the paper.

Chapter 3

Wheat genotypic variation in root architecture modifies soil pore structure and hydraulic properties

Bartolo Giuseppe Dimattia[1], Marco Bittelli[1], Fausto Tomei[2], Roberto Tuberosa[1], and Maria C. Hernandez-Soriano[3]*

[1]Department of Agricultural and Food Sciences, University of Bologna, Viale Fanin 44, 40125, Bologna, Italy

[2] Regional Agency for Environmental Protection and Energy, Emilia-Romagna Region, Viale Silvani 6, 40122, Bologna, Italy.

[3]John Innes Centre, Norwich Research Park, Norwich, NR4 7UH, United Kingdom

*Corresponding author: bartolo.dimattia2@unibo.it

Currently under review in Geoderma

Abstract

This study examined how contrasting root architectures of four wheat genotypes, two modern cultivars (Paragon, Bologna) and two landraces (Watkins 238, Senatore Cappelli), modify soil hydraulic behaviour under field conditions. Baseline (pre-sowing), bulk (fallow), and rhizosphere soils were characterised for water retention, unsaturated hydraulic conductivity, and pore size distributions derived from fitted retention curves. Root morphological traits were quantified using crown imaging and root scanning.

Genotypes differed markedly in both root traits and their associated hydraulic responses. Paragon, Watkins 238, and Senatore Cappelli exhibited bimodal pore size distributions, whereas Bologna, baseline, and bulk soil displayed unimodal behaviour, indicating a less heterogeneous pore structure. Watkins 238 achieved the most significant improvement in hydraulic properties, increasing plant-available water to 0.21 $m^3\ m^{-3}$ (vs. 0.15 $m^3\ m^{-3}$ in baseline), driven by a lower permanent wilting point (0.12 $m^3\ m^{-3}$) and higher field capacity (0.34 $m^3\ m^{-3}$). Watkins 238 also displayed higher unsaturated conductivity, with hydraulic conductivity at field capacity and wilting point significantly higher than baseline and Bologna, and an area under the $K(\psi)$ curve of 46.1, more than double that of other genotypes.

Root network area, root diameter, and branching frequency were significantly correlated with water retention parameters and conductivity metrics, indicating that root systems reshape the pore network and soil hydrological properties. These findings suggest genotype-specific modification of hydraulic processes and highlight opportunities to leverage root traits to enhance water availability and resilience under water-limited conditions.

1. Introduction

Soil health underpins agricultural productivity and resilience to climate variability, with the regulation of water availability being a central function (Bronick and Lal, 2005; Doran and Parkin, 2015). This regulation is governed by soil structure and pore network connectivity, which control water infiltration, retention, and redistribution through the soil matrix (Dexter, 2004; Young and Ritz, 2005; Rabot et al., 2018). These physical attributes strongly influence plant water supply and susceptibility to erosion or waterlogging (Bordoloi et al., 2019).

Soil hydraulic properties provide a quantitative framework for describing water retention and flow. Advances in measurement and modelling now enable improved characterisation of pore-scale processes and hydraulic behaviour (Bezerra-Coelho et al., 2018). Soil hydraulic properties are governed by soil pore architecture and mediate water retention and transport; in vegetated systems, roots and associated biota modify pore networks, thereby altering hydraulic behaviour (Lu et al., 2020).

Water retention and flow in unsaturated soils depend on the relationship between water content, water potential, and hydraulic conductivity (Bittelli et al., 2015). Saturated hydraulic conductivity (K_s) describes water transmission through saturated soil, underpinning infiltration and runoff dynamics (Hillel, 1998; Jury and Horton, 2004), while water retention and unsaturated conductivity are essential for modelling water and solute transport, as accurate parameterisation is required to solve Richards' equation (Mualem, 1976; van Genuchten, 1980). Consequently, soil hydraulic properties are foundational for estimating soil water budgets and have broad applications in hydrology and agriculture (Lal and Shukla, 2004; Šimůnek et al., 2024).

Root systems play a central role in shaping soil structure and hydraulic properties by influencing aggregation, pore formation, and water flow through mechanical and biochemical processes (Bengough et al., 2011; Gregory, 2006; Hallett et al., 2022; Lynch, 1995). Through growth,

turnover, and interactions with the soil matrix, roots drive soil structural evolution and exhibit substantial complexity and plasticity, reflecting adaptation to heterogeneous soil environments (Hodge et al., 2009; Grossman and Rice, 2012). Beyond enabling anchorage, resource uptake, and carbohydrate storage (Evert, 2006), roots act as ecosystem engineers, exerting mechanical forces, depositing organic compounds, and altering pore continuity as they explore the soil. This architectural plasticity supports plant responsiveness to biotic and abiotic stresses (Bardgett et al., 2014), thereby reshaping pore architecture and water flow pathways. Advancing our understanding of root–soil interactions and their consequences for soil structure is therefore critical for enhancing soil hydraulic functionality and supporting long-term agricultural sustainability (Dexter, 2004).

The rhizosphere, the narrow zone of soil directly influenced by root activity, is a dynamic interface where biological processes actively reshape soil structure and hydrology (Wang et al., 2022). Penetration and radial expansion of roots modify the physical arrangement of the soil matrix by creating new pore spaces and altering the size distribution and connectivity of existing pore networks (Bengough et al., 2011; Jin et al., 2013). These physical modifications have immediate effects on soil water infiltration and drainage, but also create lasting changes to soil hydraulic properties, including soil water retention capacity, permeability, and aeration (Bronick and Lal, 2005). Root exudates and organic compounds further modify the soil environment by influencing aggregate stability and pore architecture, amplifying the structural legacy that persists after root senescence (Carminati and Vetterlein, 2013).

While interspecific differences in root–soil interactions have been explored (Helliwell et al., 2017; Staszel-Szlachta et al., 2024), emerging evidence indicates that genotypes within a single crop species can also differ in their capacity to alter pore structure (Koebernick et al., 2019; Lucas et al., 2019; Zhou et al., 2021). In wheat, documented genotypic variation in root system architecture (RSA) and rhizodeposition suggests the potential for divergent impacts on soil physical properties (Bodner et al., 2014; White et al., 2015; Corneo et al., 2016; Fradgley et al., 2020). Building on our previous

findings that wheat genotypes vary in root morphology and near-root soil structure (Dimattia et al., 2025), this study investigates whether such variation translates into measurable differences in soil hydraulic properties.

The physical influence of roots on soil occurs through multiple interacting mechanisms. During growth, roots mechanically rearrange soil particles, create new macropores (>30 μm) through penetration, and can either clog existing pores or facilitate their formation depending on root diameter and branching patterns (Bodner et al., 2014; Lu et al., 2020). Root activity also modifies soil aggregation, causing macro-aggregate (>250 μm) fragmentation in the rhizosphere while promoting micro-aggregate (2–250 μm) formation through the binding effects of root exudates and associated microbial activity (Hallett et al., 2022). Following senescence, decomposing roots leave behind bio-channels that enhance macroporosity and create preferential flow paths (Bodner et al., 2014).

While the effects of agricultural management on soil hydraulic properties are well documented (Blanco-Canqui et al., 2007; Strudley et al., 2008), root-induced modifications remain challenging to quantify, particularly under field conditions and at larger spatial scales. This difficulty arises because root morphological traits—including diameter, density, and architectural configuration—can have contrasting effects on water retention and hydraulic conductivity depending on soil texture, moisture conditions, and the stage of root development or decay (Carminati et al., 2016; Lu et al., 2020)

However, quantifying root architecture under field conditions is essential for understanding its influence on soil physical processes, as field-based phenotyping approaches provide realistic measures of root system expression and spatial organisation (Trachsel et al., 2011).

In this study, we investigate how contrasting wheat root traits influence soil structure and hydraulic behaviour. We quantified root architecture under field conditions and measured soil hydraulic properties in the laboratory, enabling an assessment of genotype-specific effects on pore structure and water flow. These datasets were integrated to identify key relationships between root traits and hydraulic parameters, providing insight into the mechanisms by which roots modulate soil hydraulic properties.

2. Materials and methods

2.1 Field trial and wheat genotypes

The field experiment was conducted at the DISTAL experimental farm (Department of Agricultural and Food Sciences, University of Bologna) in Cadriano (Bologna, Italy; 44.5491° N, 11.4130° E). The climate is subhumid, characterised by a mean annual temperature of 12.8 °C and an average annual precipitation of 924 mm.

Baseline physical and chemical soil properties were characterised prior to the experiment (Supplementary Table 1). Baseline soil hydraulic properties were assessed by collecting three undisturbed soil cores before sowing using standard sampling cylinders, following the procedure described by Lipovetsky et al. (2020).

Four wheat genotypes were used to evaluate the influence of root systems on soil hydraulic properties: Watkins 238 (landrace bread wheat), Paragon and Bologna (modern elite bread wheat cultivars), and Senatore Cappelli (durum wheat landrace). These genotypes represent phylogenetically distinct material from both hexaploid and tetraploid wheat collections (Wingen et al., 2014; Maccaferri et al., 2019). They were selected following a preliminary screening of root morphology performed on 20 wheat genotypes, for which principal component analysis (Supplementary Fig. 1) identified the greatest divergence in root architectural traits. All four genotypes were included in the experiment to assess soil hydraulic properties and associated soil

parameters. The field trial was arranged in randomised complete block design with three replicates per genotype. The wheat genotypes were cultivated in plots of 6 m^2, each sown-on November 26, 2022, at a density of 23 g of seeds per m^2. The experimental area had not undergone any tillage operations for the previous two years. During the growing season, nitrogen fertiliser was applied twice at a rate of 24 kg N ha^{-1} per application: the first during the tillering stage on February 13, 2023, and the second at stem elongation on April 17, 2023.

2.2 Root characterization

Soil monoliths (40 cm length × 30 cm depth) were excavated at the flowering stage from each plot and root systems were carefully washed. For each plot, three representative plants were selected to capture the typical phenotypic expression of the genotype under field conditions. Plants were chosen based on key morphological criteria (tiller number, plant height, root dimensions) that reflect the primary drivers of root–soil interactions. Individuals exhibiting visible abnormalities (e.g., pest damage, disease symptoms, lodging, mechanical injury) were excluded to avoid confounding effects unrelated to genotype performance. This targeted selection approach is consistent with standard field sampling practices for root and rhizosphere characterisation, where destructive sampling imposes practical limitations, and the aim is to represent the modal phenotype rather than outliers (Trachsel et al., 2011; York et al., 2018). Root crown imaging and individual root component scanning were conducted according to the methodology described by Dimattia et al. (2025), which includes frontal and rotated image acquisition for root crown architecture and high-resolution scanning of seminal and nodal roots in water-filled chambers (Supplementary Fig. 2).

Root image analysis was performed using RhizoVision Explorer, an established platform for quantitative characterisation of root traits (Seethepalli et al., 2021). Crown images were subjected to whole-root architectural analysis, extracting traits describing overall spatial occupation and orientation, including root network area, convex area, morphological fragmentation patterns, and root

angle (shallow vs. steep) consistent with the framework of Le Marié et al. (2019). Scanned root components were analysed using the broken-root analysis to quantify dimensional and branching attributes, following trait definitions commonly adopted in root phenotyping research (Freschet et al., 2021; Dimattia et al., 2025). Extracted metrics included total scanned root length, diameter-class lengths (<0.45 mm and >0.45 mm), average and maximum diameter, number of root tips and branching points, and branching frequency. Root morphology data for Paragon, Cappelli, and Watkins 238 have been previously reported in Dimattia et al. (2025) and are incorporated here to enable a broader comparative assessment of genotype performance within the expanded experimental framework.

2.3 Soil sampling and measurement of hydraulic properties

Undisturbed soil cores (inner diameter 8 cm, height 5 cm) were collected using standard sampling cylinders (Lipovetsky et al., 2020). At the end of the growing season, we collected soil cores (10-15 cm depth) per genotype and per plot from within the crop row to capture soil influenced by root activity. To provide a reference baseline, three bulk-soil cores were collected from the inter-row area at an equivalent depth, representing soil minimally influenced by roots.

Saturated and unsaturated soil hydraulic properties were measured using a combination of established laboratory techniques. Soil water retention curves (SWRCs) were determined using the evaporation method (Wind, 1968) and the dew point potentiometer technique (Campbell et al., 2007). Saturated hydraulic conductivity was measured using the constant head method, a widely applied approach for core-scale saturated flow assessment (Klute and Dirksen, 2018). Unsaturated hydraulic conductivity (K) was derived by applying an inverse solution of Richard's equation to data obtained from the evaporation experiment, following the approach of Peters and Durner (2008).

Saturated hydraulic conductivity was measured using the constant head method (pressure head = 5 cm) with the KSAT system (METER Group AG, Munich), following the procedure described

by Sarkar et al. (2019). Before measurement, soil cores were saturated for 72 h to ensure complete water filling of the pore space. K_s values were replicated three times for each core and subsequently normalised to a reference temperature of 10 °C to correct for the effect of water viscosity on flow rate, in accordance with standard practice for comparative hydraulic analysis (Klute and Dirksen, 2018). After K_s determination, soil cores were re-saturated for 12–24 h to restore uniform hydration before subsequent hydraulic measurements.

SWRCs and K from 0 to approximately 120 J kg^{-1} were determined using the HYPROP2 evaporation method (METER Group Inc., Pullman, WA, USA), following the procedures described by (Peters and Durner, 2008) and (Schindler et al., 2010). During these measurements, the mass of the soil cores and the matric potential values were recorded every 10 min using two tensiometers inserted at different depths in each core. The analysis was terminated upon reaching the air entry point of the ceramic plates in the tensiometers, as indicated by the system's measurement protocol. At this stage, the entire sample, including the sampling cylinder, was weighed to determine its wet mass. The evaporation method yields matric potential measurements down to 120 J kg^{-1}, limited by the air entry value of the ceramic tensiometers. To extend the measurement range to lower water potentials, a dew point potentiometer was employed (Singh and Verdi, 2024).

Upon completion of the HYPROP2 analysis, each soil core was vertically bisected. Three subsamples were collected from the inner portion of the core for subsequent determination of water potential using a dew point potentiometer (WP4C, Meter Group Inc., USA). These subsamples were taken from: (i) the upper distal section, representing the driest zone, (ii) the central section, corresponding to intermediate moisture conditions; and (iii) the lower distal section at the height of the smaller tensiometer, where water content remained comparatively higher (Singh and Verdi, 2024).

Those subsamples were analysed with the WP4C device to determine their water potential. To measure the water content value, the subsamples were dried at 105.5 °C for 24 h after the WP4C

analysis, along with the remaining soil from the cylinder (excluding the subsamples). The dried subsamples were reintegrated with the primary core to calculate the total dry weight of the soil sample.

2.4 Parameterisation of the unsaturated hydrological properties

Soil water retention curves were parameterised using the bimodal van Genuchten model (Durner, 1994; Seki et al., 2022) to account for dual-pore systems influenced by root architecture. This model is suitable for capturing the structural and textural pore domains typically associated with root channels and soil aggregates.

(Durner, 1994)

$$S_e = \frac{\theta - \theta_r}{\theta_s - \theta_r} = \sum_{i=1}^{k} w_i \left[\frac{1}{[1 + (\alpha_i |\psi|)^{n_i}]^{m_i}} \right] \quad (1)$$

where S_e [-] is the degree of saturation, θ [m^3 m^{-3}] is the water content, θ_s [m^3 m^{-3}] is the saturated water content, θ_r [m^3 m^{-3}] is the residual water content, ψ [J kg^{-1}] is the matric potential, α is the inverse of the air-entry potential [kg J^{-1}], n [-] and m [-] are shape parameters determining the curve steepness and shape, where m = 1 - 1/n.

Field capacity (FC) and permanent wilting point (PWP) were computed from the soil water retention curve as:

$$FC = \theta(\psi = 33\, J\, kg^{-1})$$

$$PWP = \theta(\psi = 1500\, J\, kg^{-1})$$

Plant-available water (PAW) was then calculated as:

$$PAW = FC - PWP$$

Soil water potential is reported in absolute values in this study to facilitate curve-fitting procedures and graphical representation on logarithmic scales. Further details on parameter interpretation can be found in Durner (1994) and van Genuchten et al. (1992).

The fitting routine of Bittelli et al. (2015) was adapted to allow bimodal parameterisation, in which a weighting factor assigns the relative contribution of each pore domain.

$$K(\psi) = K_s S_e(\psi)^{\tau} \left[\sum_{i=1}^{k} w_i \left(1 - \left(1 - S_i(\psi)^{\frac{1}{m_i}} \right)^{m_i} \right) \right]^{r} \quad (2)$$

where $K(\psi)$ is the unsaturated hydraulic conductivity [kg s m^{-3}], K_s is the saturated conductivity [kg s m^{-3}], τ is the tortuosity parameter, and r is a parameter determined by the model used for integration of the pore size distribution (Bittelli et al., 2015). Empirical parameters l=0.5 and r=2 were used, reflecting values commonly applied in hydraulic conductivity models and selected here to ensure comparability with previous studies and to reduce parameter uncertainty. Unsaturated hydraulic conductivity was estimated using a custom Python implementation and compared against experimental observations. Further analyses of the SWRCs were carried out to evaluate model performance and hydraulic behaviour (Bittelli et al., 2015).

To investigate the effect of root traits on pore-size distribution, matric potential values from the SWRCs were converted to equivalent pore-size radii using the capillary equation (Jury and Horton, 2004). Numerical differentiation of the resulting function was then used to derive a pore-size probability density function (PDF). Indeed, by employing the capillary model approximation, the SWRCs can be interpreted as a pore size distribution, with water occupying larger pores at low matric potential and progressively smaller pores as potential increases (Durner, 1994; Tuller et al., 1999). Rearrangement of the capillary equation allows direct estimation of pore radius from matric potential, enabling quantification of root-induced shifts in pore structure.

$$r_c = \frac{2\gamma cos\beta}{\rho_l \psi_m} \quad (3)$$

where r_c is the pore radius, γ is the surface tension of water [72 * 0.001 N m^{-1}], ρ_l is the density of water [1000 kg m^{-3}], β is the contact angle [30°] converted to radians for solution of eq. 3 and ψ_m [J kg^{-1}] is the soil matric potential. Constant values are selected based on typical values for soils (Bittelli et al., 2015). Parameterisation of the SWRCs provided a continuous function of matric potential, which was converted to a cumulative pore-radius distribution (Eq. 3). The pore-size probability density function (PDF) was derived using five-point numerical differentiation with Lagrange polynomials (Burden and Faires, 1997; Bittelli et al., 2015). For bimodal distributions, the PDF exhibited two modes, whose peak positions were identified from the second derivative of the curve. The bimodal van Genuchten model was fitted independently to each of the three SWRCs replicates, and the resulting parameter estimates were treated as experimental units to preserve statistical independence for genotype comparisons and avoid pseudoreplication.

The slope of the hydraulic conductivity curve between FC and PWP in log–log space was calculated as an indicator of the decline in conductivity across the PAW range (Ahuja et al., 1985; Rawls et al., 1998). In addition, the area under the predicted K(ψ) curve (AUC) was determined by trapezoidal integration to provide an integrated measure of unsaturated hydraulic conductivity (Alexander and Skaggs, 1986). Together, slope and AUC complement point-based metrics (e.g., K_{FC} , K_{WP}) by summarising hydraulic behaviour across the full potential range.

2.5 Statistical Analysis

Data normality was evaluated using the Shapiro-Wilk test and QQ plots. To satisfy normality assumptions and stabilise variance, hydraulic parameters describing soil water retention and conductivity were log10-transformed prior to analysis. For brevity, these variables are referred to without the log-prefix throughout the text. Conversely, volumetric water content parameters (FC,

PWP, PAW) and weighting coefficients (w0, w1) were analysed in their original linear scale, as they vary within a narrow numerical range and meet parametric assumptions (Liu and Lennartz, 2019). Differences among genotypes were assessed using ANOVA for soil physical parameters and root phenotypic traits, followed by Tukey's post-hoc test where significant effects were detected.

To examine associations between root traits and soil hydraulic properties, mixed linear models (LMMs) were fitted, each testing the influence of a single root trait on a corresponding soil variable. Statistical significance was set at $p < 0.05$.

3. Results

3.1 Wheat genotypes differed in root morphological and topological traits

Root traits of Paragon, Cappelli, and Watkins 238 were previously characterised in a related study (Dimattia et al., 2025). Here, we extend the analysis by including the Bologna genotype and integrating the dataset to examine genotype-driven effects on soil hydraulic properties. Significant genotypic variation was observed across multiple root morphological and topological traits (Table 1).

Bologna exhibited the most compact root system, with significantly smaller network area than Paragon ($p < 0.05$) and Cappelli ($p < 0.01$), and smaller convex area than Cappelli ($p < 0.01$). Bologna also showed lower fragmented root morphological pattern (FRMP) values than Paragon ($p < 0.05$) and Watkins 238 ($p < 0.01$), with consistently higher steep-angle frequencies than all other genotypes ($p < 0.05$).

Table 1. Root morphological and topological traits across four wheat genotypes. Whole root analysis characterises overall root system architecture (network area, convex area, angular distribution, fragmentation). Broken root analysis quantifies individual root segments (length, diameter, branching). Values are means ± standard error. FRMP, fragmented root morphological pattern; D1, root length with diameter < 0.45 mm; D2, root length with diameter > 0.45 mm. Significance based

on ANOVA: *p < 0.1, **p < 0.05, ***p < 0.01; ns, not significant. Data for Paragon, Senatore Cappelli, and Watkins 238 were previously reported in Dimattia et al. (2025).

Root Trait	p-value	Paragon	Senatore Cappelli	Watkins 238	Bologna
	Whole root analysis				
Network area (mm2)	**	4435 ± 361	5667 ± 391	4145 ± 454	2359 ± 381
Convex area (mm2)	**	15002 ± 1460	16291 ± 2206	14714 ± 1659	11315 ± 1724
Shallow angle frequency	ns	0.22 ± 0.02	0.24 ± 0.01	0.23 ± 0.01	0.19 ± 0.02
Steep angle frequency	ns	0.51 ± 0.02	0.46 ± 0.01	0.48 ± 0.02	0.53 ± 0.02
FRMP	*	451 ± 27	637 ± 86	636 ± 75	295 ± 51
	Broken root analysis				
Root tips	***	894 ± 127	506 ± 60	237 ± 45	434 ± 32
Total root length (mm)	***	6086 ± 828	3200 ± 416	1353 ± 322	3479 ± 273
Root length D2 (> 0.45mm)	***	1157 ± 100	546 ± 175	283 ± 42	524 ± 43
Root length D1 (< 0.45 mm)	***	4928 ± 734	2654 ± 743	1170 ± 249	1954 ± 183
Branching points	***	3479 ± 612	1447 ± 189	635 ± 165	979.22 ± 98
Branching frequency (1/mm)	***	0.69 ± 0.08	0.35 ± 0.01	0.29 ± 0.03	0.34 ± 0.02
Max root diameter (mm)	**	1.93 ± 0.50	1.17 ± 0.13	1.19 ± 0.56	1.22 ± 0.34
Root diameter (mm)	**	0.93 ± 0.09	0.56 ± 0.01	0.60 ± 0.02	0.76 ± 0.08

Paragon displayed the most extensive root system, with the highest number of root tips, total root length, branching points, and branching frequency, and differed significantly from Bologna and Watkins 238 ($p < 0.001$ for most comparisons). Cappelli showed intermediate values with

significantly greater root length and branching than Watkins 238 ($p < 0.05$). Watkins 238 exhibited the finest root system with significantly smaller average and maximum diameters than Paragon ($p < 0.05$), but the lowest overall root development metrics among all genotypes.

3.2 Rhizospheric hydraulic properties differ among the wheat genotypes

Significant differences emerged among soil samples for multiple parameters derived from retention curves (Table 2, Supplementary Fig. 3). Retention curves were fitted to the pooled data from all replicates to facilitate visualisation. The bimodal van Genuchten equation fitted the data well (mean RMSE = 0.025 ± 0.015 J kg^{-1}), indicating consistency between the observed and modelled values throughout the entire range of matric potentials, with greater variability near saturation reflecting spatial heterogeneity among soil cores (Supplementary Fig. 3).

Rhizosphere soils exhibited higher saturated water content (θ_s) than bulk soil, with Watkins 238 showing the highest values ($p < 0.001$ vs. bulk; $p < 0.05$ vs. Bologna). This pattern indicates that root presence increases total porosity compared to bulk soil.

Watkins 238 also displayed the smallest α_1 value ($p < 0.001$ vs. all other soil samples), indicating smaller pore sizes near saturation than those of other genotypes. Since α_1 represents the reciprocal of the air-entry value for larger pores, this suggests that the fine, highly branched root architecture of Watkins 238 creates a denser network of smaller macropores.

The shape parameter n_1 was significantly higher in Watkins 238 than Bologna, Paragon, and baseline soil (all $p < 0.01$), indicating a broader pore size distribution in the macropore domain. Three genotypes (Paragon, Cappelli, Watkins 238) exhibited bimodal behaviour with distinct macropore and micropore domains, while Bologna, baseline, and bulk soil showed unimodal distributions. No significant differences in secondary pore parameters (α_2, n_2, w_1) were observed among the three bimodal genotypes.

Table 2. Hydraulic properties of baseline, bulk, and genotype-specific rhizosphere soils derived from retention curves. Parameters estimated using bimodal van Genuchten model fitted to pooled replicate data. θ_s, saturated volumetric water content; α_1 and α_2, shape parameters (inverse air-entry values) for macropore and micropore domains; n_1 and n_2, pore size distribution indices; K_s, saturated hydraulic conductivity; w_0 and w_1, weighting factors for bimodal distribution; FC, field capacity (water content at -33 kPa); PWP, permanent wilting point (water content at -1500 kPa); PAW, plant-available water (FC - PWP); k at FC and PWP, unsaturated hydraulic conductivity at field capacity and permanent wilting point; AUC, area under hydraulic conductivity curve; slope, gradient of log k vs. log matric potential. Values are means ± standard error. Significance based on ANOVA: *p < 0.1, **p < 0.05, ***p < 0.01; ns, not significant.

Soil Parameter	p-value	Baseline	Bulk Soil	Paragon	Senatore Cappelli	Watkins 238	Bologna
log θs	***	-0.73±0.03	-0.81±0.05	-0.66±0.03	-0.70±0.01	-0.64±0.04	-0.75±0.06
log α1	***	-1.18±0.04	-3.41±0.31	-1.41±0.66	-3.57±0.11	-4.75±1.15	-1.00±0.19
log α2	ns	-	-	-2.43±2.79	-1.02±0.11	-0.89±0.42	-
log n1	***	0.18±0.01	0.23±0.01	0.19±0.03	0.27±0.04	0.36±0.13	0.16±0.01
log n2	ns	-	-	0.88±0.39	0.53±0.25	0.53±0.19	-
log Ks	***	2.66±0.11	3.01±0.07	3.53±0.05	2.85±0.15	3.49±0.16	3.26±0.07
w0	ns	1	1	0.87±0.06	0.73±0.04	0.64±0.01	1
w1	ns	0	0	0.13±0.06	0.26±0.03	0.36±0.01	0
FC	***	0.27±0.01	0.31±0.01	0.32±0.00	0.32±0.01	0.34±0.00	0.30±0.01

PWP	**	0.12±0.00	0.13±0.00	0.16±0.00	0.14±0.01	0.12±0.01	0.14±0.00
PAW	***	0.15±0.01	0.19±0.00	0.16±0.00	0.19±0.01	0.21±0.01	0.16±0.01
log K at FC	***	-5.78±0.42	-3.73±0.12	-4.68±1.05	-3.79±0.41	-2.72±1.38	-5.57±0.31
log K at PWP	***	-9.92±0.47	-8.11±0.13	-8.85±0.90	-8.36±0.52	-7.29±1.49	-9.60±0.34
AUC	***	7.70±1.45	24.96±3.78	21.15±6.87	21.06±3.53	46.10±16.20	10.70±2.07
slope	***	-2.50±0.04	-2.64±0.02	-2.51±0.10	-2.76±0.13	-2.76±0.20	-2.43±0.03

Watkins 238 exhibited the highest field capacity (FC = 0.34 $m^3\ m^{-3}$; $p < 0.01$ vs. baseline and Bologna) and lowest permanent wilting point (PWP = 0.12 $m^3\ m^{-3}$; $p < 0.05$ vs. baseline and Paragon), resulting in the greatest plant-available water (PAW = 0.21 $m^3\ m^{-3}$), significantly exceeding baseline ($p < 0.01$), Paragon ($p < 0.05$), and Bologna ($p < 0.01$). Senatore Cappelli showed intermediate PAW (0.19 $m^3\ m^{-3}$), also higher than baseline ($p < 0.01$). These genotypic differences in water retention across the plant-available water range are illustrated in Fig. 1, which highlights a detail of the retention curves between field capacity and wilting point thresholds.

Rhizosphere soils of Paragon and Watkins 238 exhibited significantly higher K_s than baseline ($p < 0.001$), bulk soil ($p < 0.001$), and Senatore Cappelli ($p < 0.001$). Bologna also exceeded baseline ($p < 0.001$), while Senatore Cappelli showed lower K_s than Bologna ($p < 0.01$).

Based on the van Genuchten-Mualem framework (Mualem, 1976; van Genuchten, 1980), hydraulic conductivity was estimated across the full range of matric potentials (Fig. 2). Watkins 238 maintained higher conductivity throughout the entire drying range compared to other genotypes and baseline soil, with significantly higher conductivity at field capacity (K_{FC}) than Bologna ($p < 0.01$), baseline ($p <$

0.01), and Paragon ($p < 0.05$), and higher conductivity at permanent wilting point (K_{WP}) than baseline ($p < 0.01$) and Bologna ($p < 0.05$). The area under the conductivity curve (AUC), which integrates hydraulic performance across the entire moisture range (Assouline, 2001), was significantly greater for Watkins 238 (46.10) than all other treatments ($p < 0.05$ to $p < 0.001$), indicating superior water transmission capacity throughout the drying cycle.

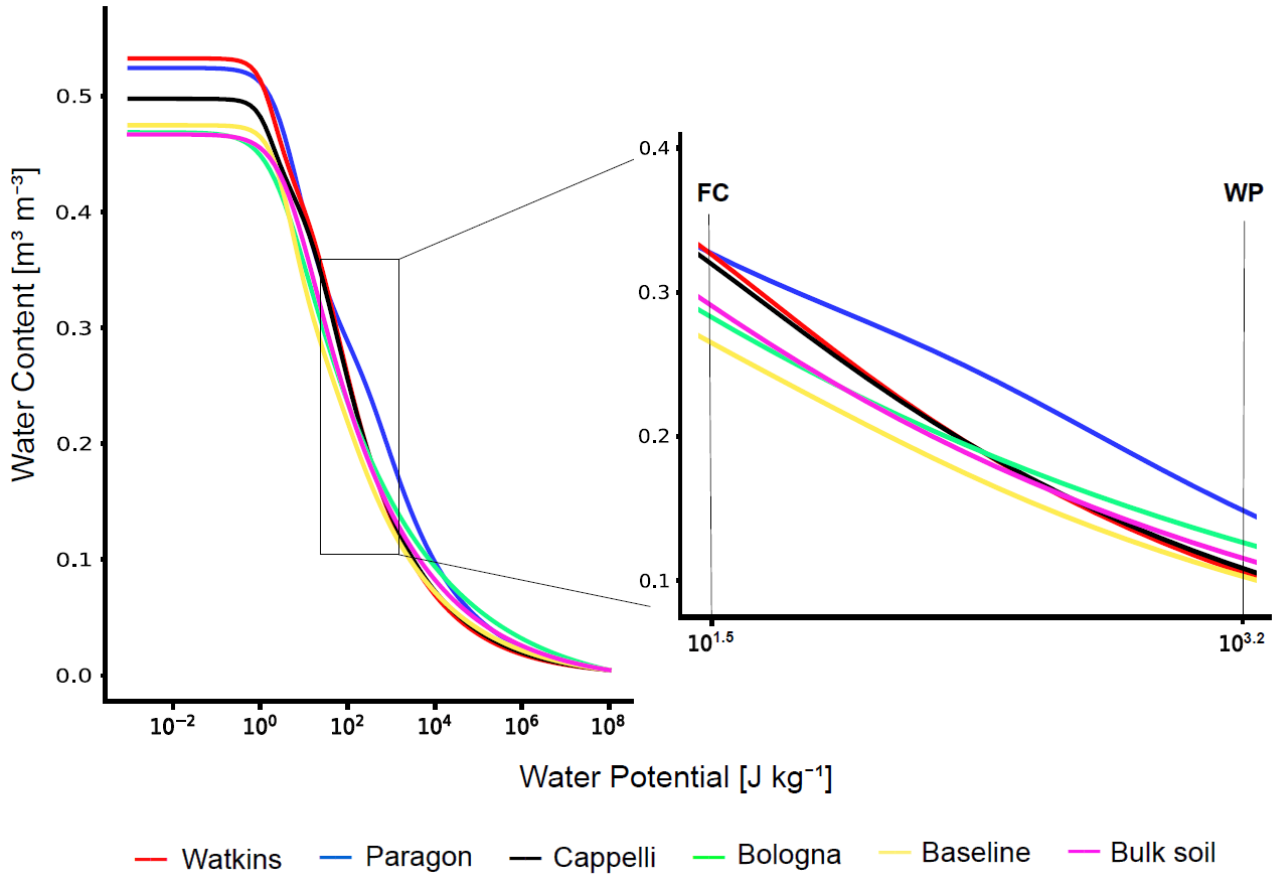

Figure 1. Soil water retention curves for soils influenced by contrasting wheat genotypes and bulk soil. Water content ($m^3\ m^{-3}$) is shown as a function of soil water potential ($J\ kg^{-1}$) for soils associated with the genotypes Watkins, Paragon, Cappelli, and Bologna, alongside a baseline soil and bulk soil control. Curves illustrate genotype-specific differences in water retention across the full matric potential range. The inset highlights the agronomically relevant range between field capacity (FC; $\sim 10^{1.5}\ J\ kg^{-1}$) and wilting point (WP; $\sim 10^{3.2}\ J\ kg^{-1}$), emphasising differences in plant-available water among treatments.

The slope of log(K) vs. log(ψ) was less negative for Watkins 238 and Senatore Cappelli than Bologna ($p < 0.01$), indicating more gradual conductivity decline during soil drying—a favourable trait for sustained water supply under water-limited conditions.

Watkins 238 displayed the smallest α_1 value, significantly different from Bologna ($p < 0.001$), Paragon ($p < 0.001$) and baseline soil ($p < 0.001$), while Senatore Cappelli and bulk soil also presented lower α_1 than Bologna (both $p < 0.001$) and Paragon (both $p < 0.01$). Additionally, bulk soil presented a lower α_1 than baseline soil ($p < 0.01$). The parameter $\alpha 1$ represents the inflection point of the first mode (larger pores), while α_2 is the inflection point of the second mode (smallest pores). From a physical perspective, the inflection point represents the pore size where water is substituted by air. Accordingly, in some SWRC models it is called the air entry value. In the van Genuchten formulation, α is the reciprocal of the air entry value. Therefore, a smaller value of α_1 corresponds to a larger value of air entry, representing the presence of smaller pores close to saturation. The significantly lower α_1 value found for Watkins 238 indicates that the root traits of this genotype might result in a decrease in pore size in the range close to saturation compared to bulk soil and the other genotypes.

Watkins 238 presented significantly higher n_1 than Bologna ($p < 0.01$), Paragon ($p < 0.01$) and baseline soil ($p < 0.01$). No significant differences were found among Cappelli, Paragon, and Watkins 238 for the parameters α_2, n_2, and w_1, suggesting similar behaviour in the secondary pore domain. However, it was not possible to perform comparisons with Bologna, baseline and bulk soil, as their water retention curves did not exhibit bimodality, and thus these parameters could not be estimated.

Watkins 238 presented a higher FC compared to baseline and Bologna (both $p < 0.01$). Also, Senatore Cappelli and Paragon showed a higher FC than baseline (both $p < 0.01$). Watkins 238 showed a lower PWP compared to baseline and Paragon (both $p < 0.05$). Watkins 238 had the highest PAW, significantly more than baseline ($p < 0.01$), Paragon ($p < 0.05$) and Bologna ($p < 0.01$). These

results indicate that the RSA has a statistically significant effect on the pore size distribution by selectively changing the PAW.

Rhizospheric soil of Paragon and Watkins 238 exhibited significantly higher K_s than baseline soil ($p < 0.001$), bulk soil ($p < 0.001$), Senatore Cappelli ($p < 0.001$). Bologna also showed greater K_s than baseline soil ($p < 0.001$), while bulk soil was higher than baseline ($p < 0.05$). In contrast, Senatore Cappelli displayed a lower K_s than Bologna ($p < 0.01$).

Based on the established relationships between SWRCs and K described by Mualem (1976) and van Genuchten (1980), we estimated the K at FC (33 J kg^{-1}) and PWP (1500 J kg^{-1}). The rate of conductivity declines and the area under the conductivity curve (AUC) were also calculated to comprehensively assess the soil's hydraulic performance across a wide range of matric potentials (Assouline, 2001; Schaap and van Genuchten, 2006).

Watkins 238 exhibited significantly higher K_{FC} than Bologna ($p < 0.01$), baseline soil ($p < 0.01$), and Paragon ($p < 0.05$), while Senatore Cappelli showed higher K_{FC} compared to baseline soil ($p < 0.05$).

Watkins 238 also exhibited significantly higher K_{WP} than baseline soil ($p < 0.01$) and Bologna ($p < 0.05$).

Watkins 238 had significantly greater AUC than baseline soil ($p < 0.001$), Bologna ($p < 0.001$), Senatore Cappelli ($p < 0.01$), Paragon ($p < 0.01$), and bulk soil ($p < 0.05$). Regarding the slope of the log(K) versus log(ψ) relationship, Senatore Cappelli and Watkins 238 presented significantly less negative slopes compared to Bologna ($p < 0.01$).

Watkins 238 showed significantly higher K_s, K_{FC}, and K_{WP}, as well as the highest AUC and a less negative slope in the log(K)–log(ψ) domain, indicating efficient water transmission across a wide range of matric potentials. Senatore Cappelli, though characterized by lower K_s, exhibited higher

conductivity in the unsaturated range, with higher K_{FC} and a flatter slope than Bologna. Both genotypes also presented lower wilting points and greater plant-available water, suggesting enhanced water retention and supply under drying conditions.

Overall, Watkins 238 showed statistically significant higher values of K over the entire range of water potentials (Fig. 2), modifying the hydraulic behaviour of the original baseline soil and also with respect to the other genotypes.

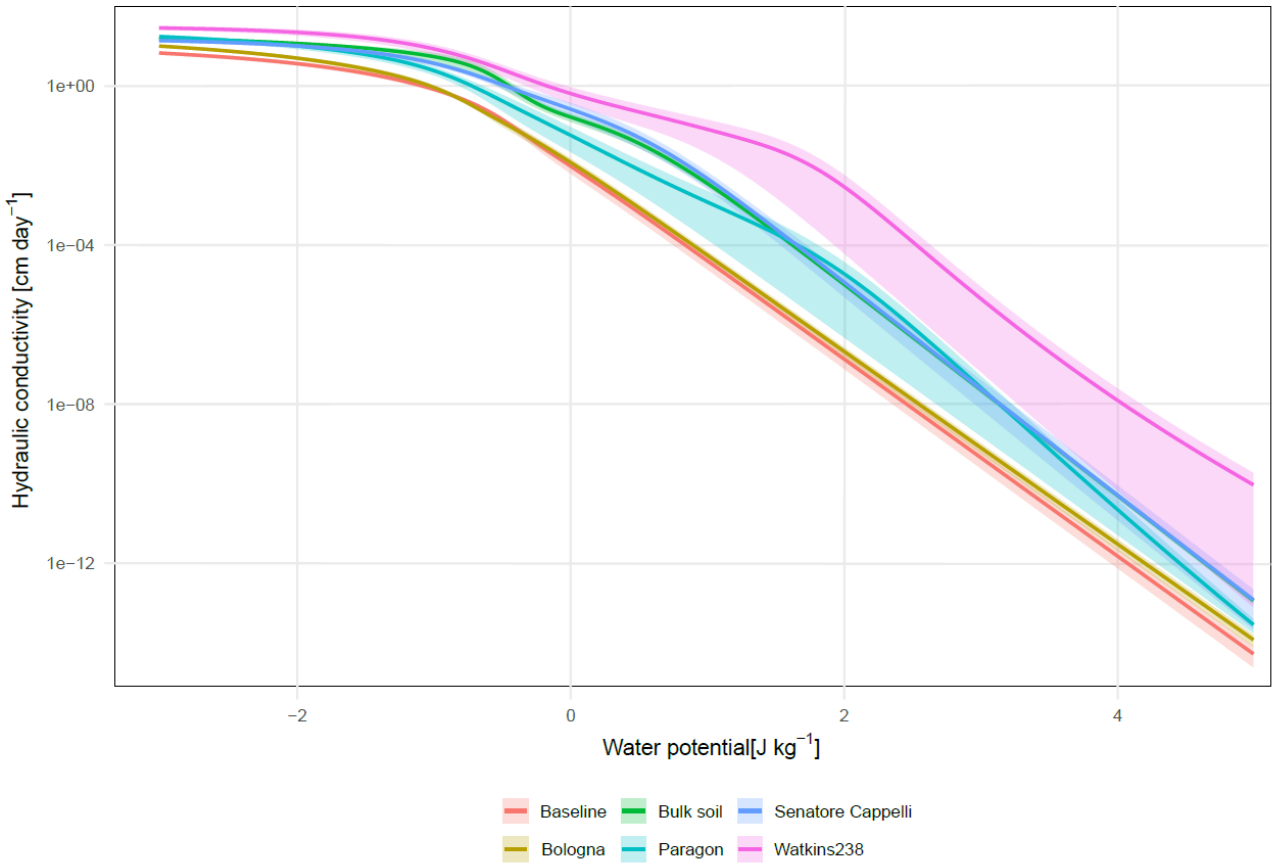

Figure 2. Hydraulic conductivity (K) curves derived from bimodal van Genuchten–Mualem models fitted to soil water retention and conductivity data. Each line represents the mean log-transformed K(ψ) relationship for a given genotype or treatment, with shaded bands indicating the standard error across replicates.

3.3 Root architectural traits correlate with soil hydraulic properties

Linear mixed models revealed significant relationships between root morphology and hydraulic behaviour (Fig. 3). Architectural traits strongly influenced water retention: crown network area correlated positively with weighting factor w_0 ($p < 0.05$), FC ($p < 0.05$), and PAW ($p < 0.01$), while FRMP (Table 1) showed negative correlation with α_1 ($p < 0.01$) but positive correlations with θ_s ($p < 0.05$), FC ($p < 0.05$), and PAW ($p < 0.05$).

Root angle distribution affected pore structure parameters: shallow-angle frequency correlated negatively with α_1 ($p < 0.01$) and n_2 ($p < 0.05$) but positively with w_1 ($p < 0.05$), while steep-angle frequency showed opposite patterns (positive with α_1 and w_0; negative with w_1; all $p < 0.01$).

Regarding the results from branching and topology parameters, root tips, total length, and length in both diameter classes (D1 < 0.45 mm; D2 > 0.45 mm) correlated negatively with α_2 ($p < 0.01$), n_1 ($p < 0.05$), and K_s ($p < 0.001$), while correlating positively with PWP ($p < 0.05$). Branching frequency showed negative correlations with n_1 ($p < 0.001$), w_1 ($p < 0.05$), PAW ($p < 0.05$), K_{FC} ($p < 0.01$), K_{WP}, and K_s (all $p < 0.001$), but positive correlations with θ_s ($p < 0.05$), α_1 ($p < 0.05$), w_0 ($p < 0.05$), PWP ($p < 0.01$), and slope ($p < 0.01$).

The average root diameter (representing primary roots) showed complex relationships—positively correlated with θ_s ($p < 0.05$) and α_1 ($p < 0.01$), indicating increased porosity but earlier pore drainage, yet negatively correlated with n_1 ($p < 0.001$), w_1 ($p < 0.001$), PAW ($p < 0.05$), K_{FC} ($p < 0.05$), and K_{WP} ($p < 0.01$). Maximum root diameter correlated positively with n_2 ($p < 0.001$), w_0 ($p < 0.01$), and slope ($p = 0.05$), but negatively with n_1 ($p < 0.05$), w_1 ($p < 0.01$), and K_s ($p < 0.01$).

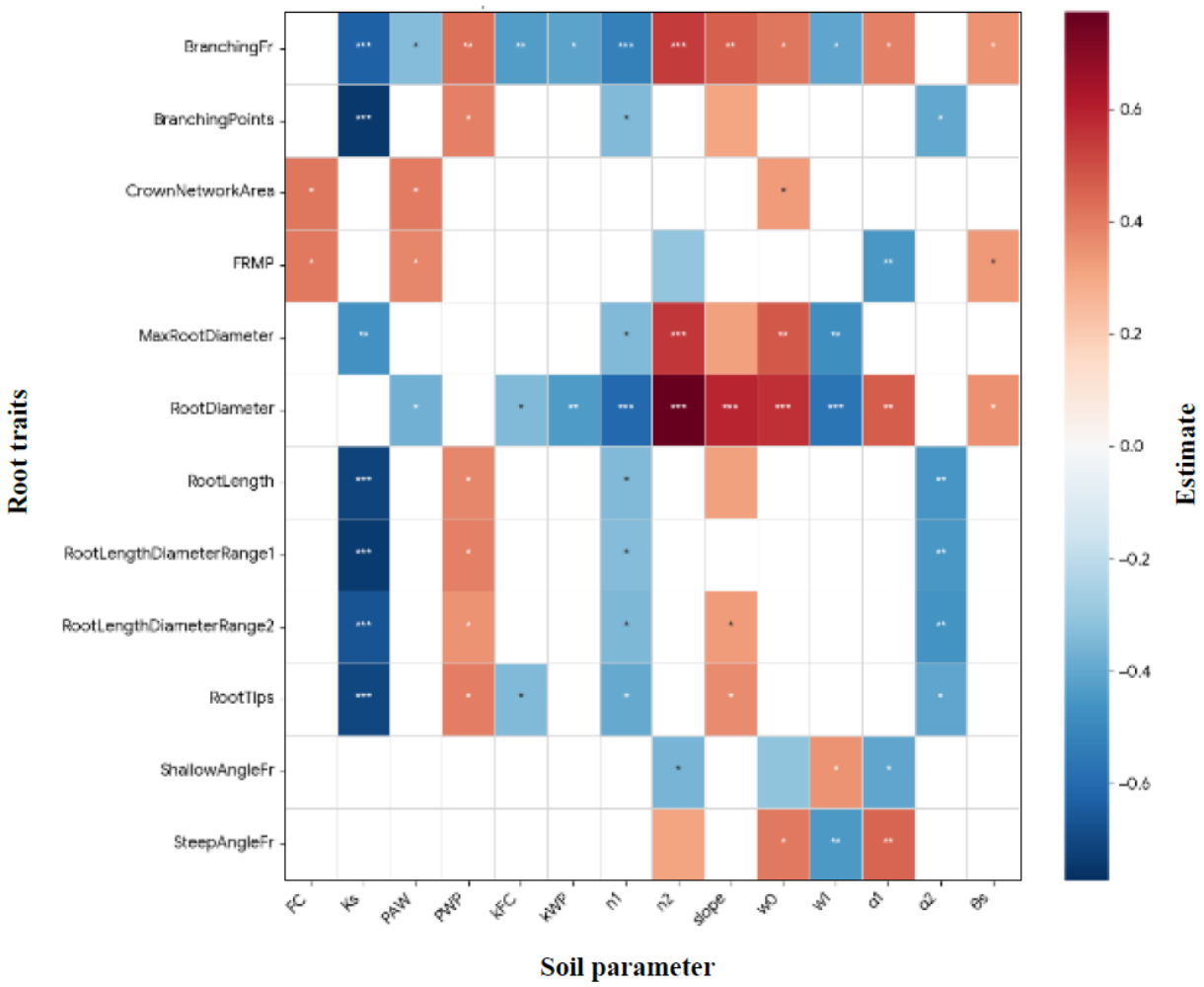

Figure 3. Associations between root architectural traits and soil hydraulic and structural variables. Heatmap showing standardized effect sizes (estimates) from statistical models relating root traits (rows) to soil physical and hydraulic variables (columns), including field capacity (FC), saturated hydraulic conductivity (Ks), plant-available water (PAW), permanent wilting point (PWP), pore size distribution metrics (kFC, kWP), pore connectivity indices (n1, n2), slope of the water retention curve, and water contents at defined matric potentials (w0, w1), as well as bulk density–related parameters (θs). Colours indicate the direction and magnitude of effects (blue = negative, red = positive), with colour intensity proportional to effect size. Asterisks denote statistical significance (* $P < 0.05$; ** $P < 0.01$; *** $P < 0.001$). White cells indicate non-significant relationships.

3.4 Roots affect pore size distribution

Pore size distributions derived from retention curves using capillary theory (Eq. 3; Fig. 4) revealed distinct patterns. Baseline and bulk soils exhibited unimodal distributions with peaks at 22.3 and 6.6

μm, respectively. Bologna, characterized by shorter, less branched roots, showed a unimodal distribution (peak at 9.9 μm) similar to bulk soil, with no significant effect on θ_s (Table 2), indicating limited influence on pore architecture.

In contrast, Paragon, Watkins 238, and Senatore Cappelli produced bimodal distributions. Paragon, with longer, thicker roots, increased total porosity (higher θ_s vs. bulk soil, $p < 0.01$) and created a bimodal distribution with peaks at 17.3 μm (macropores) and 0.162 μm (micropores).

Watkins 238 and Senatore Cappelli, characterized by finer, more elongated root systems, generated distinct bimodal distributions with larger macropore peaks (55.6 and 61.6 μm, respectively) and secondary micropore peaks around 2 μm. These genotypes exhibited lower PWP (0.12 and 0.14 m^3 m^{-3}) and enhanced PAW (0.21 and 0.19 m^3 m^{-3}), consistent with a pore architecture that retains water across a wider range of matric potentials.

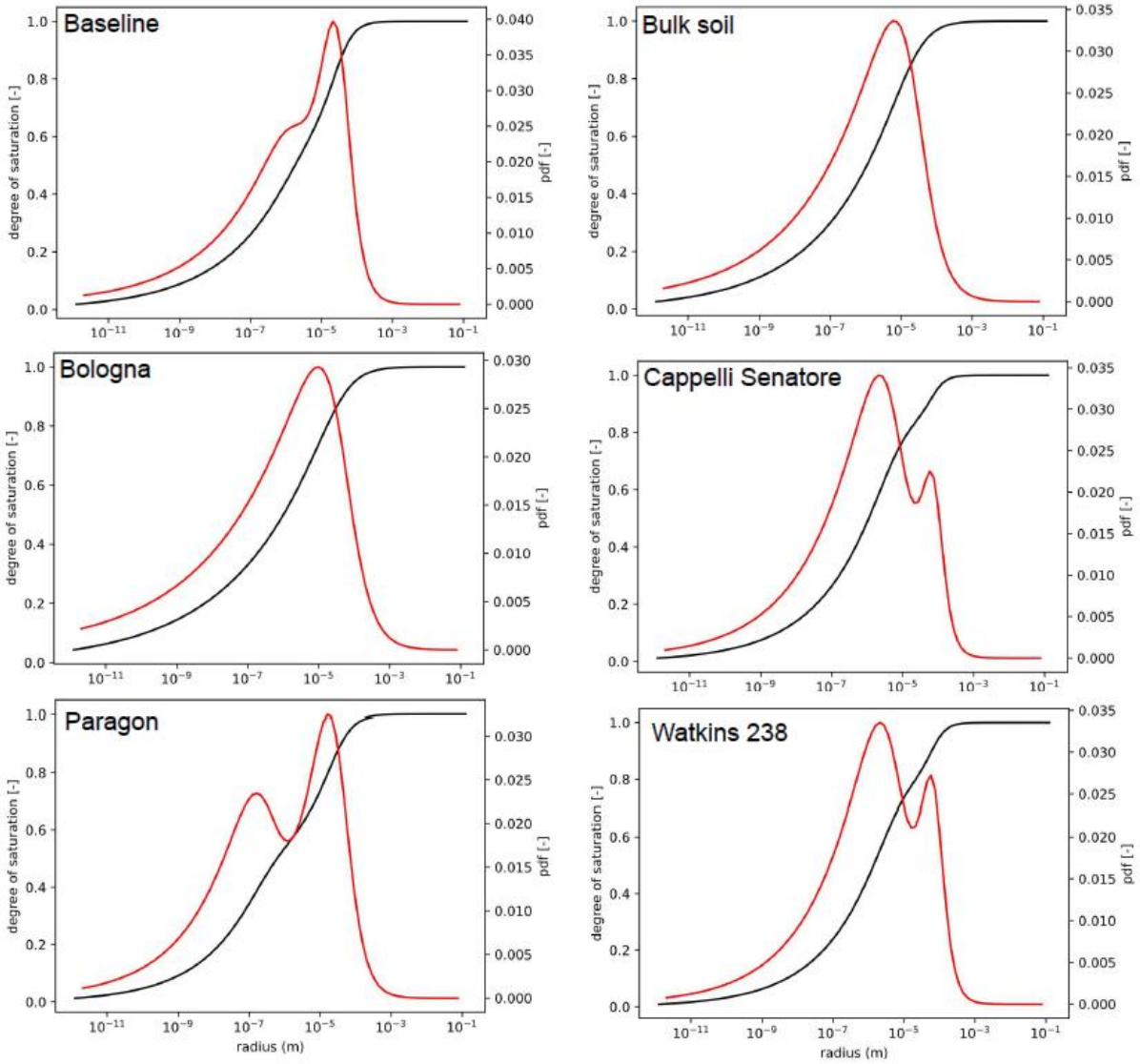

Figure 4. Pore size distribution curves derived from soil water retention data using a capillary-based model. For each soil type (baseline, bulk, and rhizosphere of the four wheat genotypes), panels display the differential water retention curve (black line) and the corresponding pore radius probability density function (red line). Peaks in the probability density function indicate dominant pore domains, with single peaks reflecting unimodal pore structures and multiple peaks identifying bimodal or more heterogeneous pore size distributions characteristic of rhizosphere modification.

4. Discussion

This study provides new evidence that genotypic variation in wheat root system architecture can modify soil hydraulic properties, including plant-available water (PAW), permanent wilting point

(PWP), and hydraulic conductivity across saturation states. These findings align with growing recognition that roots function as ecosystem engineers, physically and chemically modifying the soil matrix and hydraulic environment (Lu et al., 2020; Xiao et al., 2024). The observed differences among genotypes confirm that even within a single crop species, RSA traits shape the physical hydrology of the rhizosphere.

4.1 Root architecture as a driver of pore-scale hydraulic differentiation

Genotypes with finer or more highly branched root systems were associated with increased water retention at lower matric potentials and reduced α values, trends consistent with hydraulic behaviours typical of finer-textured or more fragmented pore architectures (Bittelli et al., 2015). The absence of bimodality in some samples, particularly Bologna and bulk soil, should not be interpreted as a limitation of the fitting procedure but rather as evidence of a structurally simpler, less aggregated pore network. As noted by Durner (1994), unimodal behaviour indicates the absence of distinct inter- and intra-aggregate pore domains, a key feature with profound implications for water retention and transport processes (Dexter, 2004; Jarvis, 2007).

Conversely, genotypes expressing bimodal pore size distributions reflected a more complex pore system, likely generated by root-induced aggregation or post-decay biopore formation, mechanisms supported by both experimental hydrology and X-ray computed tomography studies (Daly et al., 2015; Dimattia et al., 2025; Scholl et al., 2014). The hydraulic behaviour of Watkins 238, which sustained conductivity at lower matric potentials, resembles models of fine-textured soils where continuous micropore networks maintain flow under drought (Jarvis and Messing, 1995; Marshall et al., 1996). These results reinforce the hypothesis that RSA determines hydraulic properties by influencing pore connectivity and tortuosity.

4.2 Mechanisms underlying root–hydraulic interactions

The correlations observed between root traits and hydraulic parameters support the view that mechanical displacement, pore infilling, and organic deposition drive rhizospheric restructuring (Jin et al., 2017; Lu et al., 2020; Song et al., 2017). Fine-root proliferation was associated with reduced K at field capacity but a slower decline in conductivity at low water potentials, consistent with clogging of medium-sized pores but sustained flow through micropores (Hohenbrink et al., 2023). The observed increase in PWP without proportional gains in FC highlights a trade-off between total soil storage and plant-usable water, emphasising that hydraulic benefits are trait- and context-dependent.

The role of rhizodeposits also warrants consideration, as root-derived mucilage can substantially modify rhizosphere hydraulic properties. When hydrated, mucilage enhances soil water retention and promotes aggregate stability by altering interparticle forces and pore-scale connectivity (Kroener et al., 2018; Naveed et al., 2019). The spatial distribution of mucilage in the vicinity of roots further contributes to heterogeneity in rhizosphere structure and water dynamics (Holz et al., 2018). However, mucilage may undergo physicochemical changes during drying that reduce its hydrophilicity and hydraulic effectiveness, potentially reversing its influence on water retention under dry conditions (Hallett and Young, 1999; Carminati et al., 2010). Given the dry-end measurements in this study, mechanical restructuring rather than mucilage dynamics likely dominated the hydraulic responses observed. Future work should integrate structural imaging and physico-chemical assays to discriminate between biochemical versus biomechanical drivers.

4.3 Implications for breeding and sustainable water use

These genotype-specific hydraulic responses have direct agronomic relevance. Root traits that maintain functional porosity and conductivity as soils dry may contribute to improved water-use efficiency, drought resilience, and reduced irrigation demand, particularly in coarse-textured systems where PAW is inherently limited (Ober et al., 2021). Yet, the observed trade-offs—where increased

retention delivered higher PWP and reduced PAW—reinforce that selection based solely on fine-root proliferation could produce ambiguous outcomes.

These results support calls for integrating RSA traits into cropping system design and breeding programs (Ober et al., 2021; Zhang et al., 2025), while also recognizing that genotype effects interact with soil structure, management, and climate (Paez-Garcia et al., 2015; Uga, 2021). The conceptual framework presented here links root system traits to soil pore architecture (Fig. 5), subsequent hydraulic processes, and ultimately agronomic performance, providing a mechanistic basis for selecting genotypes adapted to specific soil types and water regimes.

This study demonstrates clear associations between root architectural traits and soil hydraulic behaviour, but the effects of specific traits depend on soil properties, moisture regimes, and management context. Root traits influence agronomic performance indirectly through their modification of pore architecture and hydraulic processes (Fig. 5), pathways that are strongly mediated by soil texture, initial structure, and environmental conditions. Consequently, traits that enhance water retention or conductivity in one soil–climate setting may confer different or diminished benefits elsewhere, underscoring the need to target root ideotypes to specific soil and water regimes rather than assuming universal trait advantages.

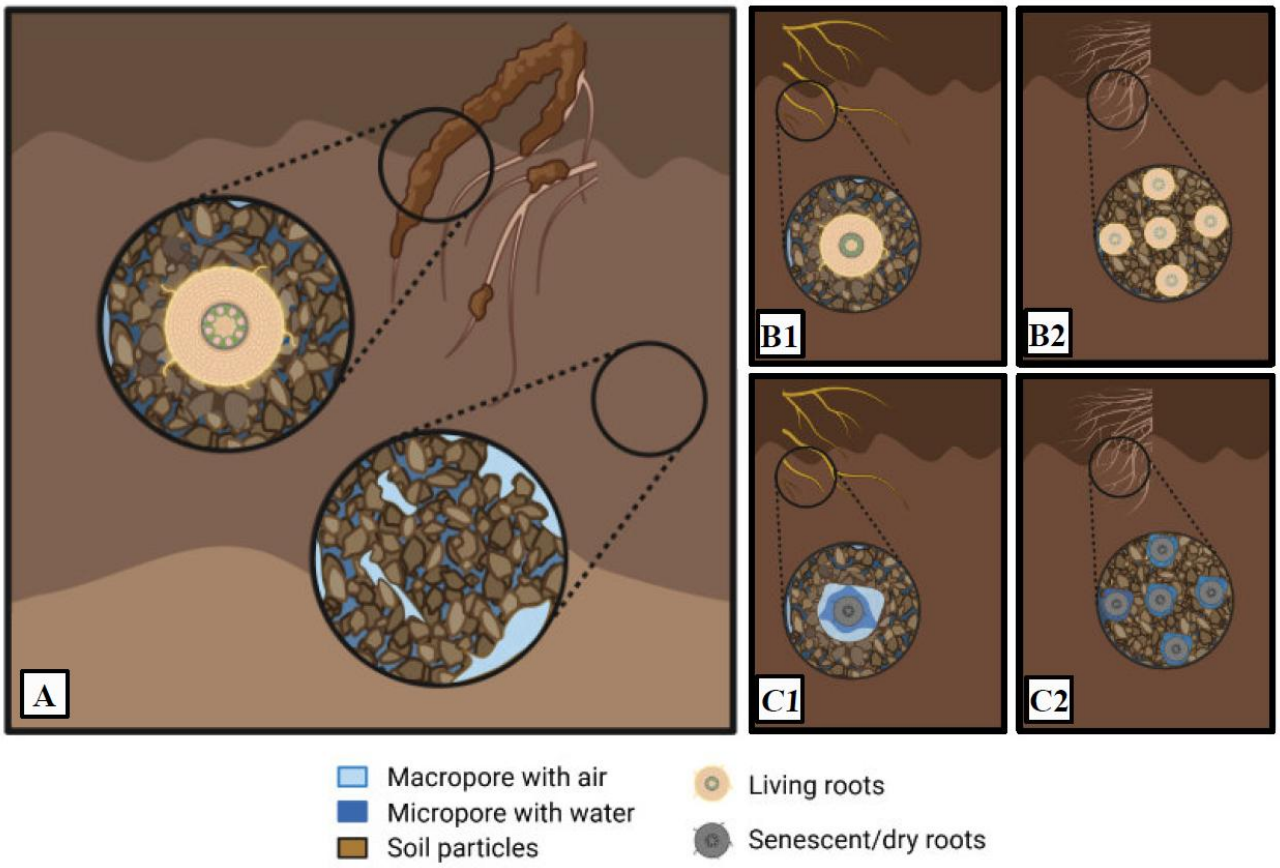

Figure 5. Conceptual model of root–soil interactions. (A) Root expansion through the soil matrix, where radial growth exerts mechanical pressure, compacting the rhizosphere. (B1–B2) Architectural divergence in living root systems: (B1) thick roots occupying large pore spaces, and (B2) dense networks of fine roots. (C1–C2) Post-senescence hydraulic impacts: (C1) senescent thick roots leave large galleries facilitating preferential flow and drainage, whereas (C2) fine-root decay leaves narrow biopores that enhance capillary water retention via high matric potential. Collectively, the model illustrates how root traits dictate soil structural modification and subsequent water dynamics.

4.4 Limitations and future directions

While the correlations reported are statistically meaningful and mechanistically plausible, they should be interpreted cautiously given the limited replication and model-derived pore size distributions. Integrating high-resolution imaging (CT, MRI), mucilage quantification, and cross-soil validation will be essential to substantiate these genotype-specific hydraulic signatures and define their stability under realistic agronomic conditions.

5. Conclusions

This study shows that variation in wheat root architecture can meaningfully modify soil hydraulic properties, emphasising the pivotal role of roots in determining rhizosphere function. These insights offer a promising avenue for breeding strategies focused on root traits that enhance soil–plant water relations, particularly in water-limited systems.

Declaration

The authors declare no competing interests.

Acknowledgements

B.G.D. received funding from the Department of Agricultural and Food Sciences (DISTAL), University of Bologna, through its Ph.D programme. M.C.H.S. gratefully acknowledges funding support from the Biotechnology and Biological Sciences Research Council (BBSRC), project BB/X003000/1. We thank Silvio Salvi for useful discussion and for participation in the development and implementation of the funded project. We are also grateful to Marco Maccaferri for providing the seeds of the cultivar Senatore Cappelli and for useful discussions, to the John Innes Centre Germplasm Resources Unit for providing the seeds of the Paragon and Watkins 238 cultivars, and to Simon Griffiths and Luzie U. Wingen for advice on the relevance of these cultivars. B.G.D. gratefully acknowledges the support of the Collegio Superiore and the Institute of Advanced Studies of the University of Bologna. We would like to thank METER Group Inc. (Munich, Germany) where the measurements of the SHPs were performed, for providing access to the soil hydraulic instrumentation and Prof. Wolfgang Durner for generously sharing his expertise and guidance throughout the study.

Data availability

The computer code, written in Python and used to fit the bimodal model, is available upon request from the authors.

Author contributions statement

B.G.D. contributed to the writing of the funded project, conceived the experiment, followed all the agronomic practices and management practices, collected samples and data, analysed the data and wrote the paper; F.T. wrote the software used for non-linear fitting and computation of hydraulic properties; M.B. contributed to the writing of the project, coordinated the experimental setup, wrote the software used for non-linear fitting and computation of hydraulic properties, contributed to data analysis and writing of the paper; R.T. contributed to the writing of the paper. M.C.H.S. is the coordinator of the project and contributed to the writing and reviewing of the manuscript.

Declaration of generative AI and AI-assisted technologies in the writing process

During the preparation of this work, the author used *Gemini (Google)* to improve the clarity and readability of the manuscript. After using this tool, the author reviewed and edited the content as needed and takes full responsibility for the content of the publication.

References

Ahuja, L.R., Naney, J.W., Williams, R.D., 1985. Estimating soil water characteristics from simpler properties or limited data. Soil Sci. Soc. Am. J. 49, 1100–1105.

Alexander, L., Skaggs, R., 1986. Predicting unsaturated hydraulic conductivity from the soil water characteristic. Transactions of the ASABE 29, 0176–0184.

Assouline, S., 2001. A model for soil relative hydraulic conductivity based on the water retention characteristic curve. Water Resources Research 37, 265–271.

Bardgett, R.D., Mommer, L., De Vries, F.T., 2014. Going underground: root traits as drivers of ecosystem processes. Trends Ecol. Evol. 29, 692–699.

Bengough, A.G., McKenzie, B.M., Hallett, P.D., Valentine, T.A., 2011. Root elongation, water stress, and mechanical impedance: a review of limiting stresses and beneficial root tip traits. J. Exp. Bot. 62, 59–68.

Bezerra-Coelho, C.R., Zhuang, L., Barbosa, M.C., Soto, M.A., van Genuchten, M.T., 2018. Further tests of the HYPROP evaporation method for estimating the unsaturated soil hydraulic

properties. J. Hydrol. Hydromech./Vodohospo. Cas. 66, 161–169.

Bittelli, M., Campbell, G.S., Tomei, F., 2015. Soil physics with Python: Transport in the soil-plant-atmosphere system. OUP Oxford.

Blanco-Canqui, H., Lal, R., Post, W., Izaurralde, R., Shipitalo, M., 2007. Soil hydraulic properties influenced by corn stover removal from no-till corn in Ohio. Soil Tillage Res. 92, 144–155.

Bodner, G., Leitner, D., Kaul, H.-P., 2014. Coarse and fine root plants affect pore size distributions differently. Plant Soil 380, 133–151.

Bordoloi, R., Das, B., Yam, G., Pandey, P.K., Tripathi, O.P., 2019. Modeling of water holding capacity using readily available soil characteristics. Agric. Res. 8, 347–355.

Bronick, C.J., Lal, R., 2005. Soil structure and management: a review. Geoderma 124, 3–22.

Burden, R.L., Faires, J.D., 1997. Numerical analysis, brooks.

Campbell, G.S., Smith, D.M., Teare, B.L., 2007. Application of a dew point method to obtain the soil water characteristic, in: Springer Proceedings in Physics. Springer Berlin Heidelberg, Berlin, Heidelberg, pp. 71–77.

Carminati, A., Moradi, A.B., Vetterlein, D., Vontobel, P., Lehmann, E., Weller, U., Vogel, H.-J., Oswald, S.E., 2010. Dynamics of soil water content in the rhizosphere. Plant Soil 332, 163–176.

Carminati, A., Vetterlein, D., 2013. Plasticity of rhizosphere hydraulic properties as a key for efficient utilization of scarce resources. Ann. Bot. 112, 277–290.

Carminati, A., Zarebanadkouki, M., Kroener, E., Ahmed, M.A., Holz, M., 2016. Biophysical rhizosphere processes affecting root water uptake. Ann. Bot. 118, 561–571.

Corneo, P.E., Suenaga, H., Kertesz, M.A., Dijkstra, F.A., 2016. Effect of twenty four wheat genotypes on soil biochemical and microbial properties. Plant Soil 404, 141–155.

Daly, K.R., Mooney, S.J., Bennett, M.J., Crout, N.M.J., Roose, T., Tracy, S.R., 2015. Assessing the influence of the rhizosphere on soil hydraulic properties using X-ray computed tomography and numerical modelling. J. Exp. Bot. 66, 2305–2314.

Dexter, A.R., 2004. Soil physical quality. Geoderma 120, 201–214.

Dimattia, B.G., Righi, A., Bettuzzi, M., Koestel, J., Morigi, M.P., Brancaccio, R., Salvi, S., Hernandez-Soriano, M.C., Bittelli, M., 2025. Root traits of different wheat cultivars influence

soil structure: an X-ray computed tomography and root morphology study. Geoderma 459, 117349.

Doran, J.W., Parkin, T.B., 2015. Defining and assessing soil quality, in: SSSA Special Publications. Soil Science Society of America and American Society of Agronomy, Madison, WI, USA, pp. 1–21.

Durner, W., 1994. Hydraulic conductivity estimation for soils with heterogeneous pore structure. Water resources research. https://doi.org/10.1029/93WR02676

Evert, R.F., 2006. Esau's plant anatomy: meristems, cells, and tissues of the plant body: their structure, function, and development.

Fradgley, N., Evans, G., Biernaskie, J.M., Cockram, J., Marr, E.C., Oliver, A.G., Ober, E., Jones, H., 2020. Effects of breeding history and crop management on the root architecture of wheat. Plant Soil 452, 587–600.

Freschet, G.T., Roumet, C., Comas, L.H., Weemstra, M., Bengough, A.G., Rewald, B., Bardgett, R.D., De Deyn, G.B., Johnson, D., Klimešová, J., Lukac, M., McCormack, M.L., Meier, I.C., Pagès, L., Poorter, H., Prieto, I., Wurzburger, N., Zadworny, M., Bagniewska-Zadworna, A., Blancaflor, E.B., Brunner, I., Gessler, A., Hobbie, S.E., Iversen, C.M., Mommer, L., Picon-Cochard, C., Postma, J.A., Rose, L., Ryser, P., Scherer-Lorenzen, M., Soudzilovskaia, N.A., Sun, T., Valverde-Barrantes, O.J., Weigelt, A., York, L.M., Stokes, A., 2021. Root traits as drivers of plant and ecosystem functioning: current understanding, pitfalls and future research needs. New Phytol. 232, 1123–1158.

Gregory, P.J. (Ed.), 2006. Plant roots: Growth, activity and interaction with soils. Wiley, Oxford, UK.

Grossman, J.D., Rice, K.J., 2012. Evolution of root plasticity responses to variation in soil nutrient distribution and concentration: Barley root plasticity. Evol. Appl. 5, 850–857.

Hallett, P.D., Marin, M., Bending, G.D., George, T.S., Collins, C.D., Otten, W., 2022. Building soil sustainability from root-soil interface traits. Trends Plant Sci. 27, 688–698.

Hallett, P.D., Young, I.M., 1999. Changes to water repellence of soil aggregates caused by substrate-induced microbial activity. Eur. J. Soil Sci. 50, 35–40.

Helliwell, J.R., Sturrock, C.J., Mairhofer, S., Craigon, J., Ashton, R.W., Miller, A.J., Whalley, W.R., Mooney, S.J., 2017. The emergent rhizosphere: imaging the development of the porous

architecture at the root-soil interface. Sci. Rep. 7, 14875.

Hillel, D., 1998. Environmental soil physics: Fundamentals, applications, and environmental considerations, 1996th ed. Academic Press, San Diego, CA.

Hodge, A., Berta, G., Doussan, C., Merchan, F., Crespi, M., 2009. Plant root growth, architecture and function. Plant Soil 321, 153–187.

Hohenbrink, T.L., Jackisch, C., Durner, W., Germer, K., Iden, S.C., Kreiselmeier, J., Peters, 2023. Soil water retention and hydraulic conductivity measured in a wide saturation range. Earth System Science Data 15, 4417–4432.

Holz, M., Leue, M., Ahmed, M.A., Benard, P., Gerke, H.H., Carminati, A., 2018. Spatial distribution of mucilage in the rhizosphere measured with infrared spectroscopy. Front. Environ. Sci. 6. https://doi.org/10.3389/fenvs.2018.00087

Jarvis, N.J., 2007. A review of non-equilibrium water flow and solute transport in soil macropores: principles, controlling factors and consequences for water quality. Eur. J. Soil Sci. 58, 523–546.

Jarvis, N.J., Messing, I., 1995. Near-saturated hydraulic conductivity in soils of contrasting texture measured by tension infiltrometers. Soil Sci. Soc. Am. J. 59, 27–34.

Jin, K., Shen, J., Ashton, R.W., Dodd, I.C., Parry, M.A.J., Whalley, W.R., 2013. How do roots elongate in a structured soil? J. Exp. Bot. 64, 4761–4777.

Jin, K., White, P.J., Whalley, W.R., Shen, J., Shi, L., 2017. Shaping an Optimal Soil by Root–Soil Interaction. Trends Plant Sci. 22, 823–829.

Jury, W.A., Horton, R., 2004. Soil Physics, 6th ed. John Wiley & Sons, Nashville, TN.

Klute, A., Dirksen, C., 2018. Hydraulic conductivity and diffusivity: Laboratory methods, in: SSSA Book Series. Soil Science Society of America, American Society of Agronomy, Madison, WI, USA, pp. 687–734.

Koebernick, N., Daly, K.R., Keyes, S.D., Bengough, A.G., Brown, L.K., Cooper, L.J., George, T.S., Hallett, P.D., Naveed, M., Raffan, A., Roose, T., 2019. Imaging microstructure of the barley rhizosphere: particle packing and root hair influences. New Phytol. 221, 1878–1889.

Kroener, E., Holz, M., Zarebanadkouki, M., Ahmed, M., Carminati, A., 2018. Effects of mucilage on rhizosphere hydraulic functions depend on soil particle size. Vadose Zone J. 17, 1–11.

Lal, R., Shukla, M.K., 2004. Principles of soil physics, Books in Soils, Plants, and the Environment.

CRC Press, London, England. https://doi.org/10.4324/9780203021231

Le Marié, C.A., York, L.M., Strigens, A., Malosetti, M., Camp, K.-H., Giuliani, S., Lynch, J.P., Hund, A., 2019. Shovelomics root traits assessed on the EURoot maize panel are highly heritable across environments but show low genotype-by-nitrogen interaction. Euphytica 215. https://doi.org/10.1007/s10681-019-2472-8

Lipovetsky, T., Zhuang, L., Teixeira, W.G., Boyd, A., May Pontedeiro, E., Moriconi, L., Alves, J.L.D., Couto, P., van Genuchten, M.T., 2020. HYPROP measurements of the unsaturated hydraulic properties of a carbonate rock sample. J. Hydrol. (Amst.) 591, 125706.

Liu, H., Lennartz, B., 2019. Hydraulic properties of peat soils along a bulk density gradient—A meta study. Hydrol. Process. 33, 101–114.

Lucas, M., Schlüter, S., Vogel, H.-J., Vetterlein, D., 2019. Roots compact the surrounding soil depending on the structures they encounter. Sci. Rep. 9, 16236.

Lu, J., Zhang, Q., Werner, A.D., Li, Y., Jiang, S., Tan, Z., 2020. Root-induced changes of soil hydraulic properties – A review. J. Hydrol. (Amst.) 589, 125203.

Lynch, J., 1995. Root architecture and plant productivity. Plant Physiol. 109, 7–13.

Maccaferri, M., Harris, N.S., Twardziok, S.O., Pasam, R.K., Gundlach, H., Spannagl, M., Ormanbekova, D., Lux, T., Prade, V.M., Milner, S.G., Himmelbach, A., Mascher, M., Bagnaresi, P., Faccioli, P., Cozzi, P., Lauria, M., Lazzari, B., Stella, A., Manconi, A., Gnocchi, M., Moscatelli, M., Avni, R., Deek, J., Biyiklioglu, S., Frascaroli, E., Corneti, S., Salvi, S., Sonnante, G., Desiderio, F., Marè, C., Crosatti, C., Mica, E., Özkan, H., Kilian, B., De Vita, P., Marone, D., Joukhadar, R., Mazzucotelli, E., Nigro, D., Gadaleta, A., Chao, S., Faris, J.D., Melo, A.T.O., Pumphrey, M., Pecchioni, N., Milanesi, L., Wiebe, K., Ens, J., MacLachlan, R.P., Clarke, J.M., Sharpe, A.G., Koh, C.S., Liang, K.Y.H., Taylor, G.J., Knox, R., Budak, H., Mastrangelo, A.M., Xu, S.S., Stein, N., Hale, I., Distelfeld, A., Hayden, M.J., Tuberosa, R., Walkowiak, S., Mayer, K.F.X., Ceriotti, A., Pozniak, C.J., Cattivelli, L., 2019. Durum wheat genome highlights past domestication signatures and future improvement targets. Nat. Genet. 51, 885–895.

Marshall, T.J., Holmes, J.W., Rose, C.W., 1996. Soil Physics, 3rd ed. Cambridge University Press, Cambridge, England.

Mualem, Y., 1976. A new model for predicting the hydraulic conductivity of unsaturated porous media. Water Resources Research 12, 513–522.

Naveed, M., Ahmed, M.A., Benard, P., Brown, L.K., George, T.S., Bengough, A.G., Roose, T., Koebernick, N., Hallett, P.D., 2019. Surface tension, rheology and hydrophobicity of rhizodeposits and seed mucilage influence soil water retention and hysteresis. Plant Soil 437, 65–81.

Ober, E.S., Alahmad, S., Cockram, J., Forestan, C., Hickey, L.T., Kant, J., Maccaferri, M., Marr, E., Milner, M., Pinto, F., Rambla, C., Reynolds, M., Salvi, S., Sciara, G., Snowdon, R.J., Thomelin, P., Tuberosa, R., Uauy, C., Voss-Fels, K.P., Wallington, E., Watt, M., 2021. Wheat root systems as a breeding target for climate resilience. Theor. Appl. Genet. 134, 1645–1662.

Paez-Garcia, A., Motes, C.M., Scheible, W.-R., Chen, R., Blancaflor, E.B., Monteros, M.J., 2015. Root traits and phenotyping strategies for plant improvement. Plants 4, 334–355.

Peters, A., Durner, W., 2008. Simplified evaporation method for determining soil hydraulic properties. J. Hydrol. (Amst.) 356, 147–162.

Rabot, E., Wiesmeier, M., Schlüter, S., Vogel, H.-J., 2018. Soil structure as an indicator of soil functions: A review. Geoderma 314, 122–137.

Rawls, W.J., Gimenez, D., Grossman, R., 1998. Use of soil texture, bulk density, and slope of the water retention curve to predict saturated hydraulic conductivity. Transactions of the ASAE 41, 983–988.

Sarkar, S., Germer, K., Maity, R., Durner, W., 2019. Measuring near-saturated hydraulic conductivity of soils by quasi unit-gradient percolation—2. Application of the methodology. J. Plant Nutr. Soil Sci. 182, 535–540.

Schaap, M.G., van Genuchten, M.T., 2006. A modified Mualem–van Genuchten formulation for improved description of the hydraulic conductivity near saturation. Vadose Zone J. 5, 27–34.

Schindler, U., Durner, W., von Unold, G., Mueller, L., Wieland, R., 2010. The evaporation method: Extending the measurement range of soil hydraulic properties using the air-entry pressure of the ceramic cup. J. Plant Nutr. Soil Sci. 173, 563–572.

Scholl, P., Leitner, D., Kammerer, G., Loiskandl, W., Kaul, H.-P., Bodner, G., 2014. Root induced changes of effective 1D hydraulic properties in a soil column. Plant Soil 381, 193–213.

Seethepalli, A., Dhakal, K., Griffiths, M., Guo, H., Freschet, G.T., York, L.M., 2021. RhizoVision Explorer: Open-source software for root image analysis and measurement standardization. bioRxiv. https://doi.org/10.1101/2021.04.11.439359

Seki, K., Toride, N., Th. van Genuchten, M., 2022. Closed-form hydraulic conductivity equations for multimodal unsaturated soil hydraulic properties. Vadose Zone J. 21. https://doi.org/10.1002/vzj2.20168

Šimůnek, J., Brunetti, G., Jacques, D., van Genuchten, M.T., Šejna, M., 2024. Developments and applications of the HYDRUS computer software packages since 2016. Vadose Zone J. 23. https://doi.org/10.1002/vzj2.20310

Singh, A., Verdi, A., 2024. Estimating the soil water retention curve by the HYPROP-WP4C system, HYPROP-based PCNN-PTF and inverse modeling using HYDRUS-1D. J. Hydrol. (Amst.) 639, 131657.

Song, L., Li, J.H., Zhou, T., Fredlund, D.G., 2017. Experimental study on unsaturated hydraulic properties of vegetated soil. Ecol. Eng. 103, 207–216.

Staszel-Szlachta, K., Lasota, J., Szlachta, A., Błońska, E., 2024. The impact of root systems and their exudates in different tree species on soil properties and microorganisms in a temperate forest ecosystem. BMC Plant Biol. 24, 45.

Strudley, M., Green, T., Ascoughii, J., 2008. Tillage effects on soil hydraulic properties in space and time: State of the science. Soil Tillage Res. 99, 4–48.

Trachsel, S., Kaeppler, S.M., Brown, K.M., Lynch, J.P., 2011. Shovelomics: high throughput phenotyping of maize (Zea mays L.) root architecture in the field. Plant Soil 341, 75–87.

Tuller, M., Or, D., Dudley, L.M., 1999. Adsorption and capillary condensation in porous media: Liquid retention and interfacial configurations in angular pores. Water Resour. Res. 35, 1949–1964.

Uga, Y., 2021. Challenges to design-oriented breeding of root system architecture adapted to climate change. Breed. Sci. 71, 3–12.

van Genuchten, M.T., 1980. A closed-form equation for predicting the hydraulic conductivity of unsaturated soils. Soil Sci. Soc. Am. J. 44, 892–898.

van Genuchten, M., Leij, F., Yates, S., 1992. The RETC code for quantifying the hydraulic functions of unsaturated soils.

Wang, P., Ding, L., Zou, C., Zhang, Y., Wang, M., 2022. Rhizosphere element circling, multifunctionality, aboveground productivity and trade-offs are better predicted by rhizosphere rare taxa. Front. Plant Sci. 13, 985574.

White, C.A., Sylvester-Bradley, R., Berry, P.M., 2015. Root length densities of UK wheat and oilseed rape crops with implications for water capture and yield. J. Exp. Bot. 66, 2293–2303.

Wind, G.P., 1968. Capillary conductivity data estimated by a simple method. Water in the unsaturated zone 1, 181–191.

Wingen, L.U., Orford, S., Goram, R., Leverington-Waite, M., Bilham, L., Patsiou, T.S., Ambrose, M., Dicks, J., Griffiths, S., 2014. Establishing the A. E. Watkins landrace cultivar collection as a resource for systematic gene discovery in bread wheat. Züchter Genet. Breed. Res. 127, 1831–1842.

Xiao, T., Li, P., Fei, W., Wang, J., 2024. Effects of vegetation roots on the structure and hydraulic properties of soils: A perspective review. Sci. Total Environ. 906, 167524.

York, L.M., Slack, S., Bennett, M.J., Foulkes, M.J., 2018. Wheat shovelomics I: A field phenotyping approach for characterising the structure and function of root systems in tillering species. bioRxiv. https://doi.org/10.1101/280875

Young, I.M., Ritz, K., 2005. The habitat of soil microbes. https://doi.org/10.5555/20073109422

Zhang, Y., Wu, X., Wang, X., Dai, M., Peng, Y., 2025. Crop root system architecture in drought response. J. Genet. Genomics 52, 4–13.

Zhou, H., Whalley, W.R., Hawkesford, M.J., Ashton, R.W., Atkinson, B., Atkinson, J.A., Sturrock, C.J., Bennett, M.J., Mooney, S.J., 2021. The interaction between wheat roots and soil pores in structured field soil. J. Exp. Bot. 72, 747–756.

Acknowledgements

MCHS gratefully acknowledges funding support from the Biotechnology and Biological Sciences Research Council (BBSRC), project BB/X003000/1. Funding was also provided by the Department of Agricultural and Food Sciences (DISTAL), University of Bologna, through its Ph.D programme. We thank Silvio Salvi for useful discussion and for participation in the development and implementation of the funded project. We are also grateful to Marco Maccaferri for providing the seeds of the cultivar Senatore Cappelli and for useful discussions, to the John Innes Centre Germplasm Resources Unit for providing the seeds of the Paragon and Watkins 238 cultivars, and to Simon Griffiths and Luzie U. Wingen for advice on the relevance of these cultivars. BGD gratefully acknowledges the support of the Collegio Superiore and the Institute of Advanced Studies of the University of Bologna. We would like to thank METER Group Inc. (Munich, Germany) where the measurements of the SHPs were performed, for providing access to the soil hydraulic instrumentation and Prof. Wolfgang Durner for generously sharing his expertise and guidance throughout the study.

Author contributions statement

B.G.D. contributed to the writing of the funded project, conceived the experiment, followed all the agronomic practices and management practices, collected samples and data, analyzed the data and wrote the paper; M.C.H.S is the coordinator of the project and contributed to manuscript review; F.T. wrote the software used for non-linear fitting and computation of hydraulic properties; M.B contributed to the writing of the project, coordinated the experimental setup, wrote the software used for non-linear fitting and computation of hydraulic properties, contributed to data analysis and writing of the paper; R.T contributed to the writing of the paper.

Chapter 4

A root phenotyping protocol suitable for both monocot and dicot annual crops

Bartolo Giuseppe Dimattia[1], Daniele Rabboni, Giuseppe Sangiorgi, Francesco Camerlengo, and Silvio Salvi[1]*

[1]Department of Agricultural and Food Sciences, University of Bologna, Viale Fanin, 44, 40125, Bologna, Italy

*Corresponding author: bartolo.dimattia2@unibo.it

Manuscript in preparation for submission to *Plant and Soil*

Abstract

Quantitative phenotyping of root system architecture (RSA) is critical for understanding genetic variation and improving crop adaptation, but methodological limitations often constrain the comparability of results across studies. The objective of this study was to develop and test a root phenotyping protocol suitable for both monocot and dicot annual crops, enabling the evaluation of complementary architectural and topological traits. We applied the protocol to eight genotypes representing wheat, barley and chickpea. Roots were excavated in the field using shovelomics and imaged, then washed and scanned in water to capture finer root segments. The same procedure was applied to seedlings grown in glass-walled rhizotrons filled with soil, combining in situ imaging with ex situ scans of cleaned roots. Images were analyzed with RhizoVision Explorer, while rhizotron datasets required an additional segmentation step with a newly trained RootPainter model optimized for fibrous roots. Within- species significant genotypic differences were detected for multiple traits in both shovelomics and rhizotron datasets. However, cross-platform (i.e. shovelomics vs. rhizotron) comparisons revealed that consistency was trait-dependent. Root angle traits were strongly correlated between methods ($R^2 \approx 0.5$), and branching-related traits such as root tip number and branching frequency also showed moderate to strong agreement (R^2 up to 0.9). In contrast, root length and volume traits exhibited weak or inconsistent correlations, reflecting both technical constraints (e.g., root loss during washing, restricted rhizotron dimensions) and developmental dynamics of trait expression. The protocol integrates complementary measurements of root crowns and washed root systems, offering a standardized framework for assessing RSA across species. This approach enhances the reliability of root trait characterization and provides a practical tool to support breeding for resource-efficient crops.

1. Introduction

The accelerating climate crisis and the growing global population urgently call for the optimization of crop production systems (Nair 2019). Among the key traits influencing yield stability and resource use efficiency, root system architecture (RSA) plays a pivotal role in the acquisition of water and nutrients, especially under suboptimal conditions (J. Lynch 1995; Meister et al. 2014). Root traits are not only instrumental in improving tolerance to abiotic stresses such as drought and nutrient deficiency but also tend to remain more stable under increased reproductive allocation, including higher grain load (D. J. Lynch et al. 2013). In this context, recent research has increasingly focused on selecting genotypes with optimized RSA to enhance productivity and sustainability (Schmidt and Gaudin 2017).

Improving crop varieties to enhance performance under abiotic stress is essential for addressing climate change and mitigating yield losses (Wasaya et al., 2018). However, the integration of root-related traits into breeding programs remains complex (Sharma and Carena, 2016). Root phenotyping is particularly challenging due to the opacity of soil and the structural complexity of root systems (Rogers and Benfey, 2015). Methodological limitations are central: existing approaches vary in throughput, resolution, and environmental realism, but none fully captures root development under natural conditions. Field-based methods such as shovelomics provide high-throughput data but are destructive and typically capture only a fraction of the root system (Trachsel et al., 2011). Controlled systems, including hydroponics or gel-based assays, allow detailed and rapid imaging, yet they inadequately represent soil–root interactions (Kuijken et al., 2015). Semi-controlled platforms such as rhizotrons represent an intermediate compromise, permitting repeated observations, though they are constrained by soil volume and environmental variability (Nagel et al., 2012). Importantly, correlations between methods are often weak: traits measured under controlled conditions do not consistently reflect field performance (Atkinson et al., 2019; Burridge et al., 2016). This underlines the necessity of multi-environment validation and cautious interpretation when translating root traits into breeding strategies.A wide range of 2D phenotyping systems has been developed to overcome the opacity of soil and enable quantitative analysis of root system architecture. Controlled, soil-free setups such as aeroponics, hydroponics, pouch-and-wick systems, and agar-based devices (e.g., RhizoTubes, Rhizoponics, Rhizoslides, RhizoChamber-Monitor, PlaRom, ChronoRoot) provide high visual contrast between roots and background, facilitating automated image acquisition and enabling high-throughput, precise characterization of root traits (Jeudy et al. 2016; Mathieu et al. 2015; Le Marié et al. 2014; Wu et al. 2018; Yazdanbakhsh and Fisahn 2009; Gaggion et al. 2021). However,

these approaches are typically restricted to early seedling stages and rely on artificial growth media, which limits their physiological relevance under agronomic conditions (Li et al. 2022).

Soil-based 2D platforms, such as RhizoPot, GROWSCREEN-Rhizo, GLO-Roots, GLO-Bot, PhenoRoots, and WinRoots, provide higher biological realism and allow long-term monitoring of roots under semi-natural conditions (Xiao et al. 2020; Nagel et al. 2012; Rellán-Álvarez et al. 2015; LaRue et al. 2021; Martins et al. 2020; Zhang et al. 2021). Nonetheless, soil heterogeneity introduces substantial environmental noise, complicates segmentation, and typically reduces imaging resolution and throughput compared to transparent, controlled media (Li et al. 2022). Field-adapted destructive methods, most notably shovelomics, represent a pragmatic balance between throughput, resolution, and realism, enabling rapid and cost-effective characterization of root crown traits in mature plants (Trachsel et al. 2011; York et al. 2018).

Three-dimensional imaging platforms allow for the non-invasive visualization of entire root systems within opaque substrates. Technologies such as X-ray computed tomography (CT) and magnetic resonance imaging (MRI) have been widely adopted for controlled soil environments, offering spatially and temporally resolved reconstruction of root architecture (Heeraman, Hopmans, and Clausnitzer 1997; van Dusschoten et al. 2016). Ground-penetrating radar (GPR) and electrical resistivity tomography (ERT) extend these capabilities to field conditions, allowing in situ root detection at larger spatial scales (Shihab and Al-Nuaimy 2004; Rossi et al. 2011). While these 3D approaches provide unparalleled insight into dynamic root development under realistic conditions, they are constrained by high costs, low throughput, and resolution limitations, particularly in resolving fine roots.

The effectiveness of any phenotyping method is strongly influenced by the availability of image analysis tools capable of extracting meaningful traits from complex root systems. A range of 2D and 3D image analysis software has been developed for root phenotyping, significantly improving the quantification of root traits (Paez-Garcia et al. 2015).

In this study, we optimized and compared a suit of root phenotyping protocols applicable to both annual monocotyledonous and dicotyledonous species. We specifically compared root traits obtained from plants grown in soil-filled rhizotrons with plants grown in field conditions. Root traits were collected using high-resolution image analysis of both entire root crowns and dissected root fragments, enabling a detailed RSA characterization. This study demonstrates the effectiveness of the protocol in capturing RSA variation in wheat, barley and chickpea lines.

2. *Materials and methods*

2.1 Study site

The field trial was conducted at the experimental farm of the University of Bologna in Cadriano (44°32′55″N, 11°24′52″E, 26 m a.s.l.), Italy. This area is characterized by a subhumid climate with a mean temperature of 12.8°C and an average annual precipitation of 924 mm. The soil is classified as loam, consisting of 11.49% clay, 52.87% silt, and 35.64% sand.

2.2 Plant materials

We tested our protocol on plants belonging to four species: bread wheat (*Triticum aestivum*), durum wheat (*Triticum turgidum* ssp. *durum*), barley (*Hordeum vulgare*), and chickpea (*Cicer arietinum*).

Durum wheat cultivar Senatore Cappelli, and bread wheat cultivars Watkins 238, Bologna, and Paragon were sown on 27/11/2022 using a Vignoli TB19 plot seeder. A total of 125 g of seeds was sown per 1 m × 6 m plot, with a seed density of approximately 400 seeds/m².

Barley cv Morex and the mutant line TMXXXX carrying a mutation in *EGT1*, a gene controlling root gravitropism (Fusi et al. 2022) from the TILLMore collection (Talamè et al 2008) were manually sown on 15/02/2024. Three rows, each 70 cm in length, were sown for both genotypes. After germination, the seedlings were thinned to achieve a spacing of approximately 2–4 cm between plants.

Chickpea lines 372 and 641 were sown in pots (5 × 5 × 15 cm) on 01/03/2024 and transplanted to the field two weeks after germination. The plants were arranged in single rows with a spacing of 10 cm between them

2.3.1 Soil filled rhizotrons

For all four species, the root system was analyzed using soil-filled rhizotrons. Prior to rhizotron setup, seeds were sterilized and pre-germinated for 24 hours at 28°C. The 2D rhizotron boxes were constructed using a black polycarbonate panel measuring 34 cm × 44 cm. The panel had an external thickness of 1 cm and an internal cavity thickness of 0.5 cm (2 cm – 1.5 cm for chickpea). These boxes were then filled with densely packed universal potting soil.

Within each rhizotron, one seed were placed for wheat and chickpea and two for barley, selected based on uniform germination. Seeds were positioned 2 cm from the upper edge and equidistant from

the lateral edges. To complete the assembly, a glass plate of the same dimensions as the panel was placed on top and secured with four metal clip holders—two near the top and two near the bottom on both sides.

The rhizotrons were installed in a tank equipped with supports, maintaining a 60° inclination with the glass side facing downward. They were placed in the DISTAL greenhouse, where lighting was provided by a combination of natural sunlight and supplemental 400-watt high-pressure sodium lamps (Sylvania SHP-TS 400W Grolux). The greenhouse environment was maintained at a daytime temperature of 22°C for 16 hours and a nighttime temperature of 18°C for 8 hours.

The plants were grown in the rhizotrons for ten days and were watered every three days.

Images were taken with the Epson Expression 12000XL scanner and processed using the Epson Scan 2 software (https://www.epson.it/it_IT/faq/KA-01831/contents?loc=it-it) at 7 days post-germination.

2.3.2 Root Image Segmentation of rhizotrones pictures Using RootPainter

Root segmentation was performed using RootPainter (version 0.2.27) following the protocol described in Smith et al. (2022) and available on the GitHub repository (Smith, 2024; https://github.com/Abe404/root_painter). The model was trained *de novo* to distinguish root tissue from background in rhizotron images acquired via flatbed scanner. A training dataset was assembled using the "Create training dataset" function, which generated cropped image tiles (750 × 750 px) from a subset of representative images ($n \approx 100$, consistent with values reported in Smith et al., 2022). The first 6–8 images were manually annotated in full, labelling all visible roots as foreground and the surrounding soil matrix as background, with background pixels exceeding root pixels by a factor of 5–10 to improve model discrimination.

Model training commenced after the annotation of the second image, following the "Corrective Training Protocol" outlined in Smith et al. (2022). Subsequent annotation rounds focused on correcting misclassified regions in the pre-segmented images produced by the evolving model. This iterative process of segmentation–correction was repeated until the model achieved consistent accuracy across images with varying root densities and soil textures.

The trained model was then applied to the entire rhizotron dataset to produce binary masks (white roots on black background). These masks were converted into RhizoVision-compatible format using the "Export segmentation" function and subsequently analysed in RhizoVision Explorer with the same image analysis parameters described for scanned roots. This workflow ensured high-contrast

segmentation, minimized background noise, and enabled extraction of architectural and morphological root traits from rhizotron-grown plants.

2.4.1 Root sampling from field

Plant sampling was conducted at full flowering (61–65 BBCH) to ensure complete development of the root crown (Trachsel et al., 2016). Initially, a uniform segment was selected from the center of each experimental plot based on homogeneity in plant tillering. This segment measured approximately 40 cm in length and 30 cm in depth. Plants within this designated area were carefully excavated using a tuscany shovel featuring a 4.5 cm diameter handle and a blade measuring 30 cm × 22 cm × 2 mm (Fig. 1A). Excavation cuts were strategically made between wheat rows to minimize root damage and retain surrounding soil integrity. Each excavated sod contained at least six plants of uniform height and similar culm numbers to ensure consistency across replicates. Extracted samples were immediately labeled, placed into large containers, and transported to a shaded area where they were submerged in water overnight to facilitate soil loosening (Fig. 1B).

After 24 hours, roots were gently washed using a low-pressure water hose to remove adhering soil without damaging delicate structures (Fig. 1C). Post-washing, individual plants were separated and positioned on a clean working surface for visual inspection. Plants were selected based on uniformity in height, number of culms, root size, and integrity. Remaining debris, weeds, or leaves present on the roots were meticulously removed.

Phenotyping of aerial plant parts was subsequently conducted by positioning three replicates individually next to a meter stick to measure the height of the main culm, excluding awns, and to record the number of culms. Following phenotyping, plants were placed in a basin containing clean water in preparation for root imaging.

2.4.2 Imaging the intact (whole) root stock

Root imaging was performed with protocols specifically developed to capture comprehensive data on root architecture. Entire root systems were initially imaged to evaluate the overall root crown structure under field conditions. Plants were placed on a clean, non-reflective black velvet surface to maximize image contrast and reduce background interference. Images were captured using a Nikon D5600 camera mounted on a U-DOLI tripod adjustable between 55 cm and 85 cm in height. The camera was positioned at an 80 cm distance from the roots, aligned at the same height, to prevent image distortion (Fig. 1D). A reference marker and a plant label, positioned without overlapping the sample, served as references for scale calibration (Fig. 1E). Each plant was photographed from a frontal view and then

rotated 90 degrees for a secondary capture, ensuring a comprehensive three-dimensional representation. Consistent lighting and standardized imaging parameters were maintained throughout to ensure data comparability.

2.4.3 Broken root imaging

Following initial root imaging from shovelomics and rhizotron-grown plants, a second phase of **broken root imaging** was conducted to acquire high-resolution scans of dissected root systems.

For shovelomics samples, the main culm roots were separated from the remaining roots, detached from the shoots, and preserved in 50 ml Falcon tubes filled with 50% ethanol, stored at 4 °C from May to September 2023. For rhizotron-grown plants, roots were carefully extracted from soil and gently washed with a low-pressure hose to remove debris.

Prior to scanning, roots were dissected using scissors to preserve their entire length, cleaned for 5 min in a basin with an Alconox soapy solution, and rinsed thoroughly with water. Clean and dissected roots were then arranged in a plexiglass tank (29.7 × 42.0 × 4 cm) with 0.3 cm matte black edges, placed on an Epson Expression 12000XL Pro flatbed scanner (Fig. 1F). The tank was filled with 1.5 L of water, and roots were carefully positioned with tweezers to minimize overlap. A reference marker was included within the scanning frame, and the tank was covered with a matte black lid (35 × 45 × 1 cm) to reduce reflections and external light interference. Images were acquired at a minimum resolution of 600 DPI, with water replaced every ten samples to maintain image clarity. After scanning, roots were systematically transferred into labeled paper envelopes for drying (Dimattia et al. 2025).

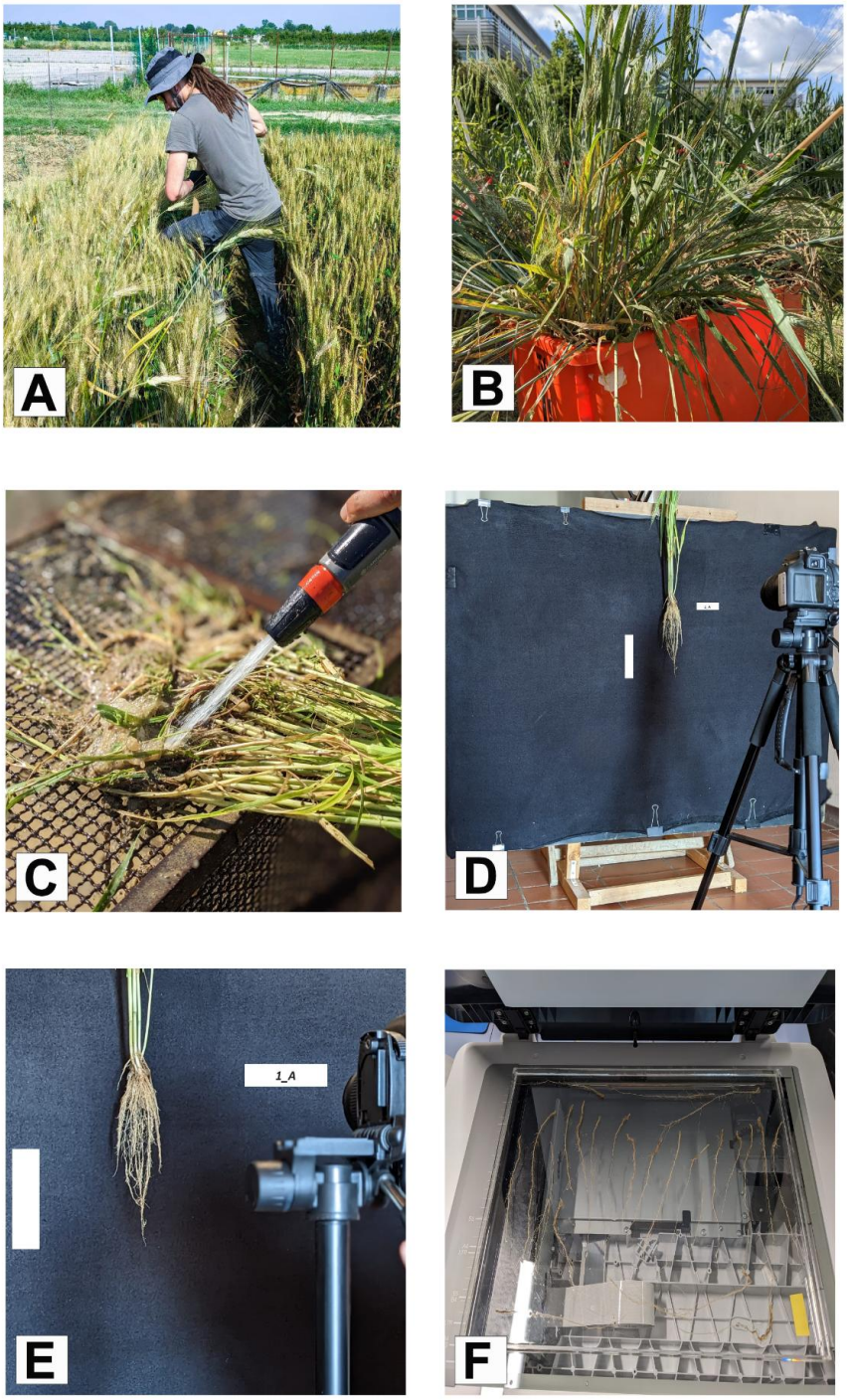

Figure 1. A) Rootstock escavation. B) Basin filled with the excavated sod and water, containing labeled plants ready for further processing. C) Samples being washed by spraying the roots with low-pressure water from a hose to remove any adhering soil particles. D) Setup station for the whole root

imaging. E) Crown root with reference marker and image code. F) Roots in the phenotyping tank positioned over the scanner, carefully arranged to prevent overlapping.

2.5 Data extraction

The collected images were processed using RhizoVision Explorer (Perez et al. 2022; Seethepalli et al. 2021). Prior to analysis, the images underwent preprocessing aimed at optimizing their quality and suitability for accurate phenotypic characterization. This preprocessing involved cropping to eliminate labels and reference markers, renaming the images with a relevant plot and replicate identifier (Plot_Rep), and enhancing contrast through adjustments to the image threshold level to ensure precise root edge detection. The conversion from pixels to physical units (mm) was performed using pixel estimations obtained through ImageJ by measuring the pixel length of a known reference marker. This procedure resulted in 7.5 pixels per mm for shovelomics-based root imaging and 17.5 pixels per mm for scanned images. Noise from background debris was minimized using the "Filter Nonroot Objects" function, while the "Edge Smoothing" and "Root Pruning" parameters were carefully calibrated to minimize artifacts and prevent loss of finer roots (Tab.1).

Table 1. Summary of RhizoVision parameters selected for this experiment. The Image Pre-processing and Feature Extraction parameters were chosen to optimally differentiate seminal roots from lateral roots.

Window	**RhizoVision parameters**	**Crown root images**	**Dissected root images**	
		Whole root	**Mode 1**	**Mode 2**
Image preprocessing	*Convert pixel to physical units*	8.6 pixel/mm	19 pixel/mm	19 pixel/mm
	Image thresholding level	170	170	200
	Keep largest component	-	-	-
	Filter nonroot objects	2	1	10
	Fill holes in root objects	-	-	-
	Edge smoothing	2	4	4
Feature extraction	*Root pruning*	2	200	4
	Range 1	0 – 1.6	0 - 0.5	0 - 0.5
	Range 2	>1.6	>0.5	>0.5

Two distinct analytical methods were employed based on the type of root images collected (Fig. 2). For crown root images obtained via shovelomics, the "whole-root analysis" was applied. Traits selected from this method were those well-established in the literature for characterizing general root

architecture, specifically root network area, convex hull area, fragmented root morphological patterns, and shallow and steep angles (Le Marié et al. 2019; Trachsel et al., 2011; Maccaferri et al., 2016; Ober et al., 2021).

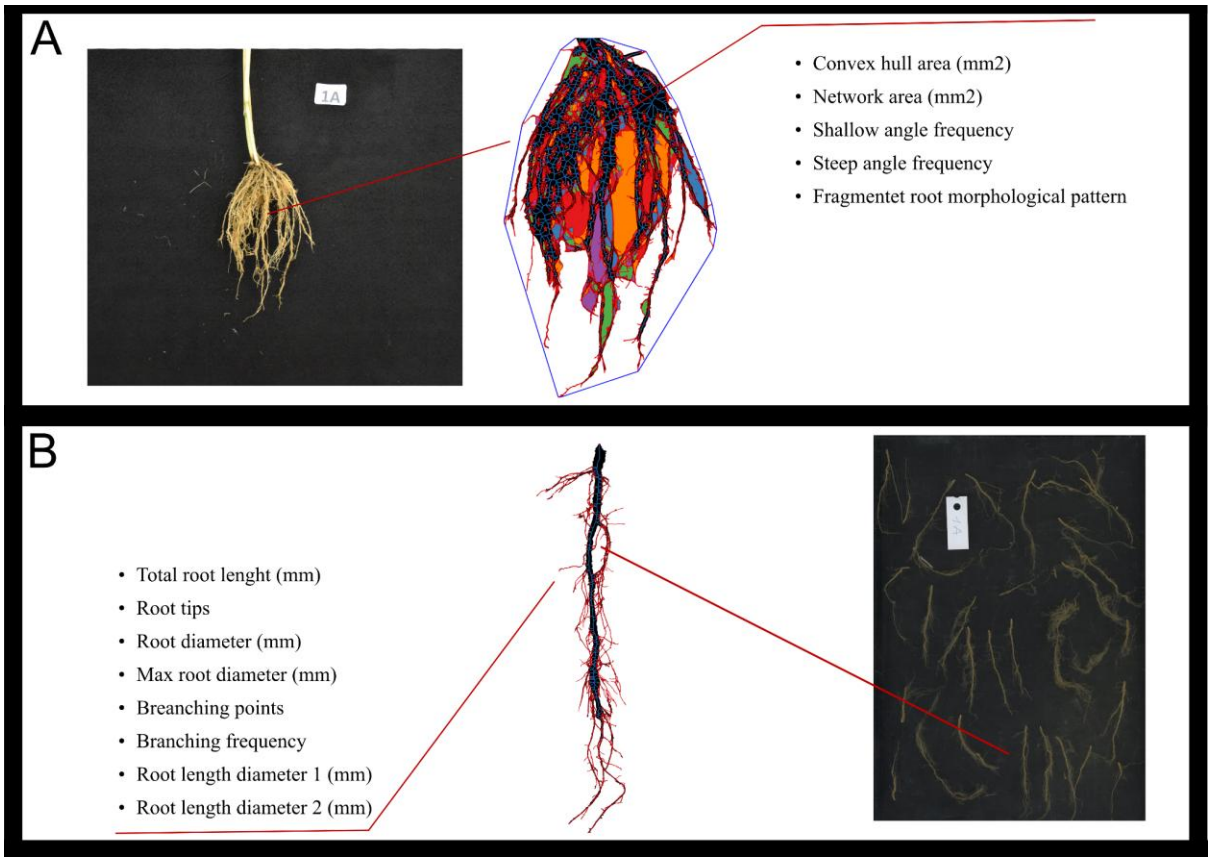

Figure 2. Whole root image (A) before and dissected root image (B) after the RhizoVision Explorer analysis with the trait selected for this experiment.

For scanned root images, the "broken-root analysis" was utilized, employing two complementary methodologies to achieve enhanced accuracy (Fig. 2 and 3). The first approach targeted axial roots (Fig. 4B), significantly reducing previous overestimations of larger diameter classes, while the second approach (Fig. 4C) was optimized for retaining finer lateral roots, root tips, branching frequency, and branching points (Fig. 5). Total root length was calculated by summing the lengths obtained from both methodologies. Additional traits extracted from the broken-root analysis included scanned root length, length of roots with diameters below and above 0.45 mm, average and maximum root diameter, number of root tips, branching points, and branching frequency (Freschet et al. 2021; Lu et al., 2020; Jin et al., 2017). Further details on the specific parametrization settings for both approaches are provided in Table 1. Overall, the integration of these methods provided a comprehensive analysis of root architecture, combining the broad structural insights from whole-root analysis with the detailed morphological resolution of broken-root analysis.

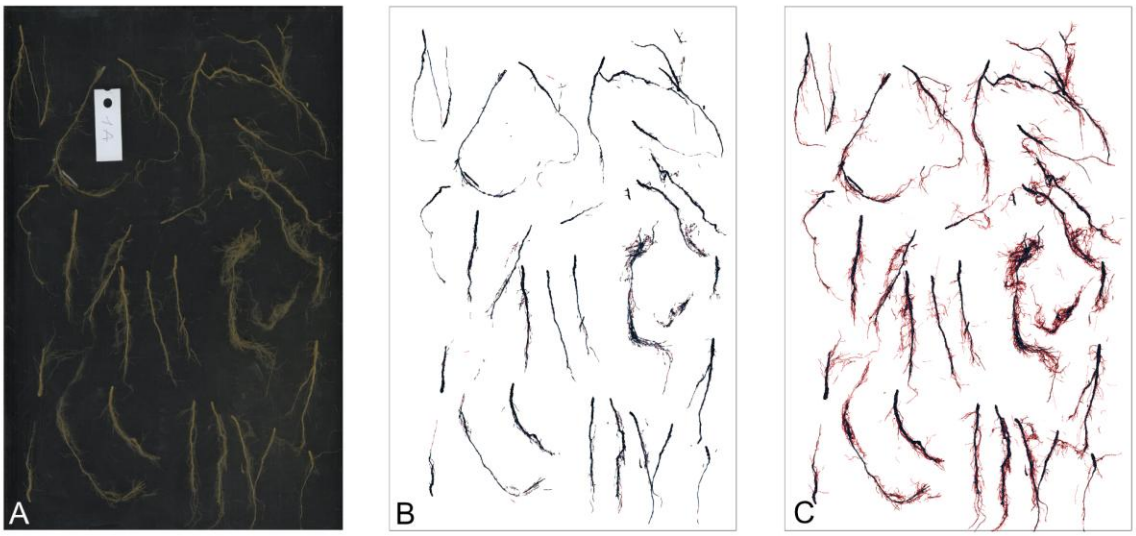

Figure 3. Broken root image (A), displayed image after the method 1 (B) and 2 (C) analysis on Rhizovision Explorer.

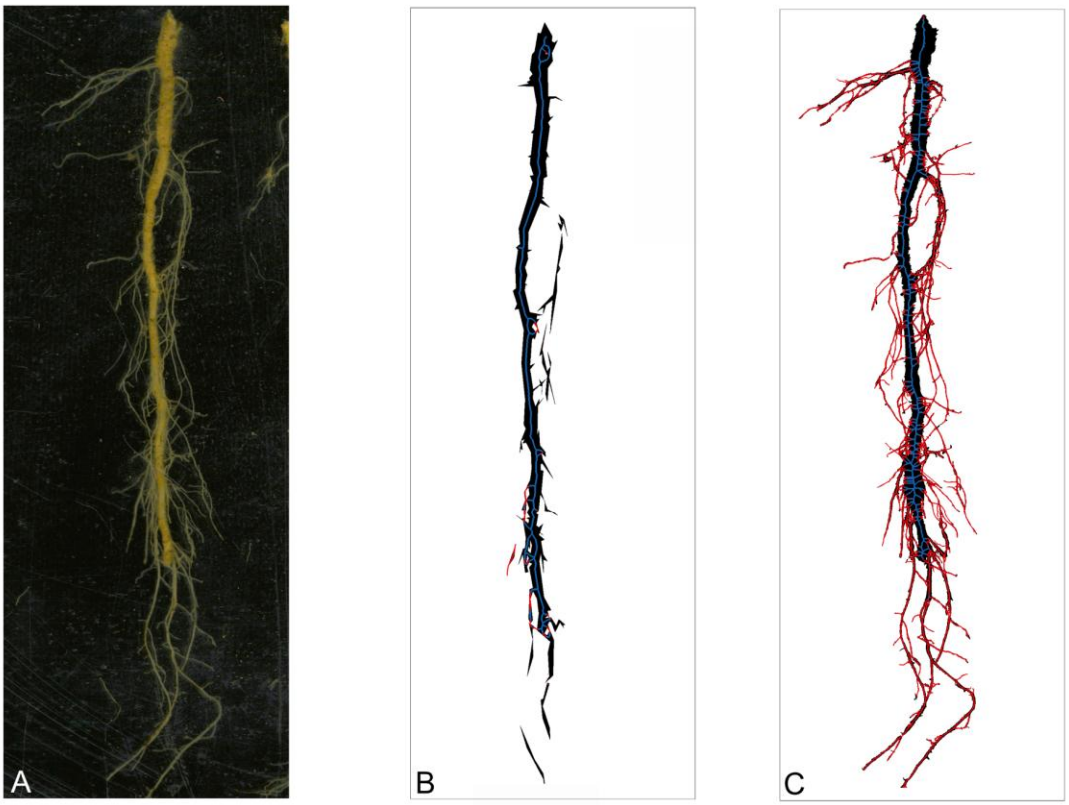

Figure 4. Single root detail before (A) and after the analysis with RhizovisionExplorer with to enhance the axial root length (B) and lateral root length (C).

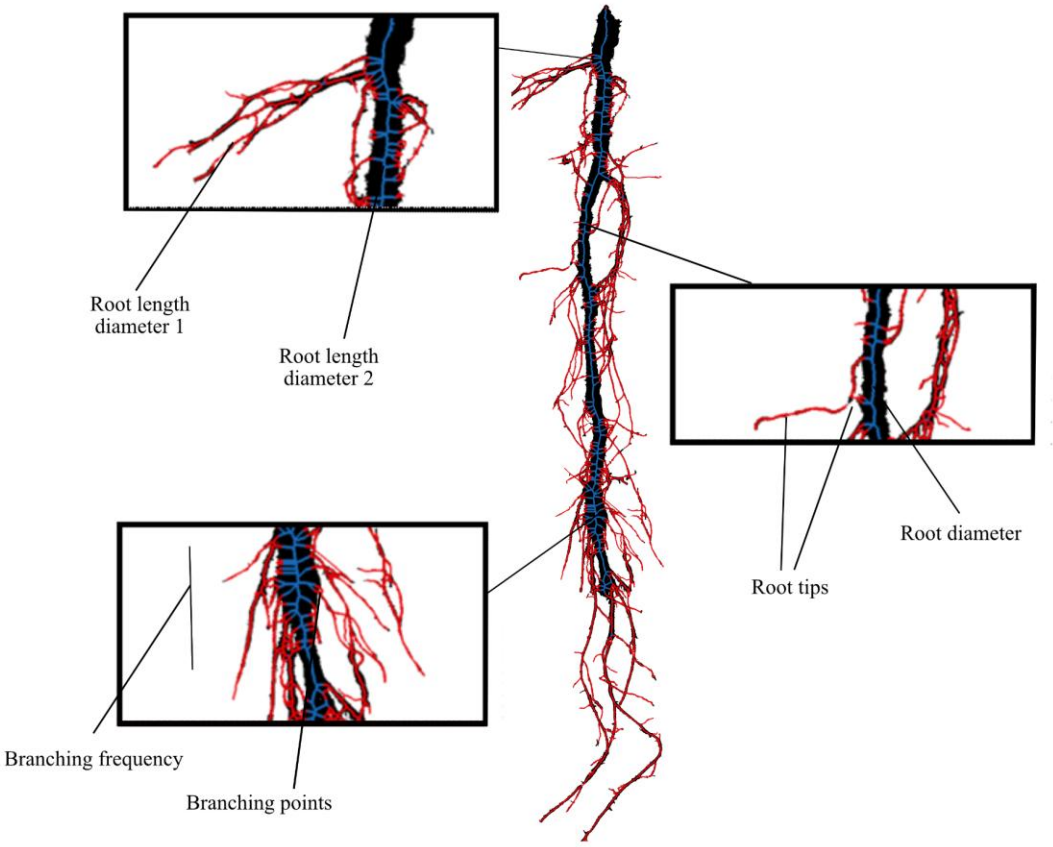

Figure 5. Example of a single root image processed with Method 2, showing key traits extracted using the broken-root analysis in RhizoVision Explorer. Root length in diameter class 2 and root diameter were estimated using Method 1, while root length in diameter class 1, number of root tips, branching frequency, and branching points were extracted using Method 2.

2.6 Statistical analysis

An analysis of variance (ANOVA) was conducted among the four wheat genotypes for all root traits extracted using RhizoVision Explorer, considering both shovelomics and rhizotron data. Fixed effects included flowering stage and replication. For barley and chickpea genotypes, a t-test was performed. A post-hoc analysis was carried out to identify specific significant differences.

Correlations between phenotyping methods were computed on the wheat and barley datasets. Agreement between shovelomics and rhizotron measurements was evaluated for all traits using correlation analysis (Pearson's correlation coefficient, or Spearman's rank correlation when normality assumptions were not met) and simple linear regression on standardized (z-scored) values.

3. Results

3.1 Root Phenotyping Data Collection Across Protocols

Phenotypic root traits were collected using a multi-scale approach combining complementary imaging protocols. Specifically, data were obtained from (i) whole-root imaging through shovelomics, (ii) broken-root analysis post-shovelomics, (iii) rhizotron-based phenotyping, and (iv) broken roots after rhizotron extraction. Each protocol captured a specific subset of architectural or anatomical traits, contributing to a comprehensive assessment of root system morphology and topology.

A flow diagram (Fig. 6) summarizes the data sources for each trait, linking the protocol with the derived root variables.

(1) Shovelomics

The following traits were extracted from whole-root crown images collected via shovelomics:

- *Root count and architecture:*
  Median_number_of_roots, Maximum_number_of_roots, Number_of_root_tips, Total_root_length (mm), Depth (mm), Maximum_Width (mm), Width_to_depth_ratio.
- *Root system morphology:*
  Network_Area (mm^2), Convex_Area (mm^2), Solidity, Lower_root_area (mm^2).
- *Root thickness and size distribution:*
  Average_diameter (mm), Median_diameter (mm), Maximum_diameter (mm), Perimeter (mm), Volume (mm^3), Surface_area (mm^2).
- *Porosity-related traits:*
  Holes (count), Average_hole_size (mm^2).
- *Root orientation and angle distribution:*
  Average_root_orientation (degrees), Shallow_angle_frequency (%), Medium_angle_frequency (%), Steep_angle_frequency (%).
- *Diameter class traits:*
  Root_length_diameter_range1/2 (mm), Projected_area_diameter_range1/2 (mm^2), Surface_area_diameter_range1/2 (mm^2), Volume_diameter_range1/2 (mm^3).

- *Processing-related:*
  Computation_time (s).

(2) Broken Roots After Shovelomics

Root fragments from the same plants were scanned individually to capture finer traits. The following variables were derived:

- *Topology and branching:*
  Number_of_root_tips, Branch_points, Branching_frequency (no. mm^{-1}).
- *Root architecture:*
  Total_root_length (mm), Network_Area (mm^2).
- *Root thickness:*
  Average_diameter (mm), Median_diameter (mm), Maximum_diameter (mm), Perimeter (mm), Volume (mm^3), Surface_area (mm^2).
- *Diameter class traits:*
  Root_length_diameter_range1/2 (mm), Projected_area_diameter_range1/2 (mm^2), Surface_area_diameter_range1/2 (mm^2), Volume_diameter_range1/2 (mm^3).
- *Processing-related:*
  Computation_time (s)

(3) Rhizotrons

(4) Broken Roots After Rhizotrons

The same sets of traits as above were extracted from rhizotron-grown plants and their respective broken roots. This ensured the consistency of measurements across soil-grown and rhizotron-grown environments.

To ensure robust and biologically meaningful characterization of root system architecture, we recommend selecting traits according to the strengths of each phenotyping method. For example, when using shovelomics and broken root analysis in combination, general architectural traits such as root angles, convex area, or hole abundance are best derived from whole-root images, which preserve the spatial integrity of the crown structure. In contrast, topological and branching-related traits—such as branching frequency, number of tips, and diameter class distribution—are better captured from broken root scans, which enhance resolution for fine root segments and internal topology. This

modular approach enables researchers to tailor trait selection according to their experimental goals and the resolution required by specific hypotheses.

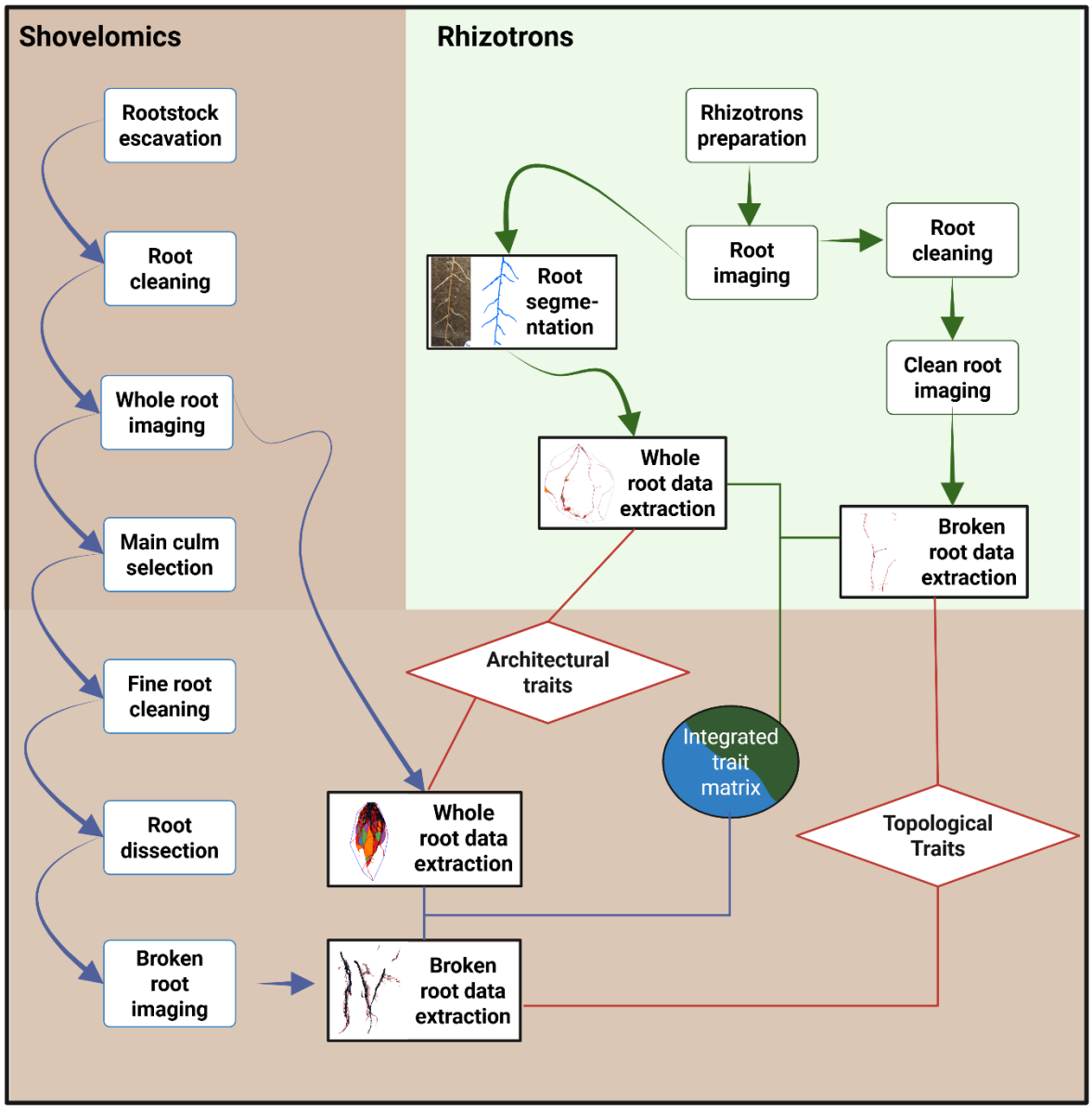

Figure 6. Workflow of the integrated root phenotyping protocol combining shovelomics and rhizotron imaging. Both approaches provide complementary datasets, with whole-root images capturing architectural traits and broken-root scans enabling detailed topological trait extraction, merged into a unified trait matrix.

3.2 Barley mutants presented differences in whole root traits

Clear differences between EGT1 and Morex (wt) were detected through shovelomics analysis (Fig. 7 and 8). EGT1 showed a higher average root orientation ($p < 0.001$), greater steep-angle frequency, and deeper rooting depth ($p = 0.034$). On the other hand, Morex exhibited a higher shallow-angle frequency ($p = 0.004$). No significant differences were found for the other traits, including those from the broken root analysis. More details are available in the supplementary material.

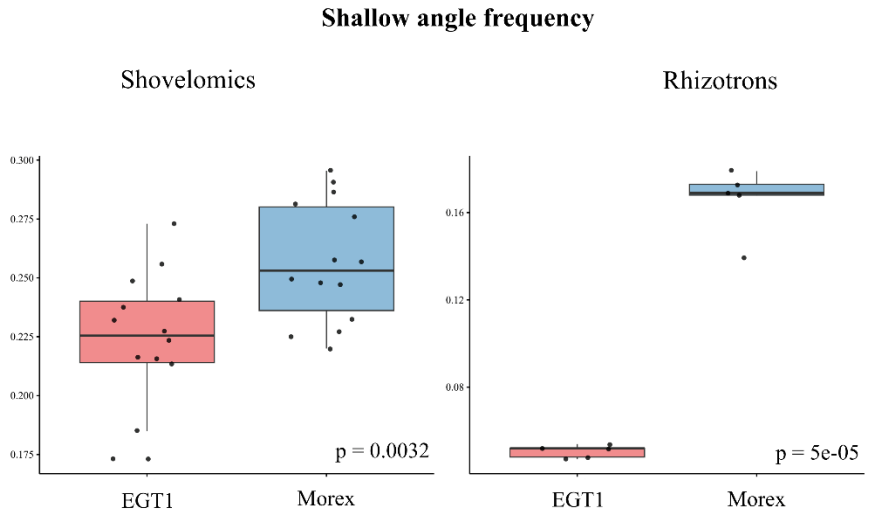

Figure 7. Boxplot showing the differences in shallow angle frequency between Morex and EGT1 both in shovelomics and rhizotrons.

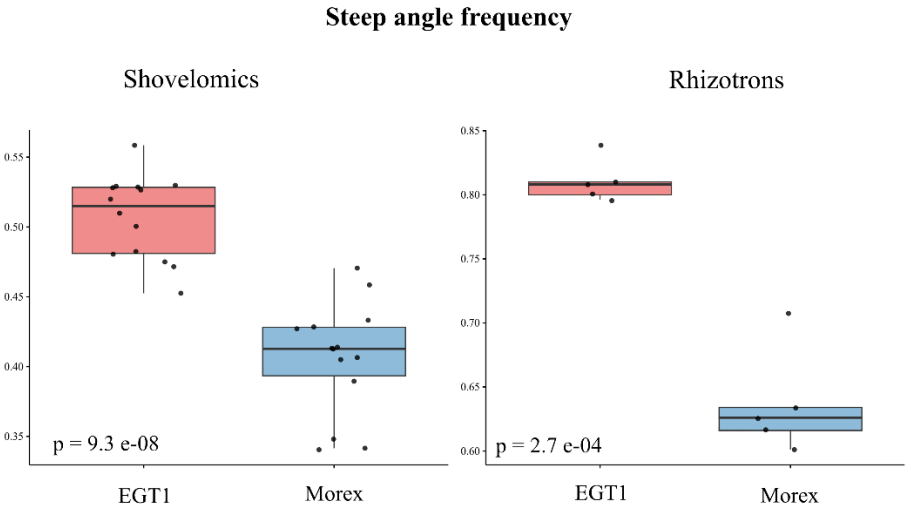

Figure 8. Boxplot showing the differences in steep angle frequency between Morex and EGT1 both in shovelomics and rhizotrons.

Similar differences in root angle between EGT1 and Morex were also observed using rhizotron phenotyping. EGT1 showed higher average root orientation ($p < 0.001$), higher steep-angle frequency ($p < 0.001$), and lower maximum width ($p = 0.001$) and shallow-angle frequency. Overall, EGT1 displayed higher values for many phenotypic traits. We hypothesize that the gravitropic roots tend to grow close to the glass, potentially leading to an overestimation of most traits. More details are available in the supplementary material.

3.3 Chickpea genotypes presented differences in whole root traits

Significant differences were found between the two genotypes using both shovelomics and rhizotron phenotyping. Shovelomics data showed that 372 had a higher steep-angle frequency ($p = 0.01$), greater root volume ($p < 0.01$), and larger maximum root diameter ($p < 0.001$) compared to 641. Rhizotron analysis confirmed that 372 had a higher number of roots ($p < 0.05$) and steep-angle frequency ($p < 0.01$). In contrast, 641 exhibited a significantly higher shallow-angle frequency ($p < 0.001$). Aggiungi grafico dell'angolo.

3.4.1 Wheat genotypes presented differences in whole root traits

ANOVA revealed significant differences in root morphology among wheat genotypes. Shovelomics data showed that Bologna had a higher steep-angle frequency ($p < 0.05$) and a slightly less pronounced difference in shallow-angle frequency ($p < 0.05$) compared to all other genotypes.

These results were confirmed by rhizotron data where Bologna exhibited a higher steep-angle frequency and a lower shallow-angle frequency compared to Paragon ($p < 0.001$) and Watkins238 ($p < 0.05$).

Shovelomics data showed that Cappelli had a larger convex hull area and network area compared to Bologna ($p < 0.05$). However, these differences were not observed in the rhizotron data. Nevertheless, in the rhizotrons, Cappelli still displayed the largest convex hull area, with a significant difference ($p < 0.05$) when compared to Paragon. The fragmented root morphological pattern (FRMP) values were also significantly lower in Bologna compared to Senatore Cappelli ($p < 0.001$), Paragon ($p < 0.05$), and Watkins238 ($p < 0.01$). However, no significant differences related to this trait were detected in the rhizotron analysis.

3.4.2 Wheat genotypes presented differences in root topological traits

Paragon and Senatore Cappelli presented significantly higher number of root tips and total root length compared to Bologna (both $p < 0.01$; $p < 0.05$) and Watkins238 (both $p < 0.001$; $p < 0.01$). Paragon

showed also in rhizotrons a high number of root tips compared with Bologna ($p < 0.05$) but no differences were found among other genotypes.

Watkins238 exhibited a significantly smaller average diameter compared to Paragon ($p < 0.05$) and marginally smaller than Senatore Cappelli ($p = 0.05$). Watkins238 also showed a significantly smaller maximum root diameter compared to Paragon ($p < 0.05$) and Senatore Cappelli ($p < 0.05$). Watkins238 showed lower root diameter in rhizotrons than Bologna, Senatore Cappelli and Paragon (all $p < 0.001$).

Paragon and Senatore Cappelli showed longer seminal and lateral roots compared to Bologna ($p < 0.01$ and $p < 0.05$, respectively) and Watkins238 ($p < 0.001$ and $p < 0.01$, respectively). Paragon also exhibited significantly more branching points and higher branching frequency compared to Bologna and Watkins238 (both $p < 0.001$). Additionally, Senatore Cappelli had significantly more branching points and frequency than Watkins238 (both $p < 0.05$). A marginal difference in branching points was observed between Senatore Cappelli and Bologna ($p = 0.08$), with no significant differences in branching frequency.

No significant differences were detected in rhizotrons for these traits. However, after root cleaning, Cappelli and Watkins238 showed a higher number of root tips, branching points, and greater lateral and seminal root length compared to Watkins238, Bologna, and Paragon (all $p < 0.001$). Cappelli also exhibited higher values for these traits compared to Watkins238 alone ($p < 0.01$).

3.5 Root traits correlation between shovelomics and rhizotrons in barley and wheat

Correlations between shovelomics and rhizotron-derived traits were calculated for all wheat and barley datasets in order to assess the degree of cross-platform consistency. Overall, the strength of association was highly trait-dependent. Figure 9 presents a subset of representative examples.

Traits reflecting the root angle were significantly correlated across methods (both $R^2 = 0.5$). This result implies that root angle frequency represents a robust architectural trait, consistently captured across contrasting phenotyping methods and therefore suitable as a reliable proxy for cross-method comparisons.

The number of root tips, surface area root diameter range 1 and root diameter range 1 displayed a consistent positive correlation ($R^2 = 0.9$; $R^2 = 0.32$; $R^2 = 0.7$), supporting the idea that branching propensity can be captured with comparable resolution in both washed root crowns and rhizotron imaging. By contrast, root volume and lengt seems to be no correlated between methods. This was particularly evident for root length diameter range 1, root volume and surface area showed inconsistent associations. These discrepancies are likely explained by methodological differences, such as the loss of delicate laterals during crown washing and the inherent limitations of two-dimensional imaging for capturing complex fine-root networks.

Average root diameter also showed moderate agreement ($R^2 = 0.32$), suggesting that relative differences in root thickness are partly preserved across those two phenotyping methods.

Shallow angle frequency

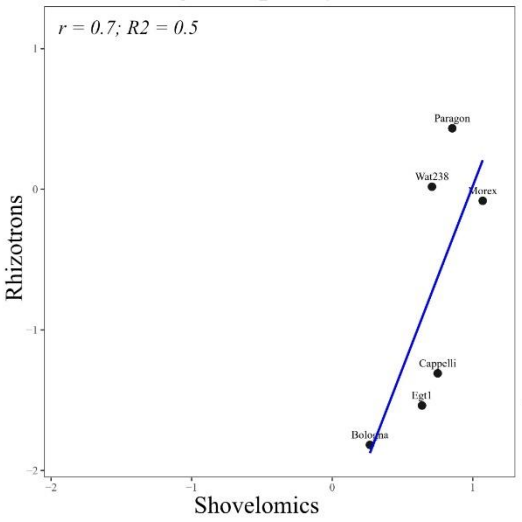

Steep angle frequency

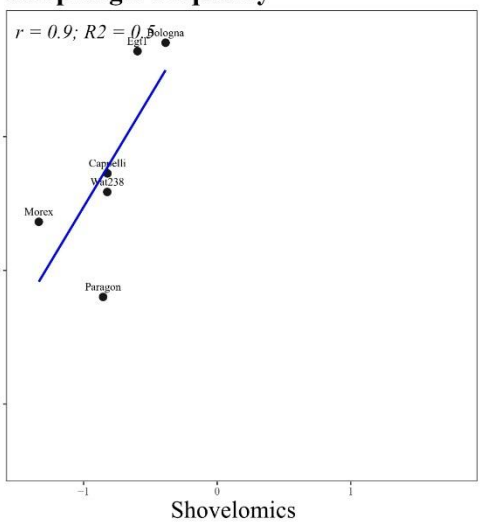

Total root lenght (mm)

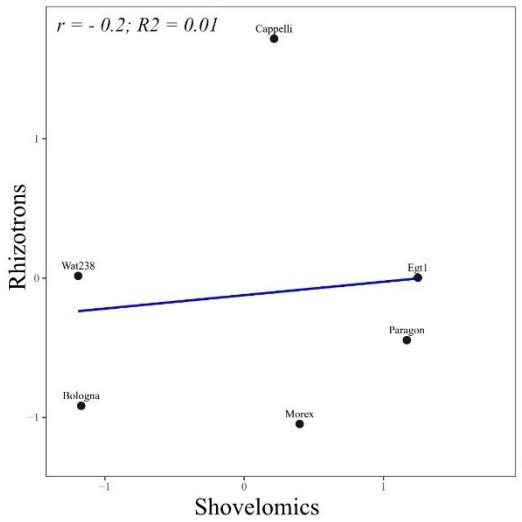

Number of root tips

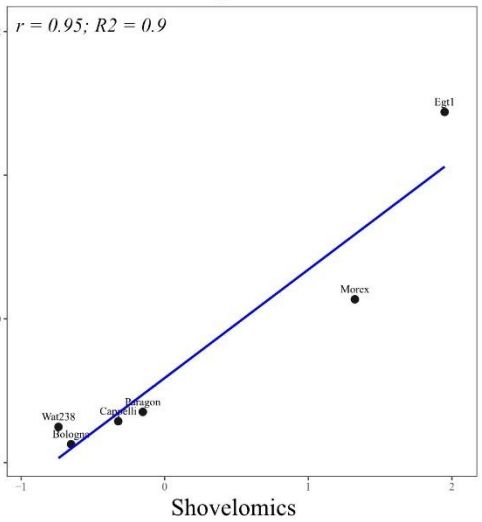

Avarage diameter (mm)

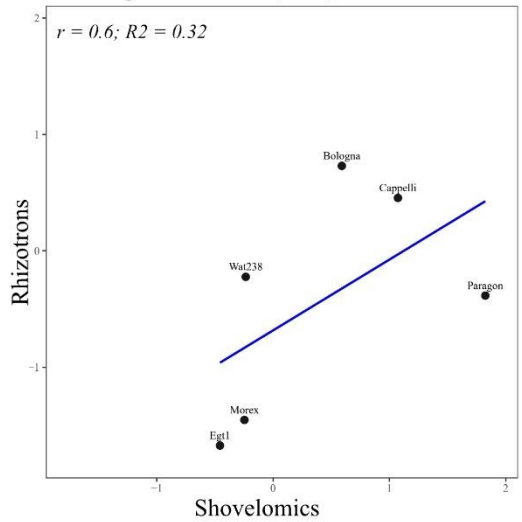

Branching frequency

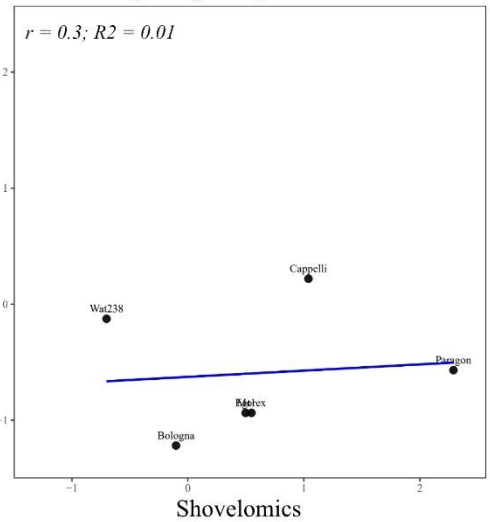

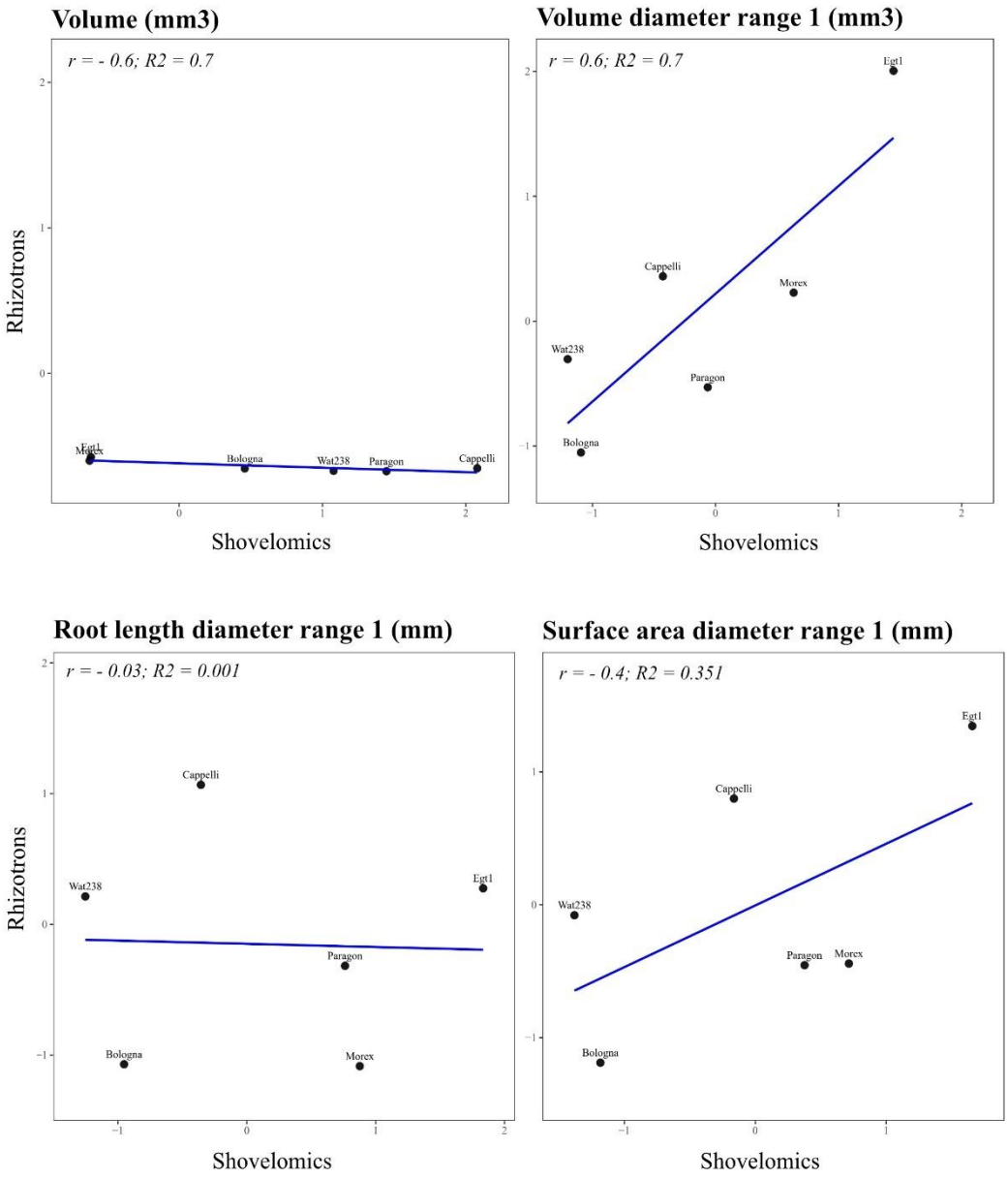

Figure 9. Correlations between root traits assessed by shovelomics and rhizotron-based measurements across wheat genotypes. Scatterplots show standardized values (z-scores) of traits derived from shovelomics (x-axis) and rhizotrons (y-axis), including shallow and steep angle frequency, total root length, number of root tips, average root diameter, branching frequency, root volume, root volume and length within the fine root diameter range, and root surface area in the same diameter range. Blue lines represent linear regression fits. Reported statistics indicate the Pearson correlation coefficient (r) and the coefficient of determination (R^2).

The partial agreement observed between shovelomics and rhizotron measurements raises an important question regarding the origin of these discrepancies. On the one hand, differences may be

attributed to technical limitations and methodological biases intrinsic to each platform. For instance, root excavation, culm selection and root washing in shovelomics can cause substantial loss of roots, leading to underestimation of total root length while leaving the root angle largely unaffected. The restricted dimensions of rhizotrons are likely to constrain total root volume, yet they do not necessarily impair the detection of discrete features such as root tip number.

On the other hand, the divergence between methods may also reflect developmental dynamics of trait expression. At seedling stage, when rhizotron imaging is typically performed, genotypic differences in some traits may not yet be fully expressed, becoming more pronounced only later in the growth cycle and thus better captured by shovelomics at maturity. Or for example, a genotype displaying relatively large root diameters at the seedling stage may later reduce its investment in thickness, resulting in comparatively smaller diameters at flowering.

Taken together, these considerations suggest that lack of correlation between methods cannot be interpreted solely as measurement error but may also reveal temporal shifts in the expression of genotypic differences. Distinguishing between these two sources of variation—technical versus biological—remains a key challenge in the cross-validation of phenotyping platforms.

Conclusions

We developed and evaluated a root phenotyping protocol suitable for annual monocot and dicot crops by integrating shovelomics with rhizotron imaging and water-based scanning of washed roots within a unified image-analysis pipeline. Applied to wheat, barley, and chickpea, this workflow enabled the joint assessment of architectural descriptors (e.g., root angle, convex/area metrics) and topological traits (e.g., diameter classes, total length, number of tips, branching frequency).

Genotypic differences were tested using ANOVA for wheat and t-tests for barley and chickpea. Across methods, both shovelomics and rhizotrons detected significant differences for several traits, indicating that each platform is sensitive to genetic variation in root system architecture (RSA). Cross-method agreement, however, was clearly trait-dependent. Correlation analyses performed on six genotypes (barley and wheat combined) showed that some traits converge across platforms, whereas others diverge.

A consistent outcome across all three species and phenotyping methods was the robustness of root angle. Angle-related traits discriminated genotypes and exhibited strong cross-method correlation between shovelomics and rhizotron measurements. This convergence suggests that root angle can be effectively screened under controlled rhizotron conditions and that relative genotypic rankings tend to be conserved in the field. While encouraging for early-stage selection, this inference should be validated with larger panels and across environments before routine deployment in breeding.

By contrast, traits such as total length and volume showed weak or inconsistent correspondence between platforms. These discrepancies likely reflect both methodological constraints (e.g., loss of delicate laterals during crown washing; two-dimensional projection and wall-growth biases in rhizotrons) and developmental dynamics (e.g., stage-dependent shifts in thickness or branching). Branching-related traits (tips, branching frequency) tended to show intermediate concordance, but their reliability appears more sensitive to image segmentation settings and diameter-class thresholds.

Two caveats temper our conclusions. First, the numbers of genotypes and biological replicates were limited, which reduces statistical power and increases the risk of both Type I and Type II errors, particularly for traits with smaller effect sizes. Second, correlation analyses pooled six genotypes across wheat and barley; although defensible for method comparison, this design may under- or over-estimate cross-platform agreement for species-specific traits. So, our findings should be interpreted with caution and viewed as hypothesis-generating rather than definitive.

What we provide with this protocol to the scientific community is a modular strategy: (i) use whole-crown images to quantify architectural traits that depend on spatial integrity (e.g., angle, convex

metrics), and (ii) use washed-root scans to capture topological and diameter-resolved traits (e.g., tips, branching points/frequency, fine-root length), with careful parameter standardization and quality control. For breeding applications, root angle emerges as a promising early-screening candidate in rhizotrons, with subsequent field verification via shovelomics.

Future work should expand genotype numbers and replication, incorporate multi-environment trials, and include explicit agreement analyses (e.g., Bland–Altman or errors-in-variables regressions) alongside correlation to quantify method bias and limits of agreement. Standardizing segmentation workflows (including training data and thresholds) and reporting uncertainty will further improve portability.

Taken together, our study indicates that no one of this single methods captures RSA complexity, but a carefully integrated protocol can deliver reproducible, biologically meaningful trait information to support selection for resource-efficient, stress-resilient crops.

References

Atkinson, Jonathan A., Michael P. Pound, Malcolm J. Bennett, and Darren M. Wells. 2019. "Uncovering the Hidden Half of Plants Using New Advances in Root Phenotyping." Current Opinion in Biotechnology 55 (February):1–8.

Bhat, Mujtaba Aamir, Vijay Kumar, Mudasir Ahmad Bhat, Ishfaq Ahmad Wani, Farhana Latief Dar, Iqra Farooq, Farha Bhatti, Rubina Koser, Safikur Rahman, and Arif Tasleem Jan. 2020. "Mechanistic Insights of the Interaction of Plant Growth-Promoting Rhizobacteria (PGPR) with Plant Roots toward Enhancing Plant Productivity by Alleviating Salinity Stress." *Frontiers in Microbiology* 11 (August):1952.

Dusschoten, Dagmar van, Ralf Metzner, Johannes Kochs, Johannes A. Postma, Daniel Pflugfelder, Jonas Bühler, Ulrich Schurr, and Siegfried Jahnke. 2016. "Quantitative 3D Analysis of Plant Roots Growing in Soil Using Magnetic Resonance Imaging." *Plant Physiology* 170 (3): 1176–88.

Gaggion, Nicolás, Federico Ariel, Vladimir Daric, Éric Lambert, Simon Legendre, Thomas Roulé, Alejandra Camoirano, et al. 2021. "ChronoRoot: High-Throughput Phenotyping by Deep Segmentation Networks Reveals Novel Temporal Parameters of Plant Root System Architecture." *GigaScience* 10 (7): giab052.

Heeraman, D. A., J. W. Hopmans, and V. Clausnitzer. 1997. "Three Dimensional Imaging of Plant Roots in Situ with X-Ray Computed Tomography." *Plant and Soil* 189 (2): 167–79.

Jeudy, Christian, Marielle Adrian, Christophe Baussard, Céline Bernard, Eric Bernaud, Virginie Bourion, Hughes Busset, et al. 2016. "RhizoTubes as a New Tool for High Throughput Imaging of Plant Root Development and Architecture: Test, Comparison with Pot Grown Plants and Validation." *Plant Methods* 12 (1): 31.

Koevoets, Iko T., Jan Henk Venema, J. Theo M. Elzenga, and Christa Testerink. 2016. "Roots Withstanding Their Environment: Exploiting Root System Architecture Responses to Abiotic Stress to Improve Crop Tolerance." Frontiers in Plant Science 7 (August):1335.

Kuijken, René C. P., Fred A. van Eeuwijk, Leo F. M. Marcelis, and Harro J. Bouwmeester. 2015. "Root Phenotyping: From Component Trait in the Lab to Breeding." Journal of Experimental Botany 66 (18): 5389–5401.

LaRue, Therese, H. Lindner, A. Srinivas, Moisés Expósito-Alonso, G. Lobet, and J. Dinneny. 2021.

"Uncovering Natural Variation in Root System Architecture and Growth Dynamics Using a Robotics-Assisted Phenomics Platform." *bioRxiv* 11 (November). https://doi.org/10.1101/2021.11.13.468476.

Le Marié, Chantal, Norbert Kirchgessner, Daniela Marschall, Achim Walter, and Andreas Hund. 2014. "Rhizoslides: Paper-Based Growth System for Non-Destructive, High Throughput Phenotyping of Root Development by Means of Image Analysis." *Plant Methods* 10 (1): 13.

Li, Anchang, Lingxiao Zhu, Wen-Li Xu, Liantao Liu, and Guifa Teng. 2022. "Recent Advances in Methods for in Situ Root Phenotyping." *PeerJ* 10 (July). https://doi.org/10.7717/peerj.13638.

Lynch, Douglas J., Roser Matamala, Colleen M. Iversen, Richard J. Norby, and Miquel A. Gonzalez-Meler. 2013. "Stored Carbon Partly Fuels Fine-Root Respiration but Is Not Used for Production of New Fine Roots." *The New Phytologist* 199 (2): 420–30.

Lynch, J. 1995. "Root Architecture and Plant Productivity." *Plant Physiology* 109 (1): 7–13.

Martins, Saulo Muniz, Giovani Greigh de Brito, Washington da Conceição Gonçalves, Bruna Mendes Diniz Tripode, Marc Lartaud, João Batista Duarte, Camilo de Lelis Morello, and Marc Giband. 2020. "PhenoRoots: An Inexpensive Non-Invasive Phenotyping System to Assess the Variability of the Root System Architecture." *Scientia Agricola* 77 (5). https://doi.org/10.1590/1678-992x-2018-0420.

Mathieu, Laura, Guillaume Lobet, Pierre Tocquin, and Claire Périlleux. 2015. "'Rhizoponics': A Novel Hydroponic Rhizotron for Root System Analyses on Mature Arabidopsis Thaliana Plants." *Plant Methods* 11 (1): 3.

Meister, Robert, M. S. Rajani, Daniel Ruzicka, and Daniel P. Schachtman. 2014. "Challenges of Modifying Root Traits in Crops for Agriculture." *Trends in Plant Science* 19 (12): 779–88.

Nagel, Kerstin A., Alexander Putz, Frank Gilmer, Kathrin Heinz, Andreas Fischbach, Johannes Pfeifer, Marc Faget, et al. 2012. "GROWSCREEN-Rhizo Is a Novel Phenotyping Robot Enabling Simultaneous Measurements of Root and Shoot Growth for Plants Grown in Soil-Filled Rhizotrons." *Functional Plant Biology: FPB* 39 (11): 891–904.

Nair, Kodoth Prabhakaran. 2019. *Combating Global Warming: The Role of Crop Wild Relatives for Food Security*. 2019th ed. Springer Climate. Cham, Switzerland: Springer Nature.

Paez-Garcia, A., C. M. Motes, W. Scheible, Rujin Chen, E. Blancaflor, and M. Monteros. 2015. "Root Traits and Phenotyping Strategies for Plant Improvement." *Plants* 4 (June):334–55.

Perez, Guillermo Ignacio, María Micaela Stoffel, Claudio Javier Baroni, María Eugenia Maina, Lucas Damián Daurelio, and Fernando Felipe Muñoz. 2022. “Biological Validation of the Free Software RhizoVision Explorer to Determine Root Parameters in Horticultural Crops.” https://www.researchsquare.com/article/rs-1389627/latest.

Rellán-Álvarez, Rubén, Guillaume Lobet, Heike Lindner, Pierre-Luc Pradier, Jose Sebastian, Muh-Ching Yee, Yu Geng, et al. 2015. “GLO-Roots: An Imaging Platform Enabling Multidimensional Characterization of Soil-Grown Root Systems.” *eLife* 4 (August). https://doi.org/10.7554/eLife.07597.

Rogers, Eric D., and Philip N. Benfey. 2015. “Regulation of Plant Root System Architecture: Implications for Crop Advancement.” *Current Opinion in Biotechnology* 32 (April):93–98.

Rossi, R., M. Amato, G. Bitella, R. Bochicchio, J. J. Ferreira Gomes, S. Lovelli, E. Martorella, and P. Favale. 2011. “Electrical Resistivity Tomography as a Non-Destructive Method for Mapping Root Biomass in an Orchard.” *European Journal of Soil Science* 62 (2): 206–15.

Schmidt, Jennifer E., and Amélie C. M. Gaudin. 2017. “Toward an Integrated Root Ideotype for Irrigated Systems.” *Trends in Plant Science* 22 (5): 433–43.

Seethepalli, Anand, Kundan Dhakal, Marcus Griffiths, Haichao Guo, Gregoire T. Freschet, and Larry M. York. 2021. “RhizoVision Explorer: Open-Source Software for Root Image Analysis and Measurement Standardization.” *bioRxiv*. bioRxiv. https://doi.org/10.1101/2021.04.11.439359.

Sharma, S., and M. J. Carena. 2016. “Grain Quality in Maize (Zea Mays L.): Breeding Implications for Short-Season Drought Environments.” *Euphytica; Netherlands Journal of Plant Breeding* 212 (2): 247–60.

Shihab, S., and W. Al-Nuaimy. 2004. “A Comparison of Segmentation Techniques for Target Extraction in Ground-penetrating Radar Data.” *Near Surface Geophysics* 2 (1): 49–57.

Trachsel, Samuel, Shawn M. Kaeppler, Kathleen M. Brown, and Jonathan P. Lynch. 2011. “Shovelomics: High Throughput Phenotyping of Maize (Zea Mays L.) Root Architecture in the Field.” *Plant and Soil* 341 (1-2): 75–87.

Wu, Jie, Qian Wu, Loïc Pagès, Yeqing Yuan, Xiaolei Zhang, Mingwei Du, Xiaoli Tian, and Zhaohu Li. 2018. “RhizoChamber-Monitor: A Robotic Platform and Software Enabling Characterization of Root Growth.” *Plant Methods* 14 (June):44.

Xiao, Shuang, Liantao Liu, Yongjiang Zhang, Hongchun Sun, Ke Zhang, Zhiying Bai, Hezhong Dong, and Cundong Li. 2020. “Fine Root and Root Hair Morphology of Cotton under Drought Stress Revealed with RhizoPot.” *Journal of Agronomy and Crop Science* 206 (6): 679–93.

Yazdanbakhsh, N., and J. Fisahn. 2009. “High Throughput Phenotyping of Root Growth Dynamics, Lateral Root Formation, Root Architecture and Root Hair Development Enabled by PlaRoM.” *Functional Plant Biology: FPB* 36 (11): 938–46.

York, Larry M., Shaunagh Slack, Malcolm J. Bennett, and M. John Foulkes. 2018. “Wheat Shovelomics I: A Field Phenotyping Approach for Characterising the Structure and Function of Root Systems in Tillering Species.” *bioRxiv*. bioRxiv. https://doi.org/10.1101/280875.

Zhang, Yangyang, Wenjing Zhang, Qicong Cao, Xiaojian Zheng, Jingting Yang, Tong Xue, Wenhao Sun, et al. 2021. “WinRoots: A High-Throughput Cultivation and Phenotyping System for Plant Phenomics Studies under Soil Stress.” *Frontiers in Plant Science* 12:794020.

Acknowledgements

The research was partially funded by the project WISH-ROOTS- "Tuning the wheat root microbiome to improve soil health and optimize rhizosphere nitrogen cycling and availability" is supported by the European Join Programme Soil ERA- NET (HORIZON 2020) research and innovation programme. MCHS gratefully acknowledges funding support from the Biotechnology and Biological Sciences Research Council (BBSRC), project BB/X003000/1. Funding was also provided by the Department of Agricultural and Food Sciences, University of Bologna, through its Ph.D programme.

Additional support to Bartolo Giuseppe Dimattia was provided by the Collegio Superiore and the Institute of Advanced Studies of the University of Bologna, whose contribution is gratefully acknowledged.

Author contributions statement

B.G.D. contributed to the writing of the funded project, conceived the experiment, followed all the agronomic practices and management practices, collected samples and data, analyzed the data and contributed to the writing of the paper, S.S contributed to the writing and revew the paper.

Conclusions

This thesis investigated whether differences in root system architecture (RSA) among wheat genotypes can influence rhizosphere soil properties. Building on an improved shovelomics protocol that integrates crown-level architectural traits with fine-scale measurements from washed-root scans, 20 bread and durum wheat genotypes were phenotyped. A subset of four contrasting genotypes was selected for detailed analyses, including X-ray imaging and functional characterization of rhizosphere soil cores.

The results of this pilot study suggest that genotypic variation in RSA may alter soil structure. Landraces tended to increase porosity and bioporosity compared to elite varieties, with root diameter and lateral root frequency emerging as promising traits associated with these differences. Hydraulic measurements further indicated genotype-dependent variation: saturated hydraulic conductivity (Ksat) and soil water retention curves (SWRCs) differed significantly among genotypes, with landraces generally showing higher field capacity, lower wilting point, and up to 33% higher plant-available water (PAW). These findings point to a potential physical, in addition to chemical, contribution of roots to soil function.

We propose that RSA traits such as root diameter and lateral density may influence soil particle packing, pore structure, and consequently water retention and flow. This could in turn affect nutrient uptake and microbial recruitment. Such a mechanism would support the development of ideotypes with *"wide, dense, and lasting"* root systems, promoting water and carbon storage in surface and intermediate soil layers and reducing external inputs.

However, these conclusions must be regarded as preliminary. The study was limited by the number of genotypes and replicates, and further work with larger and more diverse populations is needed to validate or refute this hypothesis. Nevertheless, this thesis provides the first evidence of genotypic effects on rhizosphere soil physical properties and introduces a refined shovelomics-based protocol that can support future research in this area.

Future work

The work presented in this thesis represents only a small portion of the activities carried out within the broader WISH-ROOTS project. The data collected and described in Chapter 2 will be further explored and integrated into future studies focusing on soil physics, in particular the role of root–soil interactions in shaping soil aggregation. These analyses will be complemented by investigations of soil microbiomes and chemical properties, with the aim of linking root system architecture not only to physical but also to biological and chemical dimensions of soil health. The integration of these approaches will allow a more comprehensive understanding of how genotypic variation in root traits contributes to the multifunctionality of agricultural soils.